6-30-2016

Development Of Pressure Swing Adsorption (PSA) Processor CO2 Capture From Flue Gas

Md. Atikur Rahman
University of South Carolina

DEVELOPMENT OF A PRESSURE SWING ADSORPTION (PSA) PROCESS FOR CO_2 CAPTURE FROM FLUE GAS

by

Md. Atikur Rahman

Bachelor of Science
Bangladesh University of Engineering and Technology, 2006

Master of Engineering
North Carolina Agricultural & Technical State University, 2010

Submitted in Partial Fulfillment of the Requirements

For the Degree of Doctor of Philosophy in

Chemical Engineering

College of Engineering and Computing

University of South Carolina

2016

Accepted by:

James A. Ritter, Major Professor

Armin Ebner, Committee Member

Miao Yu, Committee Member

Jamil Khan, Committee Member

John Weidner, Committee Member

Lacy Ford, Senior Vice Provost and Dean of Graduate Studies

DEDICATION

Without the fighting spirit and motivation, I would not be able to reach my destination and two persons I have learned from how to fight in the toughest situations are my mother Late Halima Rahman and my daughter Arya Tabassum Rahman. My mother passed away when I was very young after fighting with cancer. While resting on the hospital bed, she wrote on a piece of paper that she found from a shopping bag that, "Be an engineer when you grow up, it's my dream!" I do not have that paper but I always kept that line on my mind and became an engineer. I know she is smiling by sitting up in the heaven seeing me achieve this highest degree in the field of study. I would like to dedicate my dissertation to my mom.

My daughter Arya came to the world when I finished my MS and about to start my PhD studies. Her introduction to this world was not smooth. She fought in the NICU for 13 days and finally defeated all the odds and came home with us. She always gave me inspiration, motivation and fighting instincts to move forward. I would like to dedicate my dissertation to my daughter Arya too.

ACKNOWLEDGEMENTS

Doctor of Philosophy in Chemical Engineering is the biggest achievement of my life and this would not be possible without significant help of several individual during the course of my graduate studies and my life. I would like to take this opportunity to express my gratitude toward them.

I was fortunate enough to come across Dr. Armin D. Ebner, my co-advisor in University of South Carolina. He is the smartest person I have ever met and a great mentor. He was always there when I faced any theoretical or experimental problem. He also supported me and kept me on the right track during the course of my PhD studies. From him I learned the art of perseverance, problem-solving skills for both theoretical and experimental. Without his help, I would not be able to accomplish my research goal. I would like to express my heartiest gratitude toward Dr. Ebner for everything he has done for me.

I am forever in debt to Dr. James A. Ritter for accepting me as a PhD student in his research group. It was a pleasure to work with him and his input during our discussion in group meetings opened new avenue of thinking of my research. He made sure I receive a paycheck every month and I really appreciate his support. I would like to express my gratitude towards Dr. James A. Ritter.

I would like to thank Marjorie A. Nicholson for her constant help in everyday life in the laboratory whether it is for solving a problem in an analytical equipment or finding

a fitting or anything else. She took care of my as my mom would. Whenever I had headache she gave me medicine. She invited us for dinner in thanksgiving or to watch a game.

Mr. Charles Holland built every equipment and wrote the LabVIEW program for each equipment that I worked with for the last four years in Dr. Ritter's lab. I worked with three major experimental setup, Rapid Pressure Swing Absorption (RPSA) apparatus, Single Bed Pressure Swing Adsorption apparatus, and Four Bed Pressure Swing Adsorption apparatus. It was a privilege to come across such a genius person who knows a lot about design of experiment. He was always there whenever I needed to troubleshoot any equipment that saved me a lot of time. I would like to acknowledge Mr. Holland for his help.

I am grateful to all my committee members Dr. Jamil Khan, Dr. Miao Yu and Dr. John Weidner for their time, support and guidance during my research, and for being a part of my committee.

I would like to acknowledge the great support provided by very good friends Dr. Rajib Saha and Dr. Shudipto Konika Dishari during our good times and tough times. Without their support, I would not be able to get here.

I joined Dr. Ritter's group through the referral of Dr. Shubhra Bhadra after he got a job at Air Products. I would like to thank Dr. Bhadra for assisting me to join this group and hope that I was able to keep the highest level he set in the group. It was a pleasure to work with all highly motivated and friendly colleagues in Ritter's research group. I would also like to acknowledge all previous and present research group mates, Dr. Anahita Abdollahi, Dr. Ifthekher Hossain, Lutfi Erden, Hanife Erden, Joshua White, and Nima

Mohammadi for all their support. All members of Dr. Rittre's group contributed so many different ways in my PhD work.

Especially, I would like to thank my wife Tabassum Shahid, for her support, love and care. Life of a graduate student is not a smooth ride. She has always been beside me through the whole journey through difficulties. She never lost her faith in me during the darkest corner of our life. Last but not the least, I would like to acknowledge my family in Bangladesh specially my father Md. Fazlur Rahman, my elder brother Md. Asifur Rahman and my younger brother Md. Anisur Rahman for all the sacrifices in life they had to make for my long graduate student life.

ABSTRACT

Reducing the anthropogenic CO_2 emissions and lowering the concentration of greenhouse gases in the atmosphere has become one of the most important environmental issues of recent times. To this end, the development of a cost effective pressure swing adsorption (PSA) process, utilizing commercially available 13X zeolite as the adsorbent, is underway to remove and concentrate CO_2 in the flue gas of a coal-fired power plant. This systematic development effort has been carried out so far at the bench scale. It has included the following studies that defined and validated this PSA process both experimentally and via a PSA process model. First, a unique 3-bed 7-step PSA cycle schedule was developed for this CO_2-N_2 separation by performing PSA process simulations using the in-house Dynamic Adsorption Process Simulator (DAPS). To validate the results from DAPS, a number of different experiments were carried out that included measuring equilibrium and kinetic (mass transfer) data for both CO_2 and N_2 on 13X zeolite. This data was used in DAPS to validate it against PSA process experiments obtained from a unique 1-bed PSA apparatus that mimics all the steps of the 3-bed 7-step cycle. DAPS was able to predict the results from these 1-bed experiments without adjusting any of the model parameters. To validate the 3-bed 7-step PSA cycle schedule experiments were also carried out in a unique multi-bed PSA system. This set of experiments proved that the 3-bed 7-step PSA cycle could indeed meet the DOE requirements of producing 95% CO_2 purity and 90% CO_2 recovery from a 15% CO_2 in N_2 feed. Again, DAPS was able to predict the results from

these 3-bed 7-step experiments without adjusting any of the model parameters. Overall, this work validated a unique PSA process at the bench scale for separating CO_2 from the flue gas of a coal-fired power plant. This presentation will provide an overview of these experimental and modeling studies.

TABLE OF CONTENTS

LIST OF TABLES

LIST OF FIGURES

LIST OF SYMBOLS

$b_{i,k}$	Affinity constant of component i in process k in Three process Langmuir model
$b_{i,k,o}$	Pre-exponential factor of the affinity constant of component i in process k in Three process Langmuir model
$B_{i,k}$	Energy term of affinity coefficient in Three process Langmuir parameter
c_v	Flow coefficient (SLPM/$Pa^{1/2}$)
$Cp_{a,j}$	Specific heat of adsorbed component j (J/kg.K)
Cp_g	Specific heat of gas mixture (J/mol.K)
$Cp_{g,j}$	Specific heat of gas component j (J/mol.K)
Cp_w	Specific heat of the column wall (J/mol.K)
C_T	Total gas concentration (mol/m^3)
D	duration of a unit block
F	Flow rate (SLPM)
h_w	Film heat transfer coefficient between the gas phase and column wall (W/m^2.K)
i, j	Component i, j
I_i	duration of idle step i
J_i	duration between two coupled cycle steps i
k_i	mass transfer coefficient of component i (1/sec)
L	Column length (m)
n	Total number of components
N	number of beds

P	Total pressure (Pa)
P_i, P_j	Gas pressure of component i, j (Pa)
P_o	Initial total pressure (Pa)
q_i	Adsorbed phase concentration of component i (mol/kg)
q_i^*	Adsorbed gas-phase concentration in the equilibrium state of component i (mol/kg)
$q_{i,k,s}$	Saturation capacity of component i in process k in two process Langmuir model (mol/kg)
$r_{b,i}$	Internal bed radius (m)
$r_{b,o}$	External bed radius (m)
r_p	Radius of pellet (m)
R	Universal gas constant (J/mol.K)
s_g	Density of gas related to air at 294.26K
S_i	duration of a cycle step i
t	Time (s)
T	Temperature (K) or total cycle time
T_0	Exterior temperature (K)
U	duration of a unit cell
v	Velocity of gas mixture (m/s)
v_{sign}	-1 (if $v<0$), 1 (else)
y_i, y_j	Molar fraction of component i, j
x	maximum number of unit cells occupied by any cycle step except the feed step
y	number of unit cells in a unit block
z	number of beds fed simultaneously
z	Axial distance along the column (m)

ΔH_i Isosteric heat of adsorption of component i (kJ/mol)

α alpha–train of PSA process

β beta–train of PSA process

γ Purge to Feed ratio

θ Feed Throughput (L STP/hr/kg)

π Pressure Ratio

ε_b Porosity of the bed

ε_P Porosity of the pellet

ρ_g Density of gas mixture (kg/m^3)

ρ_P Pellet density (kg/m^3)

ρ_w Column wall density (kg/m^3)

μ_g Gas viscosity (Pa.s)

Γ Grand Cycle Time

LIST OF ABBREVIATIONS

CnD……Counter-current depressurization step

DAPS……..Dynamic Adsorption Process Simulator

EeD……Depressurization equalization step ($1 \leq e \leq$ number of such steps)

EeR……...Equalization Repressurization step ($1 \leq e \leq$ number of such steps)

Evac……..Evacuation step

F……..Feed step

FP……Feed pressurization step

FR……Feed re-pressurization step

HP……...Heavy product

HR……..Heavy reflux step

LP……Light product

LPP……...Light product pressurization

LR……..Light reflux purge step

P_H…….……High Pressure

P_L……..Low Pressure

PP……...Co-current depressurization step

PSA……Pressure Swing Adsorption

SLPM…….Standard liter per minute

STP……Standard Temperature and Pressure

CHAPTER 1

MASS TRANSFER COEFFICIENT DETERMINATION OF CO_2, N_2, O_2, CH_4, AND AR IN ZEOLITE 13X DETERMINED BY A RAPID PRESSURE SWING APPARATUS

1.1 Introduction

The effective design of adsorption-based gas separation processes depends upon accurate knowledge of the dynamic behavior of adsorbent/gas systems. It is usually assumed that uptake in porous adsorbents is limited by mass transfer, so studies of adsorption dynamics are often mass transfer studies in practice. Mass transfer of gases in porous adsorbents can be complex due to the existence of one or more mechanisms. Possible mechanisms include micropore diffusion, Knudsen diffusion, macropore diffusion, advection flow, and transport across a surface barrier, and external mass transfer. Also, changes in the adsorbent temperature caused by heats of adsorption can further complicate dynamic behavior.

Nitrogen, methane, carbon dioxide, oxygen and argon are important in many industrial applications, as well as in our daily life. Major research effort has been directed toward understanding the effect of increasing concentration of CO_2 on the global atmosphere. CO_2 capture from fixed point sources has been targeted [1-4]. Significant effort has been taken to develop various separation processes to capture CO_2 for various effluent gases. Relatively low energy consumption has made adsorption technologies more

attractive than available technologies and are being widely used for the separation and purification of various effluent gases in many industries [5-7]. The increasingconcentration of CO_2 in the atmosphere furnishes a major contribution to the global warming. Separation of CO_2 from mostly N_2-containing stack gases is important from this aspect [8-10]. Separation of CH_4 and CO_2 is wanted for recovering CH_4 from landfill gas emissions [11-14] and also to upgrade natural gas [15-17].

Pressure (vacuum) swing adsorption has been regarded as a promising technology to capture CO_2 and produce clean energy (H_2 and CH_4) due to its low energy consumption [16-27]. Zeolite 13X has been proved by several studies as one of the best adsorbents available commercially for post combustion applications. It is widely accepted as the benchmark material for the comparison with other materials for CO_2 separation processes [7, 27-31]. Therefore, a lot of research work presented in the literature has been focused on the uptake measurement to compare CO_2 adsorption capacities. However, relatively less work are reposted on the kinetic measurement s of CO_2 in 13X. Considerably less data are reported on the kinetic measurements of CO_2 in 13X. Onyestya´k et al. [32], Onyestya´k and Rees [33] and Onyestya´k [34] used a frequency–response technique to measure the adsorption rate of CO_2 in commercial 13X beads. They determined frequency-response (FR) sorption-rate spectra in the range of -78 and 70° C at 133 pa and found that the diffusion of CO_2 is controlled by the transport in the macropores. Knudsen diffusion was used to describe the molecular diffusion inside the macropores and a good agreement was found between the calculated and the measured values. Few years ago, Giesy et al. measure the diffusivity of CO_2 in commercial 13X beads using a novel combined pressure swing and volume swing frequency response technique [35]. His measurement proved that the

mass transfer of CO_2 in 13X is of Kundsen-type macropore diffusion controlled which agreed with the previous literature data. Recently LeVan et al. used a new combined pressure-swing and volume-swing frequency response technique to measure the diffusivity of CO_2 in commercial 13X beads [36]. They performed pressure swing and volume-swing experiments in tandem to study transport of pure CO_2 in 13X zeolite beads over the frequency range from 10^{-4} Hz to 10 Hz at pressures from 0.125 to 1 bar. Frequency response spectra showed that transport in this system is governed by a nonisothermal macropore diffusion resistance with diffusion occurring by a Knudsen-type mechanism. Measurements using different bead sizes showed evidence of a Knudsen-type macropore diffusion controlled process, confirming previous literature data. They reported the value of the diffusional time constant to be (D_p/R_p^2) to be 2.3 s^{-1}.

Valyon et al studied the sorption of N_2 and O_2 on synthetic an natural mordenites and on molecular sieves 4A, 5A and 13X by frequency response techniques [37]. The frequency response rate spectra was determined at 133 Pa, 195 or 298 K to characterize the sorption dynamics. They concluded that in powder 13X (particle size <0.063 mm) the micropore diffusion was the rate-determining step. In larger granules (~1.4-2.0 mm) the diffusion resistance of the macro- and mesopores controlled the rate of transport. Under similar conditions the mass transport of O_2 was always faster than that of N_2.

There are several other studies presented about the adsorption behavior of pelletized zeolite at different pressures for N_2, CH_4 and CO_2 on 4A, 5A and CaX [38] and CH_4 and CO_2 on zeolite 13X [38-40] through various experimental methods.

Improvements in performance and the reduction in cost of adsorption processes are dependent on parameters which are dictated by adsorbent loading per unit volume, mass-transfer properties, pressure drop, and thermal management. However, these factors are strongly influenced by the structure of the adsorbent used in the gas separation device. A major driver toward the development of future adsorptive gas separation processes lies in the development of improved sorbent materials [41]. A key area of future research is the mass-transfer characteristics. The influence of adsorbent structure on mass-transport kinetics influences the overall system efficiency. The relationship between separation performance and the macro/meso/micro hierarchy of the adsorbent has not been explored to date. Pore engineering must be integrated with systems engineering to produce an overall optimal structure.

There are several techniques available to determine mass transfer coefficient in adsorbent materials. Several researchers reported frequency response (FR) method as a useful tool for mass transfer studies [36, 42, 43]. In FR experiments, one of the system variables is perturbed periodically, about an equilibrium point, and the response of the other system parameters are used to characterize the dynamics of the system. The main drawback of the FP technique is the perturbation in the system variables is very small and always close to the equilibrium condition. Another common technique to determine the mass transfer coefficient is the zero length column (ZLC) where the measurement is done using only one single adsorbent bead [40]. Having a very small sample size ZLC does not represent a real adsorbent bed where the mass transfer characteristic can be significantly different.

The most common techniques for determining mass transfer resistance is a small step test. The response of particles is measured gravimetrically, volumetrically, or chromatographically after increasing the concentration in a step. A rate parameter is obtained by fitting an assumed model to the system response. This approached often fails to identify the controlling mass transfer mechanism in any rigorous way. Several researchers reported frequency response (FR) method as a useful tool for mass transfer studies [36, 42, 43]. In FR experiments, one of the system variables is perturbed periodically, about an equilibrium point, and the response of the other system parameters are used to characterize the dynamics of the system. The main drawback of the FR technique is the perturbation in the system variables is very small and always close to the equilibrium condition. Another common technique to determine the mass transfer coefficient is the zero length column (ZLC) where the measurement is done using only one single adsorbent bead [40]. Having a very small sample size ZLC does not represent a real adsorbent bed where the mass transfer characteristic can be significantly different. System nonlinearities often caused by large steps are not identified.

In this work the mass transfer study of single gas was carried out in a single bed rapid pressure swing apparatus by performing a two step adsorption-desorption cyclic experiment. Cyclic experiments provide insight on the mass transfer coefficients under conditions when the system is operated within a large pressure change and within the bound of a net working capacity of the adsorbent. Having a large sample size gives a good estimate of the effective mass transfer coefficient of the adsorbent bed and mimic the actual PSA adsorbent bed. The rapid pressure swing adsorption apparatus has been characterized by carrying out dynamic cyclic experiments with single gases such as He, CO_2, N_2, CH_4,

O_2 and Ar both with an empty bed and with the bed filled with beaded 13X zeolite over a wide range of cycle times and process conditions. Pressurization and depressurization step times as short as 0.25 sec are possible in this system under both positive and negative gauge pressure and at different temperatures. By fitting appropriate kinetic model with the pressure responses of a single gas in 13X for different cycle times, the mass transfer coefficient can be determined. Four models were developed and energy balances was incorporated to one of the models to incorporate temperature rise during the adsorption step.

1.2 Experimental Section

The gases used for isotherm measurements and experiments were provided by Airgas: Ultra High Pure (UHP) Nitrogen, UHP Methane, UHP Argon, UHP Oxygen, Coleman grade CO_2. The adsorbent used was zeolite 13X from Grace.

1.2.1 Isotherm Measurement

Pure component adsorption equilibrium isotherms for CO_2, O_2, N_2, Ar, and CH_4 on zeolite 13X were measured by using a volumetric system from micromeritics ASAP2010. Since ASAP-2010 is designed for surface area and porosimetry measurements and measures the nitrogen isotherm at 77 K it had to be modified to be able to measure different pure gas isotherms at various temperatures. Operation pressure range provided by this system is from 0 to 127 KPa. The molecular drag pump can create vacuums down to 1.3 $*10^{-6}$ KPa in the system.

Volumetric method involves measuring the pressure change in a known volume of sample gas exposed to an adsorbent sample. As the gas is adsorbed and allowed to come to equilibrium with the adsorbent, the measured decrease of pressure in the closed system indicates the amount of gas adsorbed under the given isothermal conditions.

Data were collected for the equilibrium pressure range of 0.001 to 110 KPa at 25, 50 and 75 degree Celsius. Obtaining each complete isotherm consists of 60 to 120 equilibrium point measurements and takes roughly about 12 hours. For each point when the rate of change for pressure is less than 0.01% criterion for equilibrium is satisfied and the system moves to the next point.

Prior to each isotherm measurement, the zeolite 13X was regenerated at 350 C for 16 hours under a vacuum of less than 1 x 10^{-4} torr. In order to prevent structural damage caused by desorbing water steam a stepwise increase in temperature with simultaneous vacuum was applied to all samples.

The pure gas adsorption isotherm along with the model fit has been shown in **Figure 1.1** and**Figure 1.2**. The experimentally determined pure gas isotherms except for CO_2 have been fitted with the Dual Process Langmuir (DPL) model. The experimental isotherm of CO_2 was fitted with three-process Langmuir (TPL) isotherm. The isotherm model parameters have been summarized in **Table 1.1**. The heat of adsorption of each gas was determined by fitting the experimental isotherm with toth isotherm. The heat of adsorption of all gases have been summarized in **Table 1.2**.

1.2.2 Rapid Pressure Swing (RPSA) Apparatus

The experimental Rapid Pressure Swing Apparatus (RPSA) designed to perform very fast pressure swing adsorption cycle (step time in the order of quarter of a second) is

shown in **Figure 1.3**. The system has been designed to perform all cycle steps of a typical pressure swing adsorption (PSA) process in a single bed and mimic a complete multi-bed PSA cycle process. It contains two sections: (1) Heavy product end (bottom section of the bed) and (2) Light product end (top section of the bed). There is a designated flowmeter and line equipped with a solenoid valve for each individual step either feed or product. For example, during the feed step, the feed is fed through the flowmeter FM-3 and the solenoid valve SV-1 is opened, the light product goes through the valve SV-9 and using the light product flow meter FM-2 the flow of the light product is read. A vacuum pump is connected to the feed thank (FD) to control the pressure of the tank which enables us to feed under vacuum. Heavy reflux (HR) gas is fed through FM-4 by opening solenoid valve SV-2 and light product during HR step is withdrawn by opening solenoid valve SV-10. There are three light-end equalization tanks (LE EQ1, LE EQ2 and LE EQ3) and one heavy end equalization tank (HE EQ) to mimic the bed-to-bed equalization step. Two vacuum pumps connected in series are used to keep the pressure of the vacuum tank (VAC) under deep vacuum ready to perform the depressurization of the bed. In order to perform the counter current depressurization (CnD) step valve SV-5 was opened and the bed was emptied by pulling with the vacuum pressure of the vacuum tank. All pressure transducers and solenoid vales are connected to the computer and operated by a LabVIEW^{TM} software. The feed tank pressure were recorded using the flow meter pressure transducer PT-3. The bed and vacuum tank pressure was recorded using the pressure transducer PT-9 and PT-1 respectively. The heavy product flow rate is recorded using the flow meter FM-5. All the flow meters were calibrated for the analysis gases using a gilibrator. There is an extra vacuum tank has been connected to the feed tank with a needle valve, by adjusting the

needle valve the pressure of the feed tank was maintained at a fixed pressure under vacuum and this way we can feed the adsorption column under vacuum.

Before loading the adsorbent to the adsorption column the two-step adsorption-desorption experiment was performed at 20 psia and 25 ^{0}C using CO_2, N_2 and He for step time from 0.25 to 10 sec. By fitting the pressure, curve of all the gases simultaneously with the Cv equation the valve Cv's of the feed line (SV-1) and CnD line (SV-5). Measured amount of adsorbent 13X zeolite was activated in an oven at 350 °C for 14 hours by flowing helium. After the adsorbent was cooled, it was loaded to the adsorbent column of the RPSA apparatus. The adsorbent was again activated in situ at 350 °C by flowing helium through the bed for another 14 hours. Two step adsorption-desorption cyclic study was carried out with loaded bed using He to determine the excluded volume. The mass balance of the He adsorption-desorption experiment is shown in **Table 1.3**. With the known excluded volume the bed properties were determine which is listed in Table 3. Then same two-step cyclic studies were carried out with the loaded bed with pure CO_2, N_2, O_2, CH_4, and Ar at different cycle times, temperature and bed pressures to determine the mass transfer coefficients between these gases and the zeolite. The experiments were performed at bed temperatures of 25, 50 and 75 °C. In order the study the effect of feed pressure on the mass transfer between these gases and the adsorbent experiments in each temperature were performed for the feed pressures of 2, 8, 20, 40 psia. For each temperature and pressure combinations half cycle of 0.25, 0.5, 1.0, 2.0, 3.0 and 10.0 were used. Activation was repeated when changing gases or deemed necessary.

1.3 Mass Transfer Models

We started with a very simple one-step isothermal macro pore model (1 Param Iso) which only considers the mass transfer resistance in the macro pore. In order to fit the pressure profile of CO_2 we slowly had to incorporate more complexity to our 1 param Iso model. In order to capture the temperature rise during the adsorption step temperature was determined by solving the energy balance simultaneously with the mass balance giving rise to one parameter non-isothermal macro pore model (1 Param Non-iso). Then a third model was developed by taking into account both macro and micro pore resistances without energy balance resulting in 2-parameter isothermal macro pore model (2 Param Iso). Finally, the energy balance was incorporated to the 2 param iso model making this to 2 parameter non-isothermal macro pore model (2 Param Non-Iso).

1.3.1 One Parameter Isothermal Macro Pore Model (1 Param Iso)

One parameter isothermal macro pore model used to describe the fixed-bed dynamics was derived from the mass balance by neglecting the energy balance. The model as based on the assumptions: the gas phase behaves as an ideal gas mixture; the temperature change is neglected.

With these assumptions, the fixed-bed model is described by the following equations. The mass balance is given by Eq. (1):

$$\frac{V_{EX}}{RT}\frac{\partial P}{\partial t} + m_a \frac{\partial \bar{\bar{q}}}{\partial t} = \dot{n} \tag{1}$$

where V_{EX} is the external volume of the bed, R is the ideal gas constant, T is the temperature average temperature of the bed, m_a is the mass of the adsorbent, $\dot{n}$ flow.

The rate of mass transfer to the particle for each gas given by Eq. (2)

$$\frac{\partial \bar{\bar{q}}}{\partial t} = k_{M,eff}(q^*(P,T) - \bar{\bar{q}}) \quad (2)$$

where $k_{M,eff}$ is the overall effective macropore mass transfer coefficient, q* is the adsorbed equilibrium concentration, i.e., q* = f (P,T) given by the isotherm and $\bar{\bar{q}}$ is the average adsorbed concentration.

The overall effective macropore mass transfer coefficient is given by Ep. (5)

$$k_{M,eff} = \frac{1}{1 + \frac{RT\rho_p}{\varepsilon_p}\frac{\partial q^*}{\partial P}_{T,\bar{P}}} k_{M1} \quad (3)$$

Where ρ_P is the particle density, ε_P is the particle porosity, $\frac{\partial q^*}{\partial P}_{T,\bar{P}}$ is the slope of the isotherm, k_M macorpore mass transfer parameter. The fitting parameter for this model is k_M.

1.3.2 One Parameter Non-Isothermal Macro Pore Model (1 Param Non-Iso)

In the first model, the temperature was held constant. However in the second model temperature change due to adsorption-desorption was considered. By including the temperature derivative the mass balance equation becomes:

$$\frac{V_{EX}}{RT}\frac{\partial P}{\partial t} - \frac{PV_{Ex}}{RT^2}\frac{\partial T}{\partial t} + m_a\frac{\partial \bar{\bar{q}}}{\partial t} = \dot{n} \quad (4)$$

The rate of mass transfer and effective mass transfer coefficient was calculated using equation 2 and 3 respectively.

The temperature was determined by solving the energy balance equation:

$$\frac{V_{EXT}P}{RT}C_{pG}\frac{\partial T}{\partial t}+\frac{V_b(1-\varepsilon_b)\varepsilon_p}{RT}\bar{P}C_{pG}\frac{\partial T}{\partial t}-V_{EXT}\frac{\partial P}{\partial t}-V_b(1-\varepsilon_b)\varepsilon_p\frac{\partial \bar{P}}{\partial t}$$

$$+m_a\left[\left(C_{ps}+qC_{pG}\right)\frac{\partial T}{\partial t}+\Delta H\frac{\partial \bar{\bar{q}}}{\partial t}\right]+hA(T-T_w)$$

$$=\dot{n}\int_{T_{in}}^{T_G}C_{pG}dT \qquad (5)$$

where C_{PG} is the molar specific heat of the gas, C_{PS} is the specific heat of the adsorbent, ΔH is the heat of adsorption of the gas, hA is the wall heat transfer coefficient, T_W is the wall temperature. The fitting parameters for this model are k_M, k_m, hA, Tw, q_0, T_0 and$\bar{P}_0$.

1.3.3 Two Parameter Isothermal Macro Pore Model (2 Param Iso)

In two parameter isothermal macro pore model two mass transfer coefficient parameters are used one for macro and the other for micro pore resistance.

The mass balance is given by Eq. (6):

$$\frac{V_{EXT}}{RT}\frac{\partial P}{\partial t}+(1-\varepsilon_b)\frac{V_b}{RT}\varepsilon_p k_{M2}\frac{Bi}{1+Bi}(P-\bar{P})=\dot{n} \qquad (6)$$

where, V_{EXT} is the exterior volume of the adsorbent bed, k_{M2} is the macropore mass transfer coefficient.

Mass balance inside the macropore is described by Eq. (7)

$$\frac{\varepsilon_p}{RT}\frac{\partial \bar{P}}{\partial t}-\frac{\varepsilon_p\bar{P}}{RT^2}\frac{\partial T}{\partial t}+\rho_p\frac{\partial \bar{\bar{q}}}{\partial t}=\frac{1}{RT}\varepsilon_p k_{M2}\frac{Bi}{1+Bi}(P-\bar{P}) \qquad (7)$$

where $\bar{P}$ is the pressure inside the macropore.

The balance inside the mircropore is described by the LDF equation:

$$\frac{\partial \bar{\bar{q}}}{\partial t} = k_{m2}(q^*(\bar{P}, T) - \bar{\bar{q}}) \tag{8}$$

where k_{m2} is the micropore mass transfer coefficient.

1.3.4 Two Parameter Non-Isothermal Macro Pore Model (2 Param Non-Iso)

Two-step macro pore model used to describe the fixed-bed dynamics was derived from the mass balance by taking into account the energy balance.

The fixed-bed model is described by the following equations. The mass balance is given by Eq. (9):

$$\frac{V_{EXT}}{RT}\frac{\partial P}{\partial t} - \frac{PV_{EXT}}{RT^2}\frac{\partial T}{\partial t} + (1 - \varepsilon_b)\frac{V_b}{RT}\varepsilon_p k_{M2}\frac{Bi}{1 + Bi}(P - \bar{P}) = \dot{n} \tag{9}$$

where, V_{EXT} is the exterior volume of the adsorbent bed, k_{M2} is the macropore mass transfer coefficient.

Mass balance inside the macropore is described by Eq. (7)

The balance inside the mircropore is described by the LDF equation, Eq (8)

The energy balance is given by Eq. (5).

In all of the above four models the flow is calculated by using the valve equation. For Feed Pressurization (FP) the flow is given by Eq. (10)

$$\dot{n} = \frac{Cv_{FP}}{\sqrt{SgT_{in}}} min\left[49.08(P_{Feed} - P_{Bed})^{\frac{1}{2}}, 41.63P_{Feed}\right] \tag{10}$$

$$Sg = \frac{Mw_g}{Mw_{Air}}$$

where Cv_{FP} is the valve coefficient of valve SV-1 (Fig. 3), T_{in} is the temperature of the feed gas, P_{Feed} is the feed gas pressure, P_{Bed} is the bed pressure.

For Counter-current Depressurization (CnD) the flow is given by Eq. (11)

$$\dot{n} = \frac{Cv_{CnD}}{\sqrt{SgT_{Bed}}} min\left[49.08(P_{Bed} - P_{Vac})^{\frac{1}{2}}, 41.63P_{Feed}\right] \quad (11)$$

Where Cv_{CnD} is the valve coefficient of valve SV-4 (Fig. 3), T_{Bed} is the average temperature of the bed, P_{Vac} is the pressure of the vacuum tank.

1.4 Result and Discussion

1.4.1 Adsorption Isotherms

The experimental single component adsorption isotherms measured for CO_2, O_2, CH_4, and Ar in 13X are shown in **Figure 1.1Figure 1.2**, respectively. Data were collected at three temperatures: 25, 50, 75 °C, and pressure up to 110 kPa. We can observe in **Figure 1.2** that isotherms of O_2, CH_4 and Ar are practically linear and marked type I for CO_2 in the range of temperature and pressure studied.

1.4.2 Mass Transfer Coefficient Measurements

The zeolite adsorbents consist of small zeolite crystals formed into larger pellets or beads. The structure of these adsorbents results in two porous domains: micropores in the individual zeolite crystals and macropores comprising the intercrystalline voids. The transport of pure gases in these “bidispersed” zeolite particles can be governed by a

combination of diffusion in macropores, transport in individual zeolite crystals, and nonisothermal effects. Because of the relevantly large aperture dimension of the zeolite framework (0.74 nm) in 13X zeolite, mass transfer is expected to be fast. Onystyak et al [32] and Ahn et al [38] have reported intracrystalline diffusivities of CO_2 in type-X zeolites that are orders of magnitude greater than intracrystalline diffusivities in type-A zeolite. Which implies that the effect of intracrystalline diffusion on the dynamic response of a bidispersed 13X zeolite bead can be negligible, and the response will only be governed by either macropore diffusion, heat transfer, or a combination of the two.

Figure 1.4 shows the pressure responses of the bed of the two step adsorption-desorption experiment for CO_2 in 13X zeolite at bed temperature of 25 °C and feed pressure of 20 psia. The experiment was performed for different step times from 0.25, 0.5, 1.0, 2.0, 3.0, and 10 sec. The experimental pressure response curves have been fitted with all four models 1 param iso, 1 param non-iso, 2 param iso and 2-param non-iso macro pore model. One param isothermal model has only one macropore mass transfer coefficient and it does not take the energy balance intro account. The 2-param non-isothermal model considers the energy balance and has two parameters for macro and micropore mass transfer resistances. It is evident from **Figure 1.4** that 2-param non-isothermal model predicts the pressure response of the bed better than other models. The pressure responses of the step times 2 sec and 0.5 sec of the experiment at 25 °C and 20 psia feed pressure were fitted against the 2-param non-iso model to determine the model parameters and using these parameters the pressure responses of the other step times (1, 3, 10 and 0.25 sec) were predicted. On the other hand pressure responses of the step times 0.5, 1, 2, and 3 sec of the experiment at 25 °C and 20 psia were fitted against the 1-param iso model to determine the

model parameters and using these parameters the pressure responses of step times 10 and 0.25 sec were predicted. The model parameters are listed in **Table 1.5**. The mass balance for different step times of the CO_2 experiment performed at 25 °C and at feed pressure of 20 psia are listed in **Table 1.6**. **Table 1.6** shows the total amount of CO_2 (in ml, STP) entering and leaving the bed per cycle averaged over 5 cycles for step times 3, 2, 1, 0.5 and 0.25 sec and averaged over 2 cycles for step time 10 sec. From this table we can see that the mass balance for CO_2 was closed with negligible error. The experimental flow in and out along with the model prediction was shown in **Figure 1.5**. The amount of CO_2 entering or leaving were calculated by calculating the area under the respective curve. The cyclic experiment with CO_2 was also performed at three different temperatures, 25. 50 and 75 °C at constant feed pressure of 8 psia. For each experimental condition, the pressure response curves of step times, 0.25 and 2 sec were fitted against the 2-param non-iso model to determine the model parameters. Using the determined parameters the pressure response curves for the other step times were predicted, in **Figure 1.6** pressure response curves along with model prediction are shown for all temperatures. All parameters for CO_2 are summarized in **Table 1.5**. In order to determine the goodness of the fit the value of R^2 was calculated and tabulated in **Table 1.7**. The values of R^2 for the 2-step MPM indicates the better fit than the 1-step MPM. In **Figure 1.7** the effective macropore mass transfer coefficient corrected by the slope of the isotherm has been plotted as a function of the cycle number (cycle number is defined as the dimensionless time, time/cycle time) along with the micropore mass transfer coefficient. From **Figure 1.7**, we can see that the transport of CO_2 in 13X zeolite is macropore limited.

Same set of cyclic experiments were performed for N_2 in 13X. The pressure response of the step times 2 sec and 0.5 sec of the experiment performed at 25 °C and 20 psia feed pressure were fitted against the 2-param non-iso model and 1-param iso model. The estimated model parameters are listed in **Table 1.8**. Due to the liner isotherm of nitrogen, we get a number of solution for a number of different values for the macropore (k_{M2}) and micropore mass transfer coefficient (k_{m2}). The values of the parameter for 1-param iso and 2-param non-iso models along with the R^2 values are listed in **Table 1.9**. In **Figure 1.8** the 1-param iso and three different solution for 2-param non-iso models were plotted against the experimental results. From **Figure 1.8**, we see that we can barely distinguish three different solutions of the 2-param non-iso model. From **Table 1.9** we can see that the R^2 values for 1-param iso model are better than those of the 2-param non-iso model. Which implies that a very simple 1-param iso model can explain the mass transfer of N_2 in 13X zeolite. In **Figure 1.9** both 1-param iso and 2-parm non-iso models predictions were plotted against the experimental pressure responses of the experiment performed at 25 °C and 20 psia feed pressure. In **Table 1.9** the R^2 values for both models were calculated in listed for all experimental conditions. It is evident that 1-param iso model is good enough to predict the experimental pressure responses in all the experimental conditions.

The cyclic experiments for O_2, CH_4, and Ar were performed for three different temperatures 25, 50, and 75 °C for step times 10, 3, 2, 1, 0.5, and 0.25 sec. The 1-param iso model was sufficient to predict the pressure responses of all these gases in 13X zeolite. The 1-param iso model parameters for all the gases for three different temperatures are listed in **Table 1.10**. The macropore mass transfer coefficient corrected by the slope of the

isotherm has been plotted as a function of cycle number for 20 and 2 psia feed pressure in Figure 10. The transport in 13X zeolite follows the order $O_2 > Ar > N_2 > CH_4 > CO_2$.

1.5 Conclusion

A detailed study of diffusion mechanism of CO_2, N_2, O_2, CH_4, and Ar in zeolite 13X beads was carried out. The main goal of this study was the understanding the gas transport process in a commercial beads such as zeolite 13X in rapid cycles. We performed the experiments in order of the step times as small as 0.25 sec and determined the mass transfer coefficient to describe the transport process at that fast cycle. The experiment covered a wide range or temperatures and partial pressures of the feed.

The transport process of CO_2 in zeolite 13X was found to be governed by the macropore resistance, which is consistent with the previous studies, found in literature. A simple 1-parameter isothermal macropore model could explain the transport process of N_2, O_2, CH_4 and Ar all.

The mass transfer parameters obtained in this study can be used in any simulator to simulate any adsorption process.

1.6 Tables

Table 1.1: Three process Langmuir isotherm parameters for all gases.

Parameter	CO_2	N_2	O_2	CH_4	Ar
qs1 (mol/kg)	1.34	3.65	0.37	3.26	0.54
qs2 (mole/kg)	2.24	1.16	0.39	2.73	0.29
qs3 (mole/kg)	1.85	0	0	0	0
b01 (1/kPa)	2.44e-08	5.43e-07	7.31e-06	7.74e-07	7.00e-06
b02 (1/kPa)	4.52e-08	5.15e-07	5.16e-07	8.01e-07	1.39e-06
b03 (1/kPa)	1.37e-08	0	0	0	0
B21 (K)	5757.03	1732.42	1725.45	2085.68	1639.64
B22 (K)	4606.08	2559.38	2157.83	2177.85	1766.64
B23 (K)	4244.86	0	0	0	0

Table 1.2: The heat of adsorption of all gases.

Gas	Heat of Adsorption [kJ/mol]
CO_2	39.33
N_2	19.54
CH_4	17.85
O_2	15.33
Ar	13.55

Table 1.3: Mass balance for He cyclic experiments at 25 °C bed temperature and 20 psia feed pressure. The table shows the total amount of He entering and leaving the bed per cycle averaged over 5 cycles.

Step Time (sec)	Flow in (Exp) (ml, STP)	Flow out (Exp) (ml, STP)	Flow in (2 Param Non-Iso) (ml, STP)	Flow out (2 Param Non-Iso) (ml, STP)
3.00	215.21	226.88	209.67	191.91
2.00	207.64	212.82	206.29	196.24
1.00	189.08	186.93	194.45	189.81
0.25	160.86	155.32	172.49	172.76

Table 1.4: Properties of the adsorbent bed packed with 13X zeolite.

Parameter	Value
Mass of adsorbent (m)	73.2 g
Pellet Density (ρ_p)*	1110 g/cc
Adsorbent volume (V_P)	0.066 L
Total Empty Volume (V_T)	0.219 L
Excluded Volume (V_{EX})	0.186 L
Skeletal Volume ($V_S = V_T - V_{EX}$)	0.033 L
Pellet Porosity (ε_P)	0.500
Bed Porosity (ε_b)*	0.350
External Volume ($V_{EXT} = V_T - V_P$)	0.153 L
Column Length (L)	0.192 m
Bed Inside Diameter (ID)	0.032 m
Bed Inside Diameter (ID)	0.032 m
Bed Packed Length (L_b)	0.126 m
Headers (L_H)	0.033 m

Table 1.5: Optimum parameters the 1 step and 2 step macropore model (MPM) of CO_2 on 13X

Model	Temperature, °C	k_{M1}	k_{M2}	k_{m2}
1 Step MPM	25	47.21	47.21	-
2 Step MPM	25	-	207.41	2.96
	50	-	203.14	8.35
	75	-	203.13	8.74
2 Step MPM	All	-	200.00	8.75

Table 1.6: Mass balance for CO_2 cyclic experiments at 25°C bed temperature and 20 psia feed pressure. The table shows the total amount of CO_2 entering and leaving the bed per cycle averaged over 5 cycles for step times 10.00, 3.00, 2.00, 1.00, 0.50, 0.25 sec and averaged over 2 cycles for step time 10 sec.

Step Time (sec)	Flow in (Exp) (ml, STP)	Flow out (Exp) (ml, STP)	Flow in (2 Step MPM) (ml, STP)	Flow out (2 Step MPM) (ml, STP)
10.00	817.65	795.87	889.04	919.33
3.00	368.80	342.20	382.53	385.70
2.00	263.08	243.32	272.73	275.16
1.00	141.36	131.14	145.65	147.41
0.50	73.21	68.24	66.11	78.89
0.25	31.96	30.10	32.40	34.37

Table 1.7: Coefficient of determination (R^2) for CO_2 cyclic experiments in 13X at different experimental conditions.

Temperature (°C)	Feed Pressure (PSIA)	Step Time (sec)	R^2 Model – 1[(b)] (1 Step MPM)	R^2 Model – 2[(a), (b)] (2 Step MPM)
25	20	10.00	0.916	0.991
		3.00	0.875	0.995
		2.00	0.906	0.994
		1.00	0.912	0.988
		0.50	0.881	0.979
		0.25	0.869	0.912
	8	10.00		0.946
		3.00		0.917
		2.00		0.896
		1.00		0.763
		0.50		0.683
		0.25		0.524
	2	10.00		0.683
		3.00		0.512
		2.00		0.476
		1.00		0.469
		0.50		0.330
50	8	10.00		0.949
		3.00		0.838
		2.00		0.798
		1.00		0.629
		0.50		0.507
		0.25		0.336
75	8	10.00		0.949
		3.00		0.815
		2.00		0.770
		1.00		0.600
		0.50		0.673
		0.25		0.698

[(a)] R^2 calculated using the experimental data. $R^2 = 1 - \frac{\Sigma(x-x_{exp})^2}{\Sigma(x-x_{bar})^2}$ where, $x_{bar} = \frac{\Sigma x_{exp}}{\Sigma n}$

[(b)] Values of k_{M1}, k_{M2}, k_{m2} are based on data given in **Table 1.5**

Table 1.8: A series of solutions for different combination of k_{m2} and k_{M2} for nitrogen at bed temperature of 25 °C and feed pressure of 20 psia.

Model	k_{M1}	k_{m2}	k_{M2}	Step Time (s)	R^2
2 Step MPM	-	60	104.14	2.0	0.994
				0.5	0.987
	-	40	110.02	2.0	0.994
				0.5	0.987
	-	20	132.44	2.0	0.994
				0.5	0.988
1 Step MPM	70.34	-	-	2.0	0.997
				0.5	0.992

Table 1.9: Coefficient of determination (R^2) for N_2 cyclic experiments in 13X zeolite at different experimental conditions for 2 Parameter Non-Isothermal model parameters k_{m2} = 60 and k_{M2} = 101.7.

Temperature (°C)	Feed Pressure (PSIA)	Step Time (sec)	R^2 Model – 1[(a), (b)] (1 Step MPM)	R^2 Model – 2[(a), (b)] (2 Step MPM)
25	20	10.00	0.998	0.997
		3.00	0.997	0.994
		2.00	0.996	0.994
		1.00	0.993	0.989
		0.50	0.992	0.987
		0.25	0.993	0.948
	2	10.00	0.980	0.981
		3.00	0.971	0.980
		2.00	0.956	0.972
		1.00	0.904	0.923
		0.50	0.849	0.865
		0.25	0.931	0.935
	40	10.00	0.999	0.996
		3.00	0.996	0.994
		2.00	0.996	0.993
		1.00	0.997	0.989
		0.50	0.999	0.983
		0.25	0.999	0.960
50	20	10.00	0.999	0.991
		3.00	0.996	0.992
		2.00	0.995	0.991
		1.00	0.998	0.995
		0.50	0.996	0.995
		0.25	0.998	0.978
75	20	10.00	0.999	0.991
		3.00	0.996	0.995
		2.00	0.996	0.993
		1.00	0.997	0.993
		0.50	0.999	0.998
		0.25	0.999	0.993

[(a)] R^2 calculated using the experimental data. $R^2 = 1 - \frac{\sum(x - x_{exp})^2}{\sum(x - x_{bar})^2}$ where, $x_{bar} = \frac{\sum x_{exp}}{\sum n}$

[(b)] Values of k_{M1}, k_{M2}, k_{m2} are based on data given in **Table 1.8**

Table 1.10: Optimum model parameters for both 1 Parameter Isothermal model and 2 Parameter Non-Isothermal model at three different temperatures for nitrogen, oxygen, methane and argon in 13X zeolite.

Gas	Temperature (°C)	k_{M1} (sec^{-1})	k_{M2}^{*} (sec^{-1})
N_2	25	70.34	104.14
	50	69.73	107.09
	75	67.67	98.72
O_2	25	46.89	72.53
	50	38.28	59.06
	75	39.80	58.98
CH_4	25	84.79	129.37
	50	81.52	114.66
	75	86.90	113.17
Ar	25	43.24	69.77
	50	34.34	44.58
	75	30.80	38.27

*Parameter for the 2 Parameter Non-Isothermal model by setting $k_{m2} = 60\ sec^{-1}$

1.7 Figures

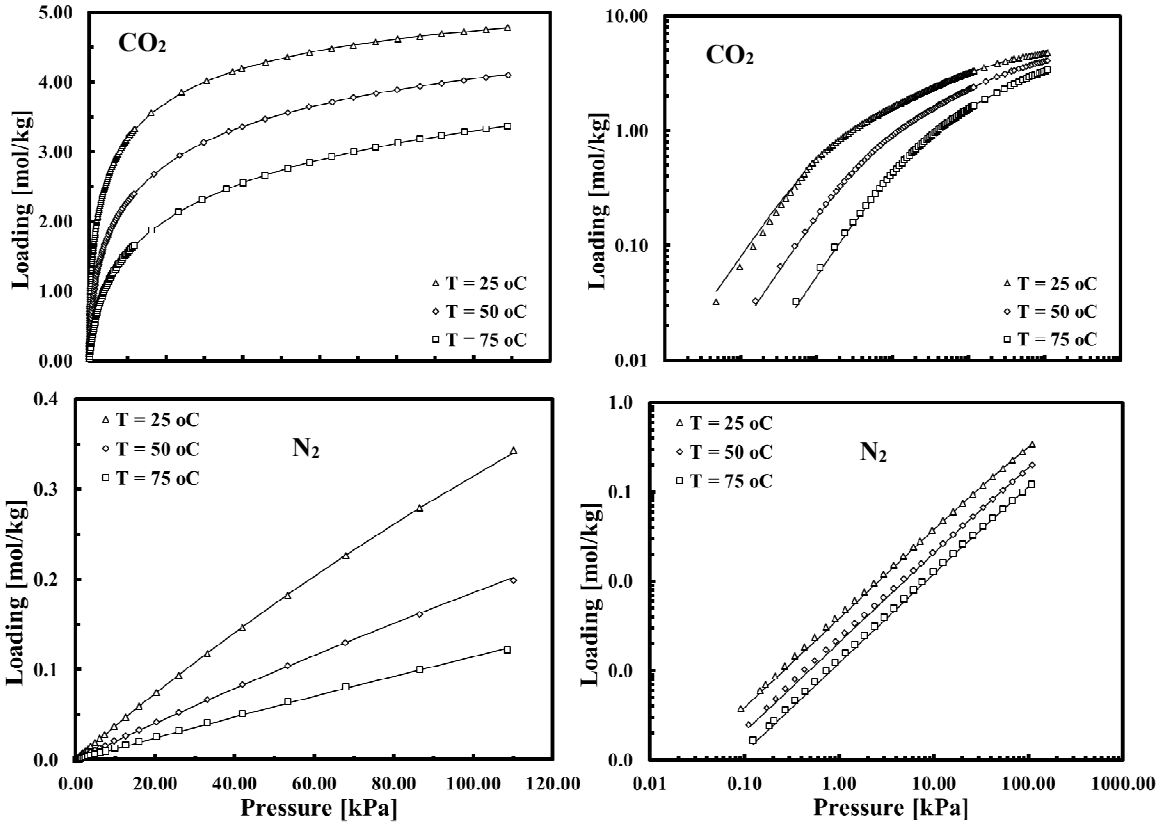

Figure 1.1: Isotherm of Carbon dioxide and Nitrogen at three different temperatures. The solid lines represent the model fits and the markers represent the experimental data. Curves on the RHS are the same curves shown on the LHS but in log –log scale.

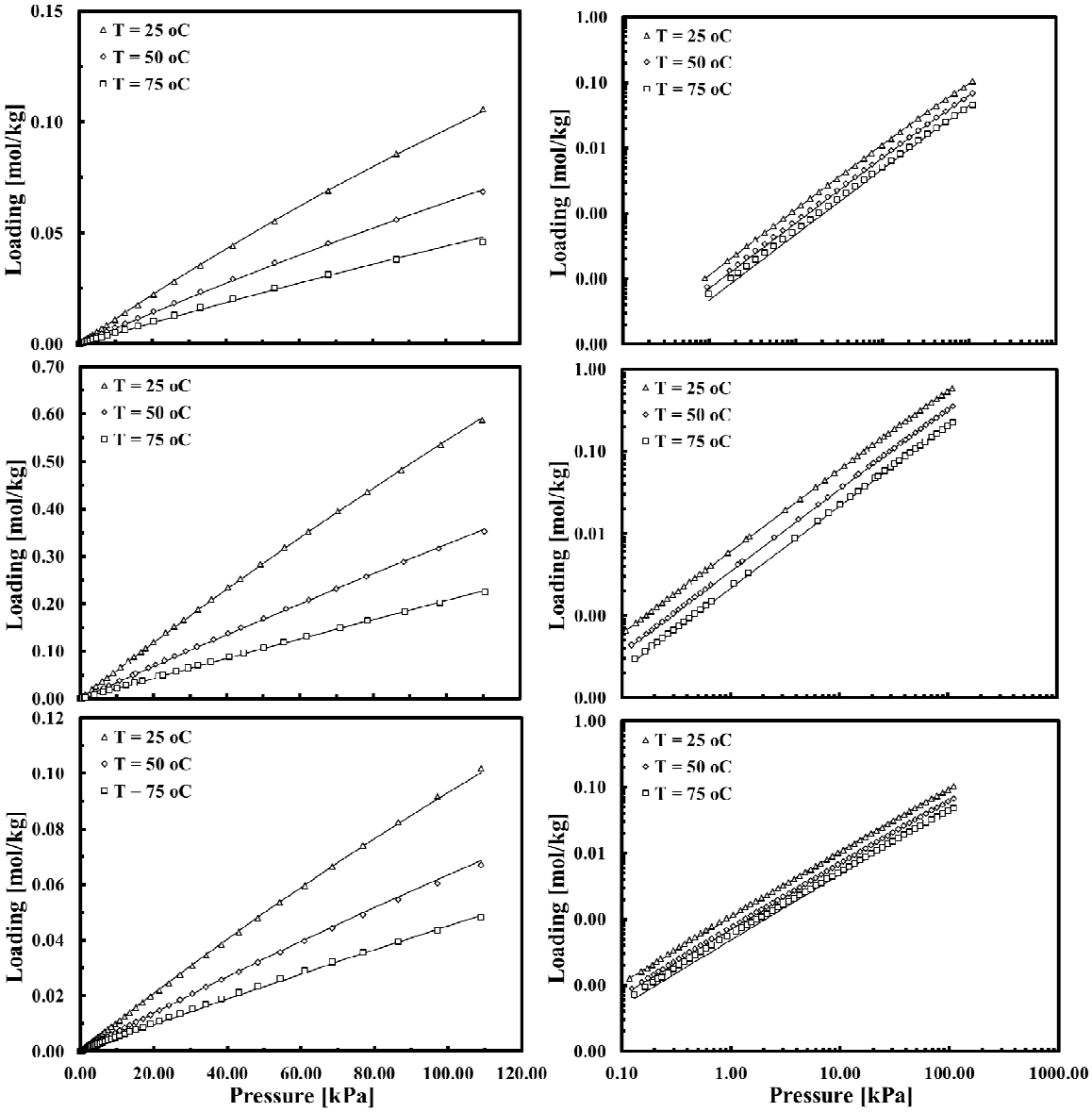

Figure 1.2 Isotherm of oxygen, methane and argon at three different temperatures. The solid lines represent the model fits and the markers represent the experimental data. Curves on the RHS are the same curves shown on the LHS but in log –log scale.

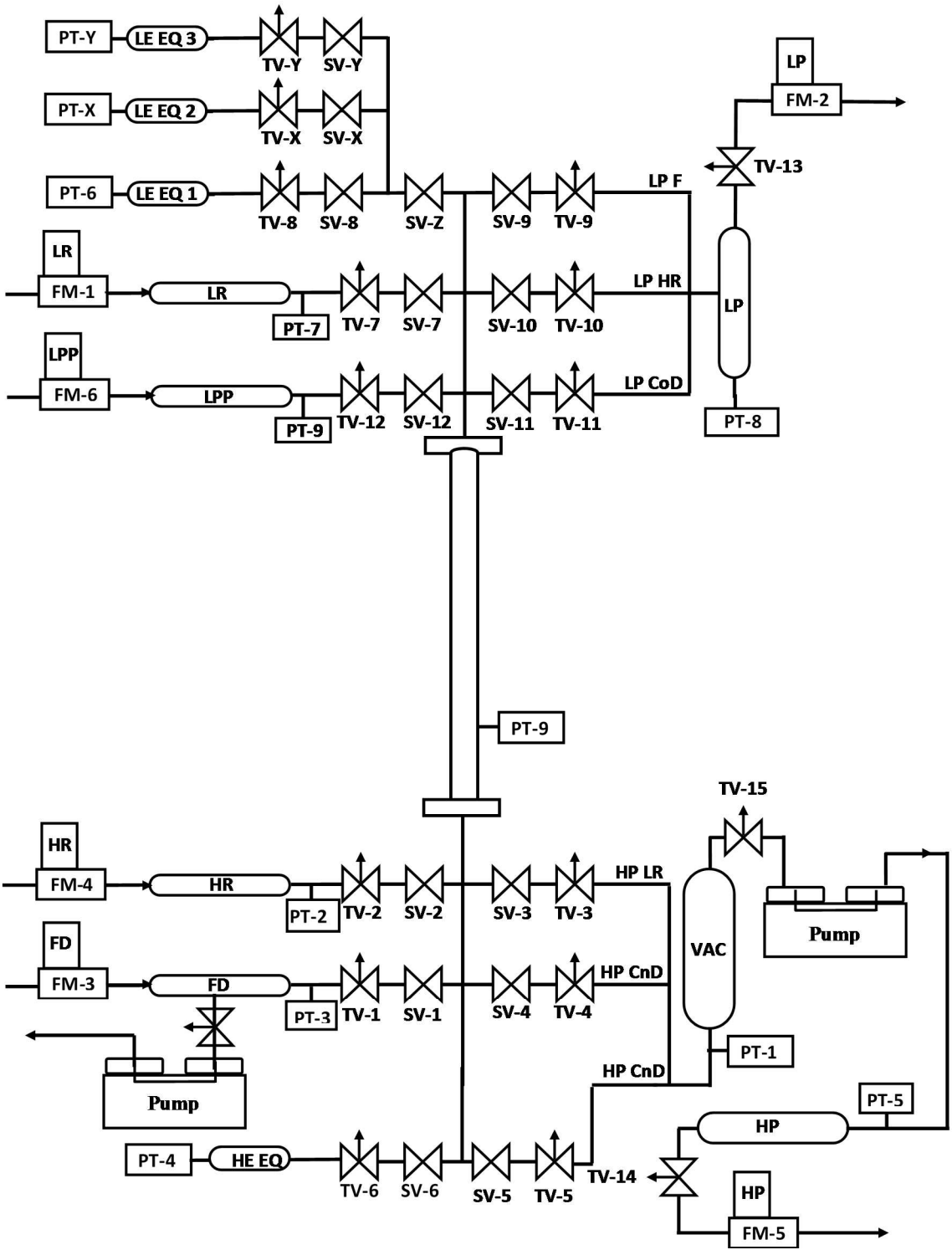

Figure 1.3: The schematic diagram of single bed rapid pressure swing (RPSA) apparatus.

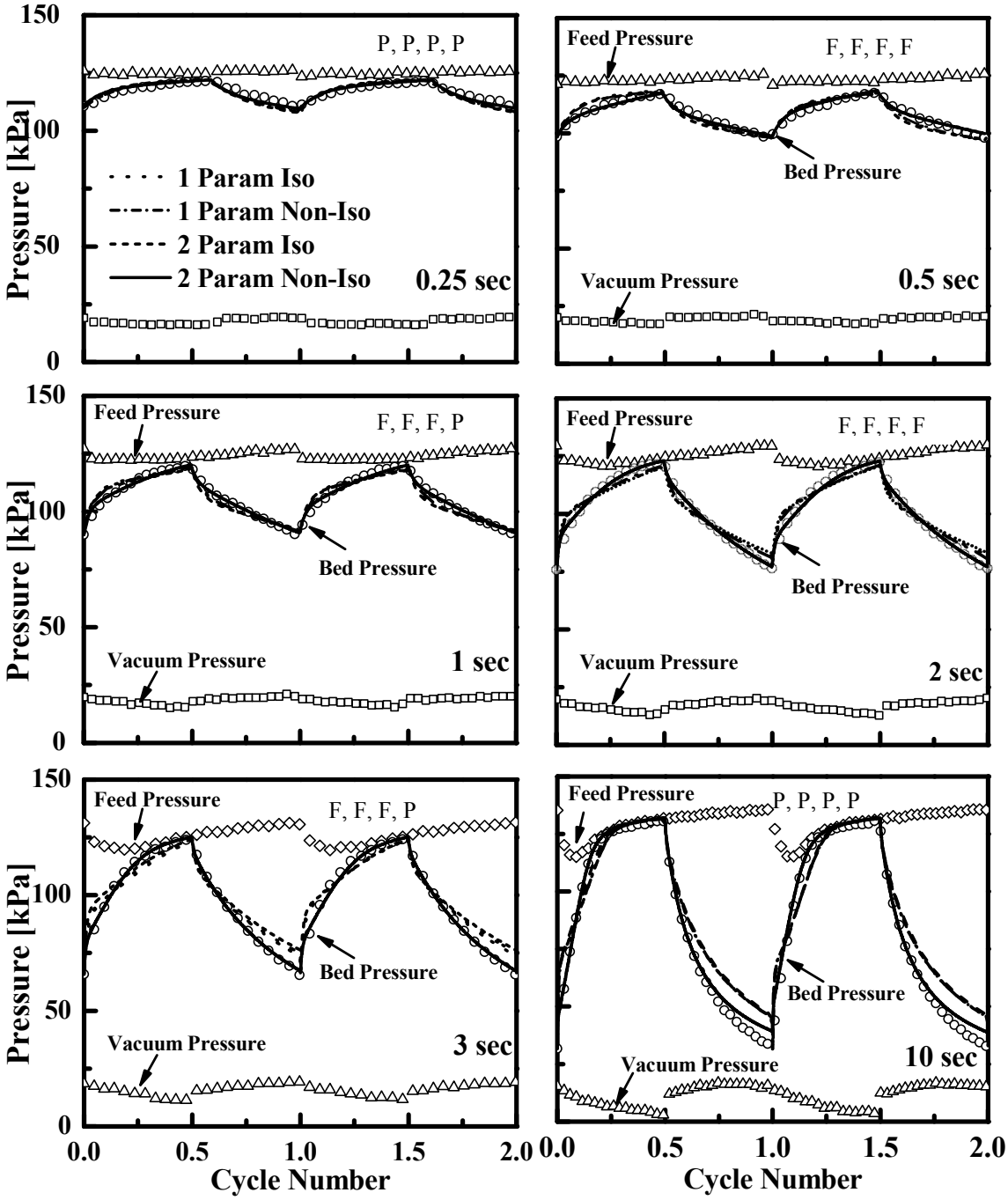

Figure 1.4: Pressure history of the adsorbent bed in the cyclic experiments of CO_2 in at bed temperature of 25 °C and feed pressure of 20 psia at different step times was fitted with both 1 step and 2 step macro pore models (MPM). Symbols represent the experimental data, the solid line represents the 2 step MPM and dashed line represents the 1 step MPM.

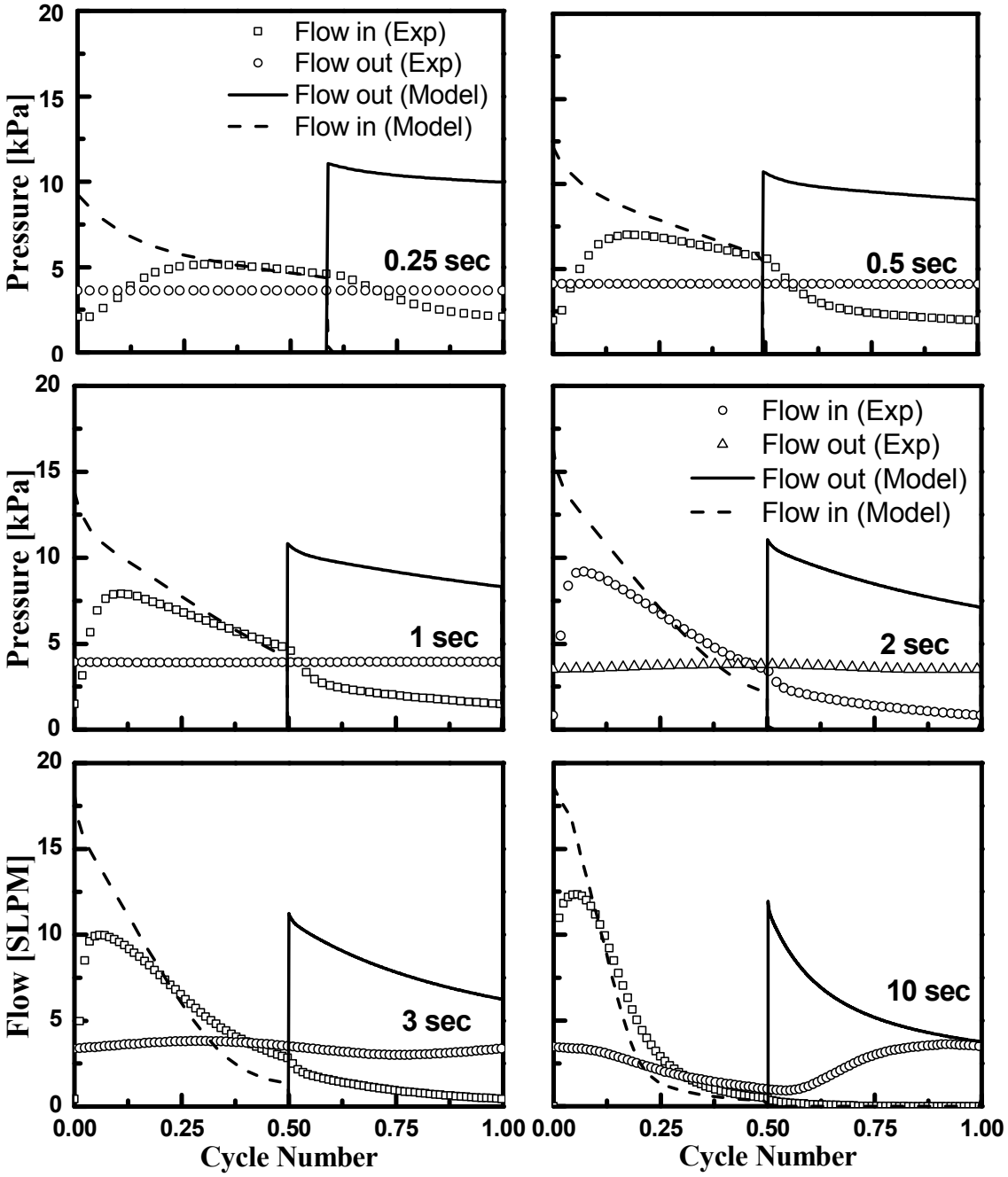

Figure 1.5: Experimental flow in and out of the bed was plotted with the model (2 Step MPM) flow in and out of the bed per cycle for the CO_2 cyclic experiments at 25 °C and 20 psia.

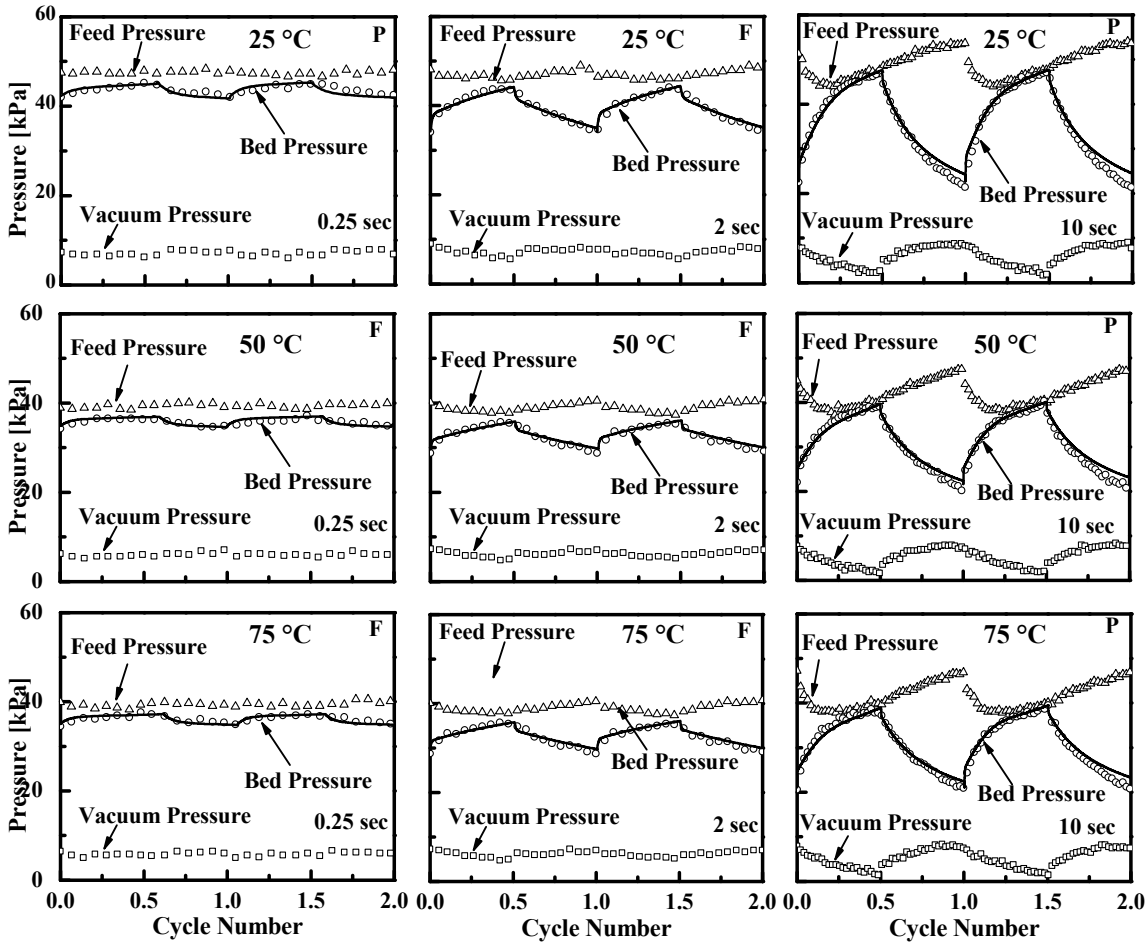

Figure 1.6: Pressure history of the adsorbent bed in the cyclic experiments of CO_2 at bed temperatures of 25, 50 and 75 °C and feed pressure of 8 psia at different step times was fitted with 2 step MPM model. Symbols represent the experimental data; the solid line represents the prediction of the 2-step MPM model.

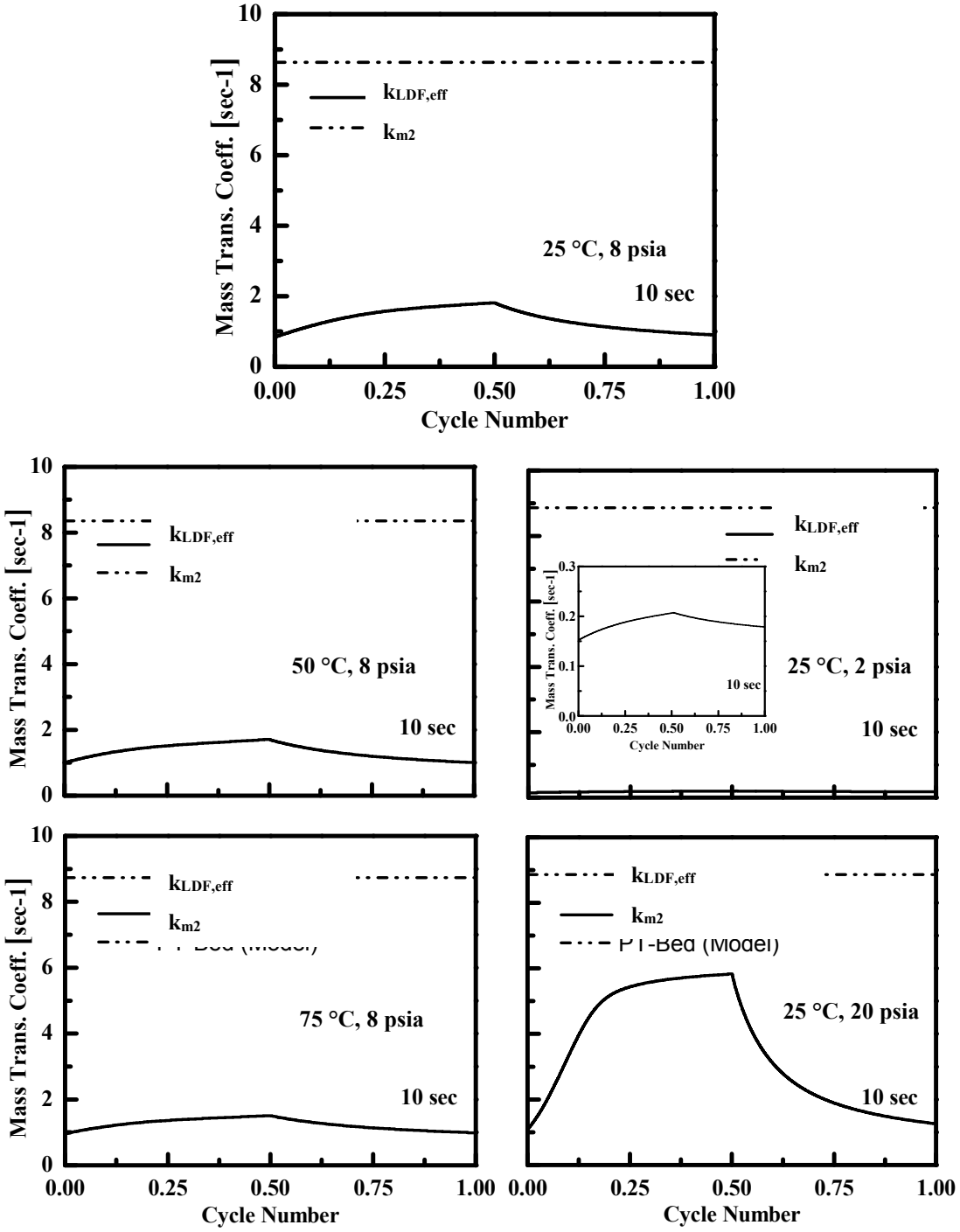

Figure 1.7: Plot of $k_{LDF,eff}$ and k_{m2} as a function of cycle time at three different bed temperatures and feed pressure of 8 psia for the cyclic experiments of CO_2 in 13X zeolite.

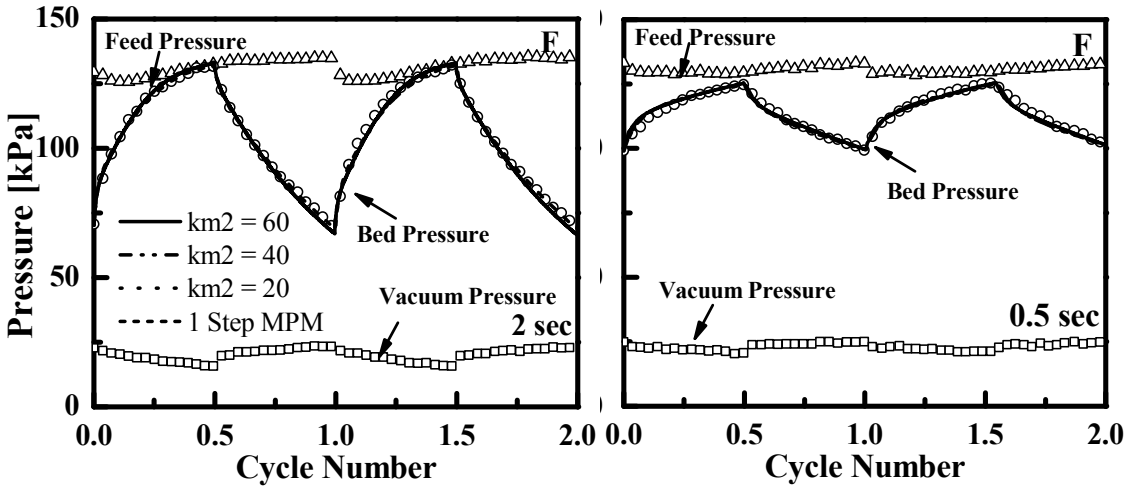

Figure 1.8: Pressure history of N_2 cyclic experiments in 13X at bed temperature of 25 °C and feed pressure of 20 psia was fitted the 2 Step MPM model for different values of k_{m2} = 20, 40, and 60.

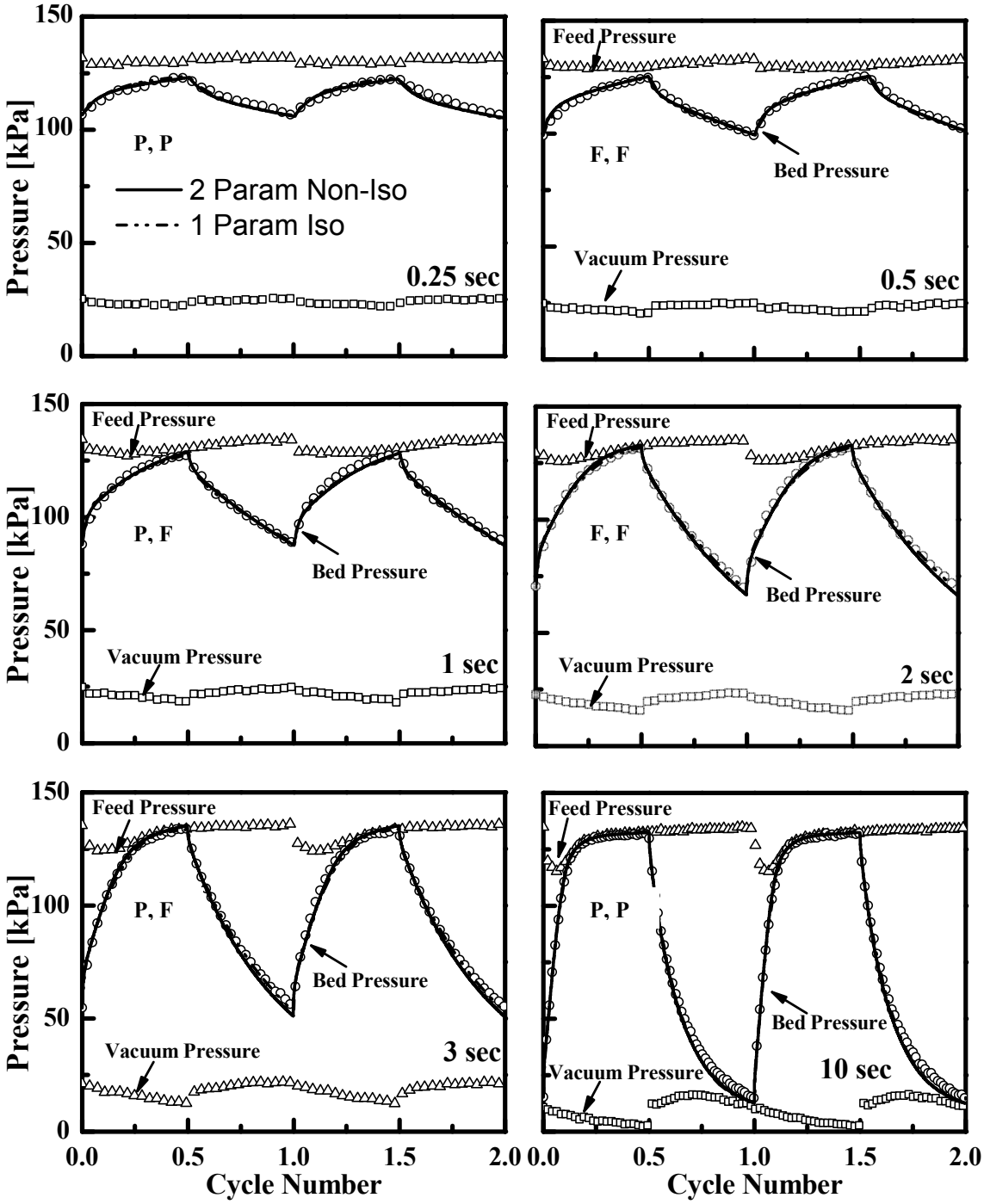

Figure 1.9: Pressure history of the adsorbent bed in the cyclic experiments of N_2 at bed temperature of 25 °C and feed pressure of 20 psia at different step times was fitted with both 1 Param Isothermal and 2 Parameter Non-isothermal models. Symbols represent the experimental data, the solid line represents the 2 Parameter Non-Isothermal and dashed line represents the 1 Parameter Isothermal.

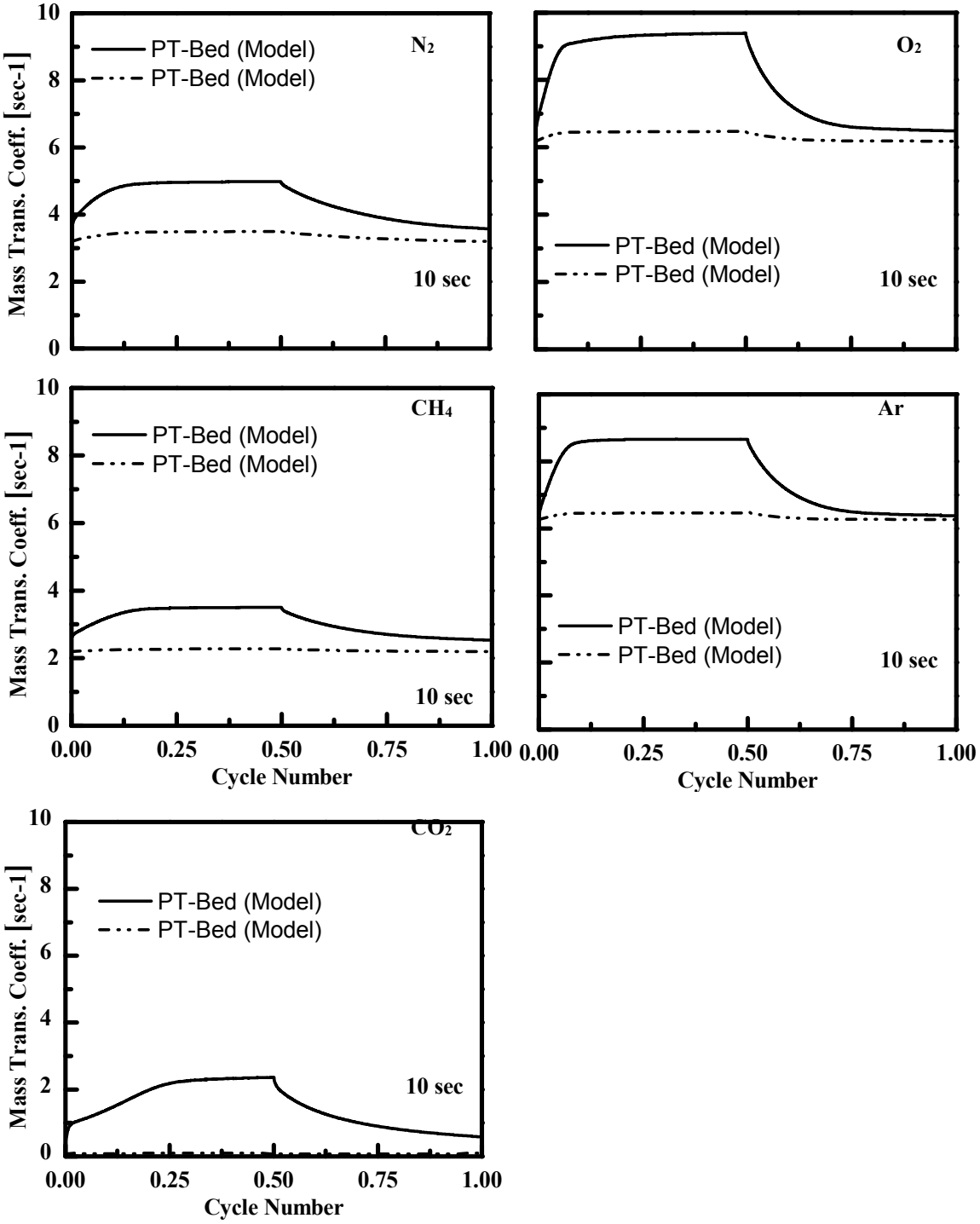

Figure 1.10: Mass transfer plots for nitrogen, oxygen, methane and argon at bed temperature of 25 °C and at two different feed pressures.

CHAPTER 2

DEVELOPMENT OF A PRESSURE SWING ADSORPTION (PSA) CYCLE FOR CO_2 CAPTURE FROM FLUE GAS USING A 1-BED PSA APPARATUS: EXPERIMENT AND MODEL VALIDATION

2.1 Introduction

It is widely accepted that the major cause for global warming is the increase in CO_2 concentration in the earth's atmosphere due to anthropogenic activities. Due to the effect of CO_2 on global warming, the CO_2 emission is becoming an increasingly serious issue. Major sources of CO_2 emissions into the atmosphere is through the burning of fossil fuels for energy. It is reported that about 85% of the world commercial energy is produced by burning coal, oil and gas. Department of Energy (DOE) has reported that about 40% of the total CO_2 emissions come from all coal-fired power plants [44]. These coal-fired power plants presents large point sources for CO_2 emissions and considerable effort has been underway worldwide to curb CO_2 emissions from these large point sources. There are several options available to reduce the CO_2 emissions from these sources. The best long term solution is to completely substitute fossil fuels with renewable sources of energy. However, a report published by DOE has shown that coal will still supply 28% of the worlds energy demand [44]. Therefore, the short term solution CO_2 and storage. This can be achieved by retrofitting existing plants with a CO_2 capture process. Typically the post combustion flue gas from a coal-fired power plant contains about 12-15% CO_2

at atmospheric pressure and the capture plant is expected to concentrate it to around 90 to 95% and sequester it underground [44].

There are several technologies available to separate CO_2 such as absorption, cryogenic distillation, adsorption, and membrane separation. The most commonly used technology for post combustion carbon capture is absorption using amine-based liquid solvents [45, 46]. However, this technology is too energy intensive due to the high energy demand for solvent regeneration [47]. The amine absorption process takes out a portion of the process steam of the power plant reducing the overall capacity of the power plant. Therefore, alternative technologies with lower energy penalty are being explored and adsorption is one of the promising alternatives [1, 46-49]. However, to date none of the technologies is economically feasible; so, significant research effort is being undergoing to come up with an economically feasible process to capture CO_2.

An article published by the International Energy Agency (IEA) in 1994, focused the use of adsorption technologies for CO_2 capture from flue gases on the basis of 500 MW power plant [50]. Both pressure swing adsorption (PSA) and temperature swing adsorption (TSA) were evaluated used a commercial adsorbent 13X zeolite. At that time the study clouded that both PSA and TSA were too energy intensive and not feasible for CO_2 capture from power plants. In 2003 another report by IEA reiterated the same results [51]. However Webley and co-workers questioned findings of both report in one of their work [52]. This work reevaluated the PSA process by calculating the energy consumption by a PSA process for CO_2 capture to be \$67/tonne CO_2 captured compared to \$97/tonne CO_2 captured as reported by IEA. This new energy consumption value of PSA compare much more

favorably to the energy consumption by the amine absorption process at \$60/tonne CO_2. The cost of PSA can be brought down significantly by proper design of the PSA cycle.

Adsorption-based processes for gas separation have been widely practiced in the industries for applications like air separation [53, 54], hydrogen purification [55, 56], hydrocarbon separation [57], and air drying [58]. Ritter et al investigated several PSA/VSA cycle specific to CO_2 capture [22]. Ishibashi et al published an article on experimental study on capture of CO_2 from a power plant flue gas with Ca-X zeolite in a two stage-process in a pilot plant [24].

Designing an adsorption-based process is very challenging and increasing development of mathematical models in the literature facilitated the model-based process design. The availability of infinite possible configurations, cycle schedules, adsorbent materials, and recycle streams make the process development very complex, and the use of a suitable model is required to assess the process performance early during the process development [59]. The reliability of a given model depends highly on the many physical parameters which are specific to the system and operating conditions. General practice to determine these parameters, the equilibrium adsorption isotherm is usually independently measured using a volumetric or gravimetric method, and the kinetic information is obtained by a fixed-bed breakthrough experiments [60-66]. Although valuable information is obtained through breakthrough experiments and these information is essential to model a full pressure swing adsorption (PSA) cycles, actual PSA adsorption process involves wide range of conditions in their different steps. So the developed model must be tested rigorously in order to have full confidence in it. Therefore, it is very important to validate

the model by comparing between experimental results of full PSA cycles and simulation results. And validation of the model is the prerequisite for its use for process development.

In this work, several PSA experiments were performed in a fully automated 1-bed PSA apparatus by changing different process parameters to cover a wide range of process conditions. The experiments two different bed temperatures, namely 70 °C and 100 °C, two different desorption (counter current depressurization) pressures, namely, 5 kPa, and 7 kPa, two different purge to reflux ratio 3% and 4%. Two different cycle times were used 720 sec and 380 sec. The adsorption pressure, i.e., the pressure during the feed step was always the same 120 kPa. The PSA cycle consists of the following steps: feed (F), heavy reflux (HR), equalization (Eq), counter-current depressurization (CnD), light reflux (LR), light product pressurization (LPP). Seven thermocouples were placed across the length of the bed to monitor the temperature profiles of the bed during each experiments and the compositions were measured by an inline mass spectrometer (MS). The main purpose of these experiments were to validate the in house dynamic process simulator (DAPS) for various process conditions. The equilibrium isotherm data for the single gas used in the process simulator were measured independently using a Micromeritics ASAP 2010. The mass transfer coefficient was determined using a rapid pressure swing apparatus. A non-isothermal one transport mass transfer model was used which only considers the macropore resistances. I this work, pressure and temperature profiles of the bed along with the process performance in terms of purity and recovery of CO2 determined experimentally were compared with simulations results. Therefore, the validation of DAPS in the context of a complete PSA process was done.

2.2 Mathematical Model

Simulations of the PSA cycles were carried out using an in house dynamic adsorption process simulator (DAPS) developed in FORTRAN that uses the finite difference method and the time adaptive DAE solver called DASPK (**Brown et al., 1994**). The following assumptions are imposed: the ideal gas law, plug flow, no heat transfer limitations between gas and solid (i.e., pellet) phases, no thermal capacitive role of the wall, no axial mass and thermal dispersion, the gas phase concentration in both bulk and pellet porosity is identical, and the mass transfer between solid and gas is defined by 1 parameter macropore limited non-isothermal model. Temperature of the wall set at a constant value equal to the temperature of the bed and heat loss to the exterior defined by heat transfer at the inner side of the wall.

For an N-component PSA process, the overall (O.M.B.) and component mass balances (C.M.B.) over a differential volume element respectively yields.

$$\left(\varepsilon_b + (1-\varepsilon_b)\varepsilon_P\right)C_T\left(\frac{1}{P}\frac{\partial P}{\partial t} - \frac{1}{T}\frac{\partial T}{\partial t}\right) + \varepsilon_b \frac{\partial v C_T}{\partial z} + \sum_{j=1}^{n} S_j = 0 \qquad (1)$$

$$\left(\varepsilon_b + (1-\varepsilon_b)\varepsilon_P\right)C_T \frac{\partial y_i}{\partial t} + \varepsilon_b C_T v \frac{\partial y_i}{\partial z} - y_i \sum_{j=1}^{n} S_j + S_i = 0 \qquad i = 1 \text{ to } N\text{-}1$$

(2a)

$$y_i + \sum_{j=1, j\neq i}^{n} y_j = 0 \qquad i = N \quad (2b)$$

with

$$C_T = \frac{P}{RT};\ S_i = (1-\varepsilon_b)\rho_P \frac{\partial q_i}{\partial t}$$

Where ε_p and ρ_p are the pellet porosity and density, respectively, ε_b is bulk porosity, v is the interstitial velocity, y_i is the molar fraction of species i in the gas phase, T is the temperature of both gas and solid phases, P is the pressure and q_i is loading of species i in the solid phase, R is the universal gas constant.

To determine the mass transfer rate for the particle for each gas one parameter non-isothermal macro pore model was used [Ref mass transfer paper]. The mass transfer of species i between the solid and gas phase is defined given by Eq. (3) (M.T.M.):

$$\frac{dq_i}{dt} = k_{M,eff}(q_i^*(P,T) - q_i) \tag{3}$$

where $k_{M,eff}$ is the overall effective macropore mass transfer coefficient, q_i^* is the adsorbed equilibrium concentration, i.e., $q_i^* = f(P,T)$ given by the isotherm and q_i is the average adsorbed concentration.

The overall effective macropore mass transfer coefficient is given by Ep. (5)

$$k_{M,eff} = \frac{1}{1 + \frac{RT\rho_p}{\varepsilon_p}\frac{\partial q^*}{\partial P}_{T,P_i}} k_M \tag{4}$$

Where ρ_P is the particle density, ε_P is the particle porosity, $\frac{\partial q^*}{\partial P}_{T,\bar{P}}$ is the slope of the isotherm, k_M macorpore mass transfer parameter. The fitting parameter for this model is k_M.

The equilibrium loading of component i, q_i^* is calculated from the Three Process Langmuir isotherm:

$$q_i^* = \sum_{k=1}^{3} \frac{b_{i,k} P_i q_{i,k,s}}{1 + \sum_{j=1}^{n} \left(b_{j,k} P_j \right)}$$

where $b_{i,k} = b_{i,k,o} \exp\left(\frac{B_{i,k}}{T} \right)$ and $q_{i,k,s} = q_{i,k,s}^* + q_{i,k,st} * T$ [k = 1 to 3]

where q_i^* is the total loading of component i in mol/kg, n is the number of components, $q_{i,k,s}$ is the saturation loadings of component i in mol/kg on sites k, P_i is the partial pressure of component I, T is the temperature in K.

The energy balance (E.B.) is expressed as

$$\left(\varepsilon_b + (1-\varepsilon_b)\varepsilon_P\right)\left(Cp_g C_T \frac{\partial T}{\partial t} - \frac{\partial P}{\partial t} \right) + \left((1-\varepsilon_b)\rho_P Cp_p\right)\frac{\partial T}{\partial t} + \varepsilon_b Cp_g C_T v \frac{\partial T}{\partial z} +$$

$$(1-\varepsilon_b)\rho_P \sum_{j=1}^{n}\left(Cp_{a,j} q_j \frac{\partial T}{\partial t} + \Delta H_i \frac{\partial q_i}{\partial t} \right) + \frac{2}{r_{b,i}} h_w (T - T_w) = 0 \qquad (5)$$

with

$$Cp_g = \sum_{i=1}^{n} \left(y_j Cp_{g,i} \right)$$

where $Cp_{g,i}$ and $Cp_{a,j}$ are the molar heat capacities of species i in the gas and adsorbed phase, respectively (typically assumed identical), Cp_p is the heat capacity of the pellet, ΔH_i is the heat of adsorption of species i, h_w is the heat transfer coefficient at the

inner side of the wall of the bed and r_i is the internal radius of the bed and T_w is the wall temperature.

The pressure drop along the bed is evaluated via Ergun's equation, i.e. the momentum balance (E.B.):

$$\frac{\partial P}{\partial z} + 1.5\times10^{-1}\mu_g\left(\frac{1-\varepsilon_b}{2r_p\varepsilon_b}\right)^2 v + 1.75\times10^{-3}C_T M_g \frac{1-\varepsilon_b}{2r_p\varepsilon_b} v|v| = 0 \qquad (6)$$

where μ_g and M_g are the viscosity and the average molecular weight of the gas phase and r_p is the effective radius of the pellet.

At given boundaries the flow rate (F) whether it's goes in or out of the bed is defined according to the valve equation (V.E.), which is defined according to Eq (10):

$$F = C_v v_{sign} \frac{1}{\sqrt{S_g T_-}} min(49.08|P_-^2 - P_+^2|^{0.5}, 41.63P_-) \qquad (7)$$

where c_v is the valve coefficient, S_g is the molecular weight of the gas relative to that of air, P_- and P_+ is the pressure upstream and downstream the valve, T_- is the temperature upstream the valve.

The equations described above constitute a complete mathematical model for multi-component pressure swing adsorption process once the initial and boundary conditions for particular steps are specified. For a system containing N components, there are a total of 2N+3 variables and equations that have to be solved at each node.

The initial and boundary conditions depends on the PSA process cycle configuration used. The initial and boundary conditions for different steps are given in **Table 2.2**:

2.3 Experimental Section

2.3.1 Adsorption Isotherm Measurement

Pure component adsorption equilibrium isotherms for CO_2 and N_2, on zeolite 13X were measured by using a volumetric system from micromeritics ASAP2010. Since ASAP-2010 is designed for surface area and porosimetry measurements and measures the nitrogen isotherm at 77 K it had to be modified to be able to measure different pure gas isotherms at various temperatures. Operation pressure range provided by this system is from 0 to 127 KPa. The molecular drag pump can create vacuums down to $1.3 * 10^{-6}$ KPa in the system.

Volumetric method involves measuring the pressure change in a known volume of sample gas exposed to an adsorbent sample. As the gas is adsorbed and allowed to come to equilibrium with the adsorbent, the measured decrease of pressure in the closed system indicates the amount of gas adsorbed under the given isothermal conditions.

Data were collected for the equilibrium pressure range of 0.001 to 110 KPa at 25, 50 and 75 degree Celsius. Obtaining each complete isotherm consists of 60 to 120 equilibrium point measurements and takes roughly about 12 hours. For each point when the rate of change for pressure is less than 0.01% criterion for equilibrium is satisfied and the system moves to the next point.

Prior to each isotherm measurement, the zeolite 13X was regenerated at 350 °C for 16 hours under a vacuum of less than 1 x 10^{-4} torr. In order to prevent structural damage caused by desorbing water steam a stepwise increase in temperature with simultaneous vacuum was applied to all samples.

The pure gas adsorption isotherm along with the model fit has been shown in **Figure 2.3**. The experimentally determined pure gas isotherms except for CO_2 have been fitted with the Dual Process Langmuir (DPL) model. The experimental isotherm of CO_2 was fitted with three-process Langmuir (TPL) isotherm. The isotherm model parameters have been summarized in **Table 2.1**.

2.3.2 Description of the Experimental Setup

The schematic diagram of the 1-bed PSA apparatus is shown in **Figure 2.1**, where all basic steps of a PSA process, i.e., feed (F), heavy reflux (HR), equalization (E), counter-current depressurization (CnD), light reflux (LR) and light product pressurization (LPP) can be performed. It consists of a single adsorbent bed packed with W.R. Grace Zeolite 13X. For feed gas, high purity grades of carbon dioxide and nitrogen were obtained from Praxair. There are six mass flow controllers of different ranges and for different gases are connected with the system. Each mass flow controllers can feed the bed from top or bottom of the bed. Before performing any experiment each mass flow controllers were calibrated using the respected gas. Using the appropriate mass flow controllers CO_2 and N_2 were blended together to mimic the flue gas composition for feed and heavy and light reflux streams. The flow of the heavy and light product was recorded using two mass flow meters. Seven exposed tip k-type thermocouples places axially along the length of the column were used to record the temperature profiles of the bed. The position of the concentration wave

along the bed was determined by observing the temperature profiles. The pressure of the bed was measured by using a pressure transducer placed at the bottom of the column and a low range transducer was used to measure the pressure when the pressure were below vacuum. Flows can be directed in so many different ways in and out of the bed using multiple solenoid vale trains giving enough flexibility to study any possible combinations of PSA cycle steps including pressure equalization. Three equalization tanks were used to mimic the bed-to-bed pressure equalization step. There are two product tanks were connected to the system, one for the light product and the other for the heavy product. The system was designed to analyze both average and instantaneous concentration of the gas coming out of the column. The average concentration of the light and heavy product were determined by analyzing the gas from the light or heavy product tank whereas the instantaneous concentration was analyzing by bypassing the product tanks. Three vacuum pumps were connected in parallel to generate column pressure above and below atmospheric pressure. The concentrations of the different streams were analyzed using a mass spectrometer by withdrawing a fraction of the stream to be measured.

2.3.3 PSA Experiments

A number of experiments were performed on the single bed PSA system by changing different process parameters such as feed flow, cycle time, low pressure, bed temperature etc. to study of their effect on the overall process performances. A simplified schematic diagram of the PSA cycle schedule is shown in **Figure 2.2**. By blending CO_2 and N_2 with flow controllers FC 2-2 and FC 2-3 respectively simulated flue gas containing 15% CO_2 and balance N_2 was produced. The simulated flue gas enters the adsorption column at high pressure P_H from the bottom during the feed step. Zeolite 13X adsorbs CO_2

preferentially and N_2 rich gas leaves the column from the top and enters the light product tank (T). The concentrations and flows of the all the steps was found from the preliminary simulation studies. The concentration of the heavy reflux (HR) was achieved again by blending CO_2 and N_2 using the respective flow controllers and was fed at the high pressure P_H. The purpose of this step is to enrich the loading of CO_2 in the solid phase and remove the gas phase N_2 through to the light end. These step help increase the purity of CO_2 in the heavy product that was produced in the subsequent counter-current depressurization (CnD) step. The bed is emptied in the CnD step to the low pressure P_L producing the heavy product. In order to reduce the size of the vacuum pump used in the CnD step the pressure of the bed was reduced before the CnD step by taking advantage of bed-to-bed equalization step. In bed-to-bed equalization, step one bed at high pressure is connected to another bed at low pressure and pressure of both beds are let to equalize. Since this is a single bed set up, the bed-to-bed equalization step was mimic by equalizing with two empty tanks. After the HR step, the pressure of the bed is partially reduced from P_H to an intermediate pressure P_{EI} during the first equalization step. During the equalization step the light end of the bed is connected to the first equalization step, gas in the light end (mostly N_2) enter the equalization tank due to the pressure difference. The pressure of the bed is further reduced from P_{E1} to P_{E2} by connecting it to the second equalization tank. Next step is the CnD during which the bed pressure reaches to the lowest pressure P_L. During the CnD step, the heavy end of the column was exposed to the vacuum pump by keeping the light end closed. The decrease in the column pressure causes CO_2 to desorb from the adsorbent and exit the bed through the heavy end. The effluent from the CnD step enters the heavy product tank (T). In order to further regenerate, the bed N_2 is flown through the top of the column (light

end) counter-currently during the light reflux (LR) step. The LR step operate at the column low pressure P_L to facilitate the desorption of CO_2. The effluent from the LR step rich in CO_2 also enters the heavy product tank. Usually the LR stream is recycled back the HR step in a multi-bed process. Since the concentration of the LR step stream is lower than that of the CnD step stream the heavy product gets diluted. In order to determine the actual purity of the heavy product the heavy product tank was bypassed at the periodic behavior of the process and the effluent coming out of the bed was directly analyzed with the mass spectrometer. After the LR step the column again undergoes two equalizations steps where the column pressure increases from P_L to P_{E2*} and P_{E1*} respectively. After the equalizations steps the column pressure was increased from P_{E1*} to P_H by using pure N_2 to pressurize the bed through the light end.

2.3.4 PSA Cycle Process Performance Indicators

The PSA process was designed to produce enriched CO_2 as the heavy product and take out N_2 in the light product. The recovery and purity of CO_2 in the heavy product and the recovery and purity of the N_2 in the light product was used to judge the overall performance of the process, the average mole fraction of CO_2 in the heavy product during the CnD step was taken as the purity of CO_2 in the heavy product. The average mole fraction was calculated by averaging the mole fraction of the streams coming out of the CnD step. The recovery of this process was defined as the total amount of CO_2 produced divided by the total amount of CO_2 fed during the feed and HR step. The N_2 recovery in the light product is defined as the total moles of N_2 produced in the light product divided by the total amount of N_2 fed during feed, HR, LR and LPP steps.

Total five runs were carried out to study the effect of different process parameters on the overall process performance. The parameters studies was the feed flow rate, total cycle time, light reflux flow rate, bed temperature. The bed properties and run conditions during each run (Runs 1 to 6) are shown in **Table 2.4**.

The performance indicators of the PSA process are evaluated in terms of purity, recovery and throughput, which are defined below for feed concentration y_F of CO_2:

$$Purity(\%) = \frac{CO_2(mol)obtained\ as\ product\ during\ A\ step.100}{total\ Product(mol)obtained\ during\ A\ step} \quad (11)$$

$$Recovery(\%) = \frac{CO_2(mol)obtained\ as\ product\ during\ CnD\ \&\ LR\ step.100}{COH_2(mol)\ fed\ during\ Feed\ \&\ HR\ setp\ Feed\ step} \quad (12)$$

$$Throughput\left(\frac{L(STP)}{kg.h}\right) = \frac{Fresh\ total\ Feed(L(STP))\ used\ in\ Feed\ step.60}{Mass\ of\ adsorbent(kg)in\ all\ beds} \quad (13)$$

The compressor energy was calculated using the following formula:

$$E_i\left(\frac{kj}{mol}\right) = \frac{1}{n_{CO_2}}\int_0^{t_{step}}\left(\frac{\gamma}{\gamma-1}\right)RT\left[\left(\frac{P_{high}}{P(t)}\right)^{\frac{\gamma-1}{\gamma}}-1\right]\frac{1}{\eta}n(t)dt \quad (14)$$

where t_{step} is the duration of the step feeding the compressor, n_{CO2} is the total moles of CO_2 removed into the heavy product (HP) per cycle during the CnD step and P(t) and n(t) are the time varying pressure and molar flow, respectively, of the stream being fed into the compressor.

2.4 PSA Experiments Results and Discussions

Five runs were carried out to study the effect of various process parameters. The parameters studied include feed flow, cycle and individual step time, reflux ratio in the light reflux step, CnD pressure and temperature. **Table 2.5Table 2.6** summarize all the process conditions for the run 1 through 5. The base case is run 1 (E-1) which was conducted at 70 °C bed temperature, total cycle time was 720 sec, reflux ratio 3% and CnD pressure 5 kPa. The CnD pressure was controlled by fine-tuning with a needle valve in the vacuum line. In E-2, the reflux ratio was changed to 4% by keeping all other parameters, same as base case E-1. In E-3, the CnD pressure was raised from 5 kPa to 7 kPa compared to the base case E-1 while the other parameters were kept the same. In E-4, all the step times were made half of those in the base case E-1 except for the equalization steps and the feed flow rate was doubled. Experiment E-5 was ran at 100 °C bed temperature and all other parameters were same as those in the base case E-1.

Figure 2.4 shows the temperature profiles of the seven thermocouples (T-1 to T-7) along the bed at the periodic state of the bed. The temperature profiles shows the progression of the concentration wave through the bed. The first temperature peak corresponds to the temperature rise due to the feed gas. However, the higher temperature peak corresponds to the temperature rise due to higher concentration heavy reflux stream. **Figure 2.5**(a) shows the periodic state pressure profile of the bed for a complete PSA cycle of the base case E – 1. **Figure 2.5**(b) shows the zoomed view of the pressure profile during equalization, CnD and LR step. In the base case E - 1 the CO_2 purity and CO_2 recovery obtained was 96.79% and 91.06% respectively, and this will be compared with the results of the other 4 runs.

In run E-2, only the reflux ratio was changed from 3% to 4% compared to the base case E – 1 while keeping the other parameters same. During the LR step, pure N_2 was fed to the column from the light end. This wave of pure N_2 forces all the CO_2 in void spaces and some from the solid phase to be pushed out from the bed through the heavy end. This step pushes the CO_2 front further down the bed causing better regeneration of the bed. The effluent from both step, CnD and LR goes to the heavy product tank. The concentration coming out of the LR step heavily dependent of the flow of the light reflux step. However only the concentration of CO_2 of the stream coming out of the CnD step was considered as the CO_2 purity of the process. The higher reflux ratio helped the bed regenerate better which should yield higher recovery of CO_2. From Table 4 we can see that the CO_2 recovery was increased in run E – 2 compared to E – 1.

In run E – 3 the CnD pressure was limited to 7 kPa compared to 5 kPa of the base case E – 1, keeping the other process conditions the same. A lower vacuum pressure helps desorb more CO_2 and be removed in the heavy product. Better regeneration improves the bed capacity for CO_2 and therefore CO_2 recovery increases. The recovery of CO_2 in the heavy product was much deceased as compared to base case E – 1 because it was run at a higher vacuum, which caused poor regeneration of the bed causing more CO_2 to breakthrough thereby reducing the CO_2 recovery in the heavy product.

In experiment E – 4 all the step times was reduced to half except for the equalization steps compared to the base case E – 1 also the flow rates was made twice. The reduction in time in the CnD step caused poor regeneration of the bed causing the CO_2 wave pushed further up and as a result more CO_2 breakthrough to the light product. Because of this, the CO_2 recovery decreases significantly compared to E – 1.

The last experiment (E – 5) was conducted at 100 °C keeping all other process parameters the same. The loading of both CO_2 and N_2 decreases significantly at higher temperature, however the loading of N2 decreases significantly at higher temperature that explains the higher CO_2 purity in the heavy product in run E – 5.

2.5 Model Validation

Every model needs to validate against experiment before it can be used to design a process. The DAPS model was also validated against the experimental data obtained in the five runs. The simulations was performed using the equilibrium and kinetic information of the 13X zeolite for the given gases independently in separate measurement methods. As explained before the equilibrium isotherm of both CO_2 and N_2 on 13X zeolite was obtained using the micromeritics ASAP 2010 for three different operating temperatures. The mass transfer coefficients of CO_2 and N_2 was obtained using the rapid pressure swing apparatus (RPSA). In these simulations one parameter mass transfer coefficient with energy balance was used. The main heat transfer resistance is between the solid and gas phase inside of the column wall. In order to remove the heat transfer of the wall and outside the wall thickness was considered negligible. The heat transfer coefficient was obtained by fitting the temperature profile of the bed of a pure N_2 purge run. Heat transfer and mass transfer coefficients were not changed in any simulation. Only the valve coefficient of different steps was changed in order to match the pressure history of the bed during a complete cycle.

In **Figure 2.6** the model predicted pressure profile of the bed was plotted against the experimental pressure profile of the bed at the periodic state for the entire PSA cycle. The PSA cycle consists of 8 steps namely feed step (F), heavy reflux step (HR), first

equalization down step (Eq-1), second equalization down step (Eq-2), counter-current blowdown step (CnD), light reflux step (LR), first equalization step up (Eq-2*), second equalization step up (Eq-1*) and light product pressurization step (LPP). The experimental data was represented as the open circle whereas the solid line shows the model prediction. As it can be seen from the figure the DAPS can predict exactly the experimental pressure profile of the bed. It is very important to have a correct estimation of the individual component isotherms, mass transfer coefficients and heat transfer coefficients. The pressure profile was matched only adjusting the respective valve coefficients of each step no other parameter was adjusted.

In **Figure 2.7** the experimental temperature profiles at periodic state for seven different thermocouples in the bed was plotted against the DAPS predicted temperature profiles. The open circles represent the experimental data whereas the solid lines represent the model predictions. The experimental and model prediction of seven thermocouples (T-1 to T-7) were plotted separately in **Figure 2.7**(a) – (g) in order for better comparison. In **Figure 2.7**(h) the model prediction of all the thermocouples (T-1 to T-7) are plotted together. The relative locations of the thermocouples along the bed are T-1: 12.68%, T-2: 24.02%, T-3: 35.73%, T-4: 47.26%, T-5: 58.78%, T-6: 70.31%, and T-7: 81.83%. Because of a higher heat of adsorption of CO_2 there is a temperature rise during adsorption and the temperature rise indicates the location of the concentration front in the bed. The first peak in the **Figure 2.7**(a) – (g) is due to the feed gas. The second peak in **Figure 2.7**(a) - (d) is due to the heavy reflux gas. The temperature rise during the heavy reflux is more than that happens during feed because CO_2 concentration is higher in the heavy reflux stream. The feed concentration is 15% CO_2 whereas the concentration in the heavy reflux stream is in

the range 75 - 85% CO_2. The progression of the concentration front can be tracked by observing the temperature rise peak in the temperature profile of all the thermocouple. We can see that the second peak only reaches until thermocouple T-4 which is 47.26% in the bed that means the front location is between 47.26% and 58.78% of the bed. However, the feed wave front reached until T-7 and a very small amount of CO_2 broke through during this experiment. Using the equilibrium isotherms of individual component determined using micromeritics ASAP 2010 and mass transfer coefficients determined from the single gas cyclic experiment in RPSA setup, the model was able to predict accurately the temperature profiles and position of the higher concentration front during the heavy reflux step for the entire PSA cycle for E – 1. The comparison of the experiment with simulation prediction of CO_2 purity and CO_2 recovery in the heavy product for all five runs are shown in **Table 2.8**. The results show a close agreement between experiments and model. Therefore, the DAPS model was validated and now can be used to simulate a variety of PSA cycles and process conditions for CO_2 capture.

2.6 Conclusion

A nine-step PSA cycle was studies using the single bed PSA apparatus to separate CO_2 from flue gas (15% CO_2, 85% N_2) using Zeolite 13X from Grace as adsorbent. Several PSA cycle experiments were performed by varying different process parameters. The cycle steps involved were feed, heavy reflux, equalization, counter current depressurization, light reflux, and light product pressurization. The process performances was judged by the CO_2 purity and recovery in the heavy product. The process parameters studied was feed flow, light reflux ratio, cycle/step time, CnD pressure and bed temperature. The experimental

results were used to validate the dynamics adsorption process simulator (DAPS) using equilibrium isotherms of the individual components measured at three different temperatures independently using micromeritics ASAP 2010 and the mass transfer coefficients determined using the single gas cycling using a rapid pressure swing adsorption apparatus. The model successfully predicts the pressure and temperature profiles and performance of each experiment. DAPS successfully capture the location of the concentration front in the bed without any adjustable parameters. The agreement between the experiment and simulation results also validate the single component adsorption isotherm and mass transfer coefficient measure independently. The reason simulation predicted temperature profiles did not match perfectly with the experiment was that there is only one lumped heat balance was used. However, the model does excellent job in predicting the location of the temperature peaks.

In spite of the minor differences in the temperature profiles and the performance predictions, we are convinced that DAPS captures all the crucial phenomena and predicts all the important trends observed in the PSA process for the separation of CO_2 from a simulated flue as containing 15% CO_2 and 85% N_2 using 13X zeolite, and it does so in a quantitative manner. Now DAPS can be used to model process design and optimization a CO_2 separation process using PSA.

2.7 Tables

Table 2.1: Isotherm parameters.

Parameter	CO_2	N_2
	k = 1	
$q^*_{i,1,s}$ (mol/kg)	1.338	0.438
$q_{i,1,st}$ (mol/kg/K)	0.0	0.0
$b_{i,1,o}$ (1/kPa)	2.4419E-8	7.5950E-7
$B_{i,1}$ (K)	5757.03	2370.32
	k = 2	
$q^*_{i,2,s}$ (mol/kg)	2.238	0.733
$q_{i,2,st}$ (mol/kg/K)	0.0	0.0
$b_{i,2,o}$ (1/kPa)	4.5204e-08	7.5950e-7E-6
$B_{i,2}$ (K)	4606.08	2370.32
	k = 3	
$q^*_{i,3,s}$ (mol/kg)	1.853	0.607
$q_{i,3,st}$ (mol/kg/K)	0.0	0.0
$b_{i,3,o}$ (1/kPa)	1.3737E-8	7.5950e-7E-6
$B_{i,3}$ (K)	4224.86	2370.32

Table 2.2: The initial and boundary conditions of other steps of the PSA cycle:

Step	Time and Bed Location	Initial, Boundary conditions and balances
		PSA cycles
Feed (F)	t = 0	$y_i=y_{i,LPP}$, $T = T_{LPP}$, $q_i = q_{i,LPP}$ (at all z)
	z/L = 0	$y = y_{i,F}$, $F = F_F$, LDFE, $T = T_F$, M.B. (at all t)
	z/L = 1	C.M.B., O.M.B., LDFE, E.B. ($T_o = T_F$), V.E. ($P_o=P_H$) (at all t)
Heavy Reflux (HR)	t = 0	$y_i=y_{i,F}$, $T = T_F$, $q_i = q_{i,F}$ (at all z)
	z/L = 0	$y = y_{i,HR}$, $F = F_{HR}$, LDFE, $T = T_{HR}$, M.B. (at all t)
	z/L = 1	C.M.B., O.M.B., LDFE, E.B. ($T_o = T_F$), V.E. ($P_o=P_H$) (at all t)
Counter-current depressurization (CnD)	t = 0	$y_i=y_{i,HR}$, $T = T_{HR}$, $q_i = q_{i,HR}$ (at all z)
	z/L = 0	C.M.B., O.M.B., LDFE, E.B. ($T_o = T_F$), V.E. (at all t)
	z/L = 1	C.M.B., v = 0, LDFE, E.B. ($T_o = T_F$) (at all t)
Light reflux (LR)	t = 0	$y_i=y_{i,CnD}$, $T = T_{CnD}$, $q_i = q_{i,CnD}$ (at all z)
	z/L = 0	C.M.B., O.M.B., LDFE, E.B. ($T_o = T_F$), V.E. (at all t)
	z/L = 1	$y = y_{i,LR}$, $F = -F_{LR}$, LDFE, $T = T_F$, M.B. (at all t)
Light Product pressurization (LPP)	t = 0	$y_i=y_{i,E1R}$, $T = T_{E1R}$, $q_i = q_{i,E1R}$ (at all z)
	z/L = 0	C.M.B., v = 0, LDFE, E.B. ($T_o = T_F$) (at all t)
	z/L = 1	$y = y_{i,LPP}$, $F = -F_{LPP}$, LDFE, $T = T_F$, M.B. (at all t)

Table 2.3: The cycle schedule of the experiment performed.

FEED	HR	E-1	E-2	CnD	LR	E-2*	E-1*	LPP
I	I	E-1	I	I	I	I	E-1*	I
I	I	I	E-2	I	I	E-2*	I	I

Table 2.4: Properties and Operating conditions.

Properties	Values
Bed Characteristics	
Length (m)	0.50165
Internal Radius (m)	0.0254
Bed porosity	0.425
Bulk density (kg/m^3)	632.8
External Heat transfer Coefficient ($kW/m^2/K$	0.0024
Wall	
Material	SS 316
Thickness (mm)	4.0
Heat capacity (kJ/kg/K)	0.468
Density (kg/m^3)	8.24
Adsorbent	
Total Mass (kg)	0.7204
Material	Zeolite 13X
Pellet density (kg/m^3)	1100.0
Pellet porosity	0.54
Pellet heat capacity (kJ/kg/K)	1.1
Operation	See table 3
Feed flow (SLPM)	14.54, 29.07
CO_2 concentration (Balance N_2, %)	15.9
Feed and external temperature (^oC)	25.0
Light reflux ratio*	0.02-0.05
High pressure, P_H (kPa)	121.0
Low pressure, P_L (kPa)	5.0, 7.0, 10.0
Cycle Times and Step Times	See Table 3
Gasses	
CO_2	
Isotherm	See Table 4
Mass transfer Coefficients, k_{M1} (1/s)	47.21
Nitrogen	
Isotherm	See Table 4
Mass transfer Coefficient, k_{M1} (1/s)	70.34

Table 2.5: Experimental Conditions of the PSA Experiments.

T [°C]	Exp	Cycle Time [sec]	Step Times [sec]								
			F	HR	E-1	E-2	CnD	LR	E-2*	E-1*	LPP
70	E-1	720.0	240	120	10	10	100	120	10	10	100
	E-2	720.0	240	120	10	10	100	120	10	10	100
	E-3	720.0	240	120	10	10	100	120	10	10	100
	E-4	380.0	120	60	10	10	50	60	10	10	50
100	E-5	720.0	240	120	10	10	100	120	10	10	100

Table 2.6: Experimental Conditions of the PSA Experiments

Bed Temp [°C]	Exp. No	Feed Throughput [L_{STP}/hr/kg]	Feed CO_2 Conc. [%]	Reflux Ratio [%]	P_H [kPa]	P_L [kPa]	P_H/P_L
70	E-1	403.61	15.90	3.0	120.10	4.94	24.32
	E-2	403.60	15.91	4.0	120.07	4.95	24.24
	E-3	403.47	15.90	3.0	119.68	7.15	16.73
	E-4	764.48	15.94	3.0	119.47	6.11	19.54
100	E-5	403.57	15.92	3.0	119.84	4.93	24.29

Table 2.7: Summary of PSA Cycle experimental results.

Temp	Exp	Feed Throughput	Cycle Time	P_L	R.R.	CO_2 HP		N_2 LP	
[°C]		[L_{STP}/hr/kg]	[sec]	[kPa]	[%]	% Pur	% Rec	% Pur	% Rec
70	E-1	403.61	720.0	4.94	3.0	96.79	91.06	96.38	94.55
	E-2	403.60	720.0	4.95	4.0	96.72	92.45	96.73	94.09
	E-3	403.47	720.0	7.15	3.0	95.24	82.20	92.63	92.00
	E-4	764.48	380.0	6.11	3.0	96.51	83.70	92.23	94.64
100	E-5	403.57	720.0	4.93	3.0	97.51	91.42	95.96	94.81

Table 2.8: Summary of PSA cycle experimental results compared with Simulation results.

Temp	Exp	Cycle Time	P_L	R.R.	HP CO_2 Rec [%]		HP CO_2 Pur [%]	
[°C]		[sec]	[kPa]	[%]	Experiment	Modeling	Experiment	Modeling
70	E-1	720.0	5.02	2.0	91.06	94.56	96.79	96.71
	E-2	720.0	5.01	3.0	92.45	94.82	96.72	96.86
	E-3	720.0	5.12	4.0	82.20	83.70	95.24	95.52
	E-4	380.0	6.94	4.0	83.70	84.60	96.51	96.08
100	E-5	720.0	5.02	3.0	91.42	93.90	97.51	98.00

2.8 Figures

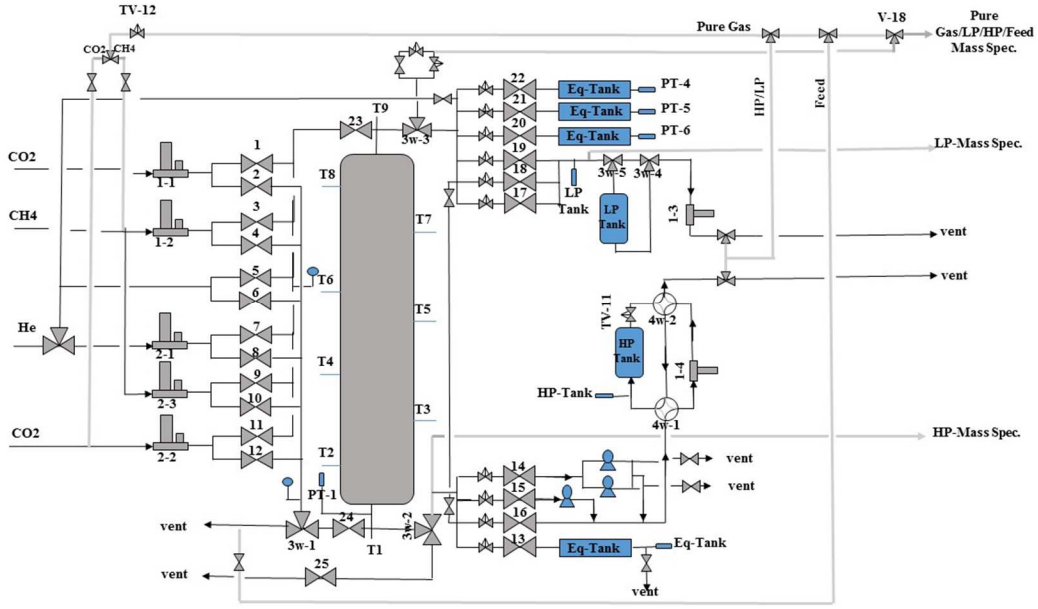

Figure 2.1: Simplified schematic diagram of the single bed PSA experimental apparatus.

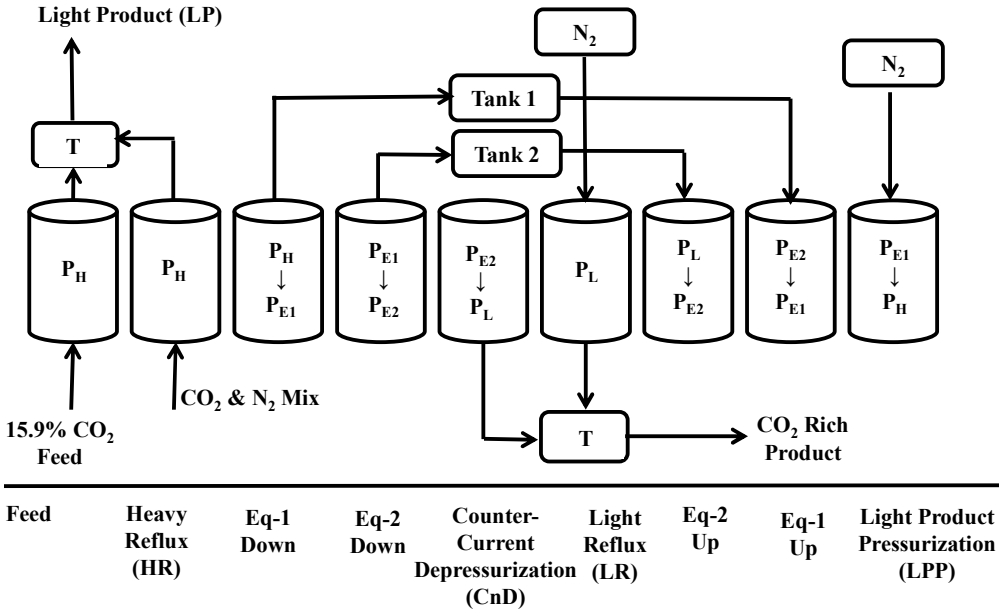

Figure 2.2: Schematic diagram showing all steps in the PSA cycle investigated in the single bed experimental system. 1: Feed (F) step; 2. Heavy-Reflux step (HR); 3, 4, 7, and 8: Pressure equalization steps (Eq); 5: Counter Current depressurization (CnD) step; 6: Light-reflux (LR) purge step; 7: Light product pressurization (LPP) step.

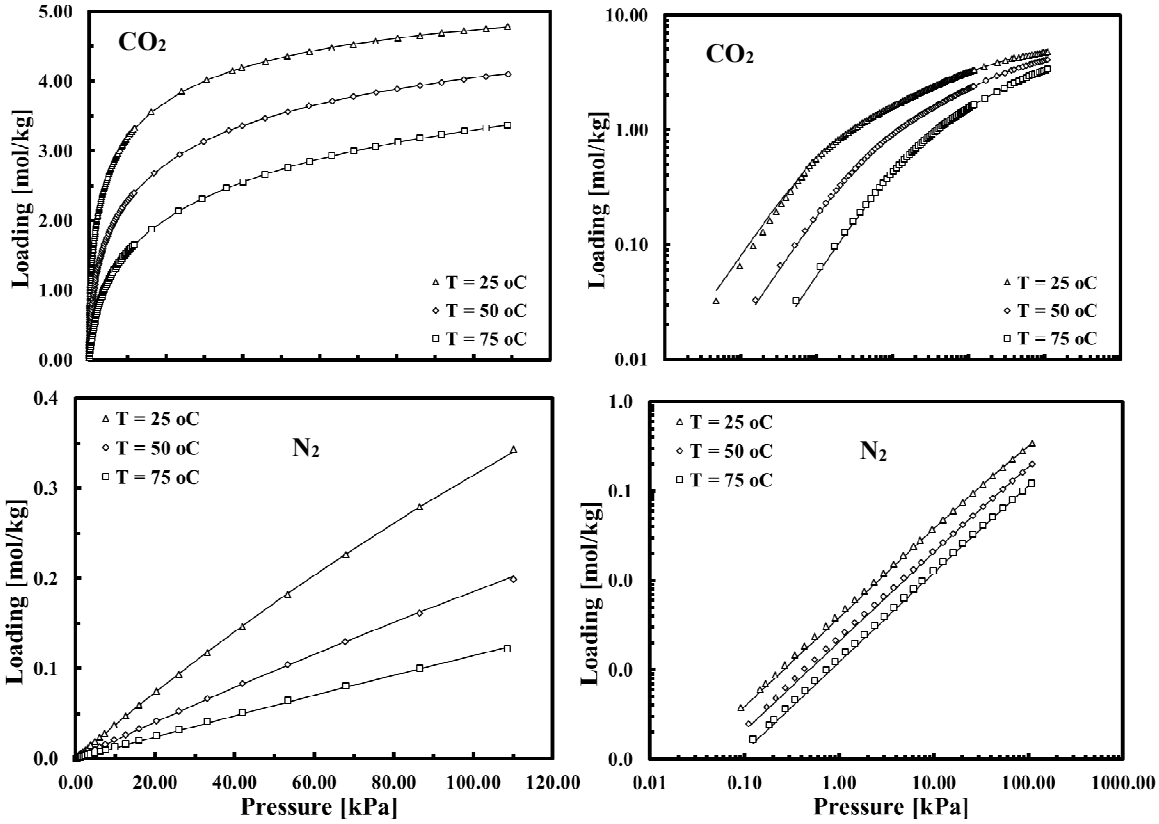

Figure 2.3: Isotherms of Carbon dioxide and Nitrogen at three different temperatures in linear (left) and log-log scale (right). The solid lines represent the model fits and the markers represent the experimental data.

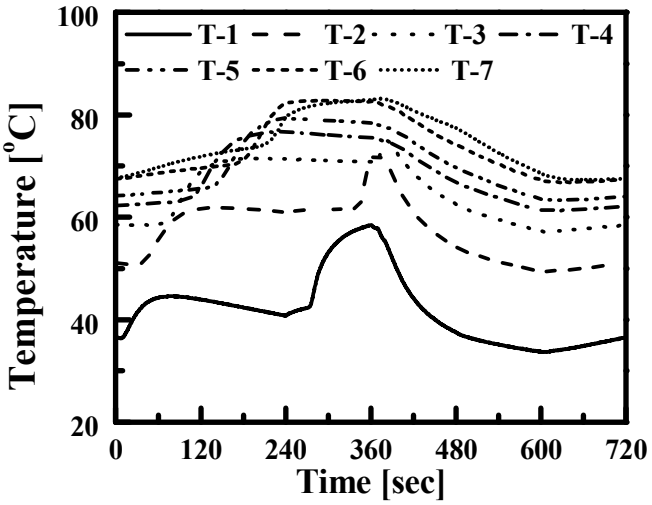

Figure 2.4: Temperature history of each bed and one bed for 7 different equidistant locations (1:12.68%, 2:24.20%, 3:35.73%, 4:47.26%, 5:58.78%, 6:70.31%, 7:81.83%) for experiment E-1 during one entire cycle.

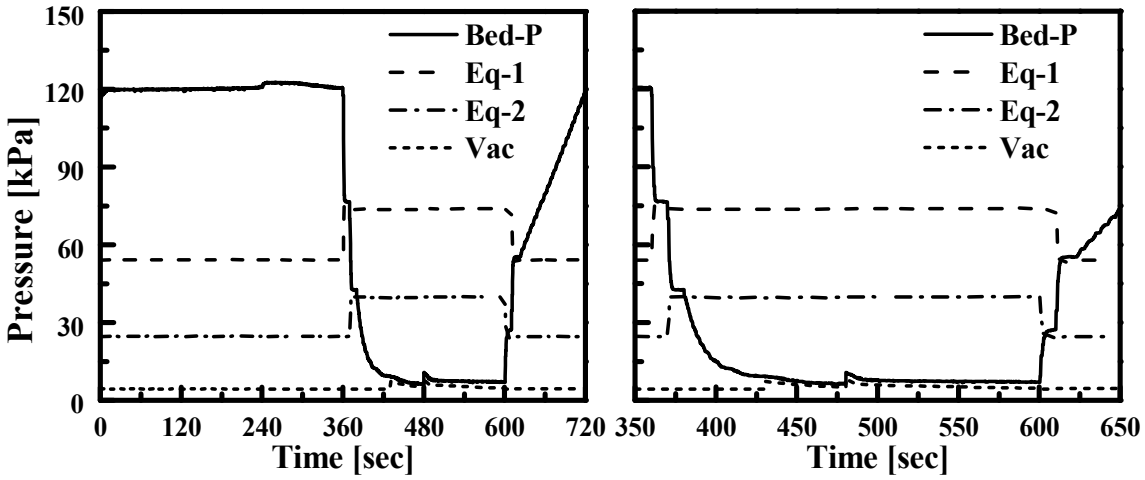

Figure 2.5: Pressure history for all 3 beds during one entire cycle (left) and pressure history for only bed-1 during one entire cycle (right) of experiment E-1.

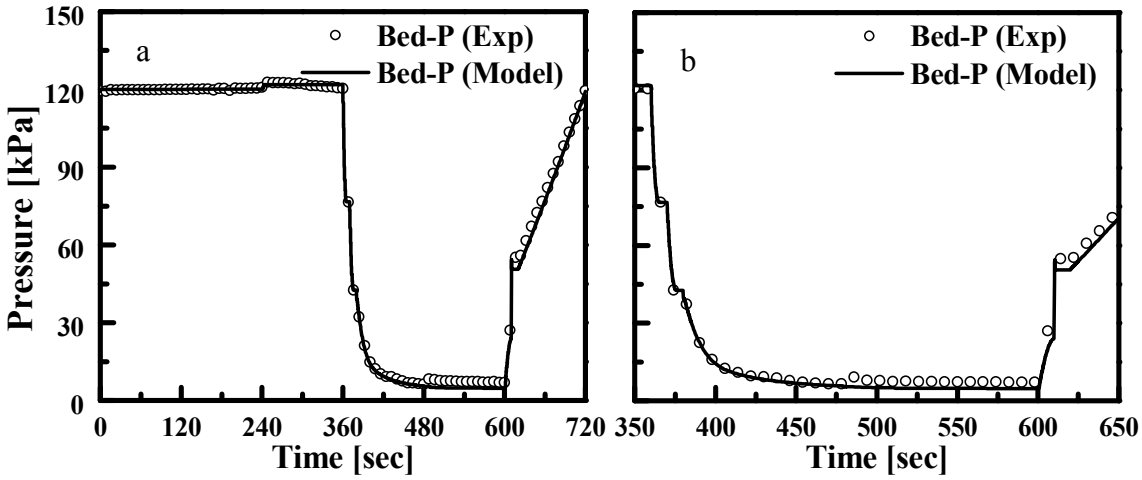

Figure 2.6: Pressure history of Bed-1 during one entire cycle for E1, plotted against the pressure history as predicted by simulation (M-1).

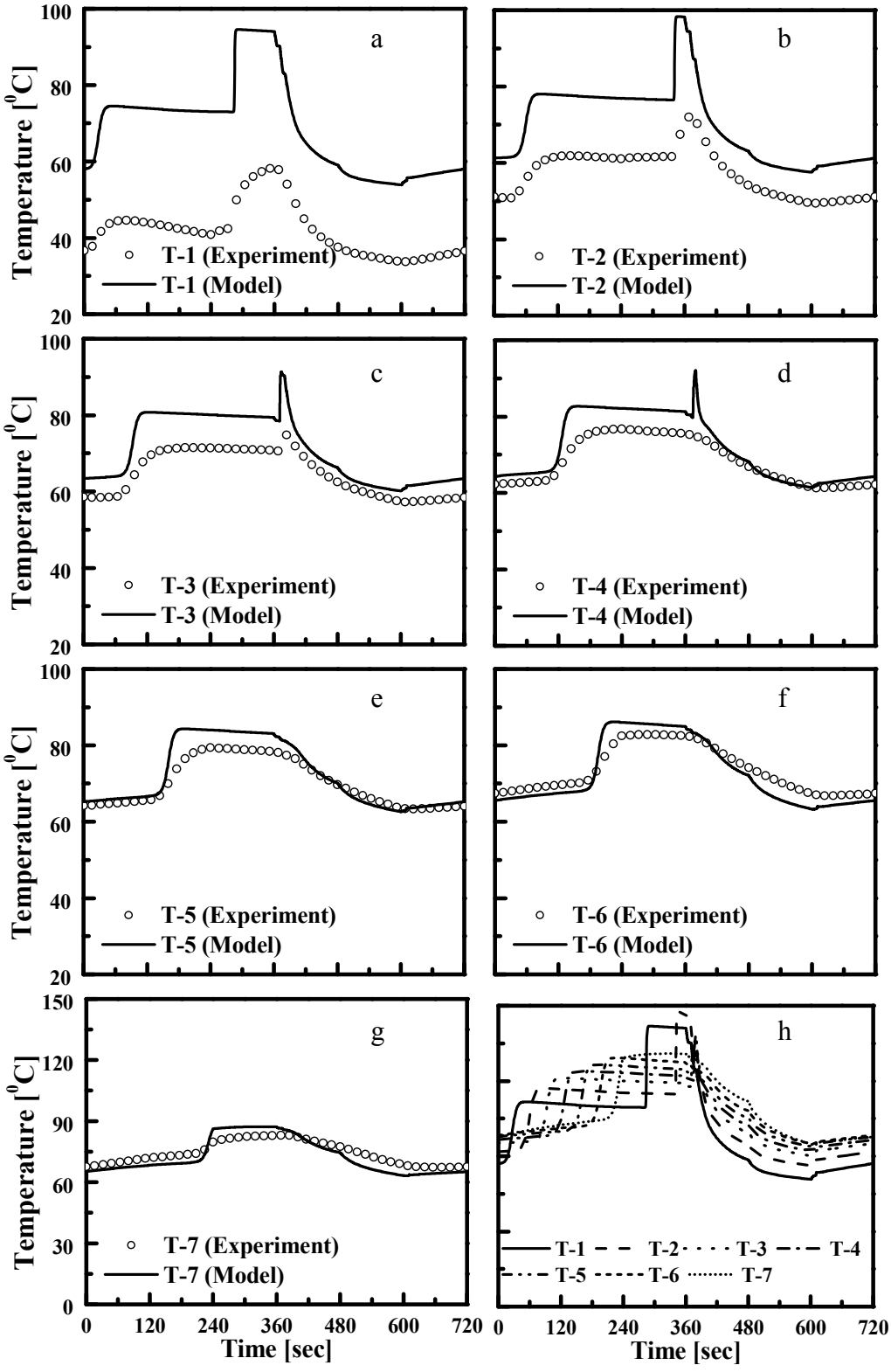

Figure 2.7: Periodic state experiment and model prediction temperature profiles in the bed for E-1 at seven different thermocouples (T-1 to T-7) along the bed (T-1:12.68%, T-2:24.20%, T-3:35.73%, T-4:47.26%, T-5:58.78%, T-6:70.31%, T-7:81.83%).

CHAPTER 3

DEVELOPMENT OF A PRESSURE SWING ADSORPTION (PSA) CYCLE FOR CO2 CAPTURE FROM FLUE GAS USING A 4-BED PSA APPARATUS: EXPERIMENT AND MODEL PREDICTION

3.1 Introduction

It is widely accepted that the major cause for global warming is the increase in CO_2 concentration in the earth's atmosphere due to anthropogenic activities. Due to the effect of CO_2 on global warming, the CO_2 emission is becoming an increasingly serious issue. Major sources of CO_2 emissions into the atmosphere is through the burning of fossil fuels for energy. The emission of CO_2 can be reduced by switching to renewable energy such as solar or wind energy [67-75] or through CO_2 capture and sequestration [44]. It is reported that about 85% of the world commercial energy is produced by burning coal, oil and gas. Department of Energy (DOE) has reported that about 40% of the total CO_2 emissions come from all coal-fired power plants [44]. These coal-fired power plants presents large point sources for CO_2 emissions and considerable effort has been underway worldwide to curb CO_2 emissions from these large point sources. The goal is to capture CO_2 from the flue gas of power plants and concentrate it to around 90 to 95% and sequester it underground [44].

There are several technologies available to separate CO_2 such as absorption, cryogenic distillation, adsorption, and membrane separation. However, to date none of the

technologies is economically feasible; so, significant research effort is being undergoing to come up with an economically feasible process to capture CO_2. Among the available technologies, physical absorption using amines is the most widely accepted technology. However, the operating cost is significantly higher in the amine absorption to regenerate the solvent. The amine absorption process takes out a portion of the process steam of the power plant reducing the overall capacity of the power plant. The energy penalty of the cryogenic distillation is prohibitively high. The membrane process suffers some serious drawbacks such as low flux, degradation, fouling, capital cost and stability at the extreme process conditions.

An article published by the International Energy Agency (IEA) in 1994, focused the use of adsorption technologies for CO_2 capture from flue gases on the basis of 500 MW power plant [50]. Both pressure swing adsorption (PSA) and temperature swing adsorption (TSA) were evaluated used a commercial adsorbent 13X zeolite. At that time the study clouded that both PSA and TSA were too energy intensive and not feasible for CO_2 capture from power plants. In 2003 another report by IEA reiterated the same results [51]. However Webley and co-workers questioned findings of both report in one of their work [52]. This work reevaluated the PSA process by calculating the energy consumption by a PSA process for CO_2 capture to be \$67/tonne CO_2 captured compared to \$97/tonne CO_2 captured as reported by IEA. This new energy consumption value of PSA compare much more favorably to the energy consumption by the amine absorption process at \$60/tonne CO_2. The cost of PSA can be brought down significantly by proper design of the PSA cycle.

Many industries have been developing pressure swing adsorption (PSA) for years. Japanese power industries started developing cyclic PSA/VSA for CO_2 removal in early

nineties [24, 76-79]. Since early ninety, a number of different PSA/VSA cycle have been developed and reported in the literature. A summary of these studies is tabulated in table 1. The definition of different variables used in the table are, y_f is the % of CO_2 in the feed, p_{CO2} and r_{CO2} are the purity and recovery of CO_2 in the heavy product stream. However, most of the studies listed in Table 1 are bench-scale studies with extremely small feed throughput.

Ritter research group has studied a number of different cycles of PSA for CO_2 capture at high temperature using K-promoted hydrotalcite as the adsorbent [80-82]. Their main emphasis was to obtain heavy product at a high purity by introducing a heavy reflux step. In their work, they compared seven different 4-bed 4-step, 4-bed 5-step and 5-bed 5-step configurations with and without heavy reflux step. In another study, they compared nine different PSA configurations to maximized the CO_2 purities and recoveries, however all were at a very small feed throughput [83]. Kikkinides et al was able to improve the purity and recovery of CO_2 in a 4-bed 4-step process by allowing significant breakthrough of CO_2 from the light end of the column undergoing heavy reflux after that recycling the effluent from this light end back to the column with the feed [25]. Chue et al. studied a 3-bed 9-step VSA process using activated carbon and zeolite 13X [7]. They concluded that zeolite 13X performs better that the activated carbon despite having a high heat of adsorption. Zeolite 13X outperforms activated carbon because of its higher working capacity, lower purge requirement and higher equilibrium selectivity. Kikkinides et al was able to improve the purity and recovery of CO_2 in a 4-bed 4-step process by allowing significant breakthrough of CO_2 from the light end of the column undergoing heavy reflux after that recycling the effluent from this light end back to the column with the feed [25].

Chue et al. studied a 3-bed 9-step VSA process using activated carbon and zeolite 13X [7]. They concluded that zeolite 13X performs better that the activated carbon despite having a high heat of adsorption. Zeolite 13X outperforms activated carbon because of its higher working capacity, lower purge requirement and higher equilibrium selectivity. PSA cycle employing both heavy and light reflux steps were investigated by Takamura et al. [84] and Park et al. [85]. Park et al. compared three different configurations of VSA process while Takamura et al. investigated a 4-bed 8-step VSA process. Although the pure CO_2 rinse step improved the CO_2 purity and recovery, it did not decrease the power consumptions. The power requirements for the 2-bed 6-step and 3-bed 5-step cycle were 106.91 kWh/tonne CO_2 and 147.64 kWh/tonne CO_2 respectively. However, the feed throughput was quite low (0.331 kgmol/hr) in those studies. Gomes et al. [23], studied the 2-bed 4-step Skarstrom cycle. He did not employ vacuum to recover CO_2. Their study also shows that the pure heavy component cannot be achieved by employing only the light reflux step.

Chou et al. [21] studies two different PSA configurations consisting of 2-bed and 3-bed respectively. The 2-bed process did not have any light or heavy reflux step while the 3-bed process used both light and heavy reflux steps. Flow reversal was implemented in between the pressurization and depressurization steps in the 2-bed process. The maximum CO_2 purity achieved was 63% using a 3-bed 6-step cycle. In a study, Ko et al. [86] was able to achieve a CO_2 purity of 90% and CO_2 recovery of 94% by an optimized 1-bed 4-step fractionated VPSA process. Grande et al. [87], studied 3-bed 5-step process which include a pure CO_2 rinse step after the adsorption step. They were able to achieve a purity of 83% and a recovery of 66% at a very high feed throughput of 48.57 kmol/hr. Chaffee et al. [52] studied a 3-bed 6-step VSA process at a feed throughput of 0.193 kgmol/hr and

were able to achieve a lower power consumption of 192 kWh/ton CO_2. On the other hand Zhang et al. [48] achieved a power consumption of 240 kWh/ton CO_2 at the same feed throughput of 0.193 kWh/ton CO_2 with a 3-bed 9-step VSA process. Xiao et al. [88] achieved a CO_2 recovery of 75% with a similar 3-bed 9-step cycle. Zhang and Webley [89] investigated a number of different VSA configurations and concluded that, by incorporating heavy reflux and equalization steps CO_2 purity can be increased

The main objective of the current study is to develop a PSA process to capture CO2 from the flue gas containing 15% CO_2 and balance N_2 using 13X zeolite. It is very important to have a reliable process simulator to design any process. The in-house FORTRAN based dynamic adsorption process simulator (DAPS) was validated by fitting the experimental results of the PSA experiment conducted in a single bed apparatus using PSA experiment performed in a single bed PSA apparatus.

3.2 Mathematical Model

Simulations of the PSA cycles were carried out using an in house dynamic adsorption process simulator (DAPS) developed in FORTRAN that uses the finite difference method and the time adaptive DAE solver called DASPK (**Brown et al., 1994**). The following assumptions are imposed: the ideal gas law, plug flow, no heat transfer limitations between gas and solid (i.e., pellet) phases, no thermal capacitive role of the wall, no axial mass and thermal dispersion, the gas phase concentration in both bulk and pellet porosity is identical, and the mass transfer between solid and gas is defined by 1 parameter macropore limited non-isothermal model. Temperature of the wall set at a

constant value equal to the temperature of the bed and heat loss to the exterior defined by heat transfer at the inner side of the wall.

For an N-component PSA process, the overall (O.M.B.) and component mass balances (C.M.B.) over a differential volume element respectively yields:

$$(\varepsilon_b + (1-\varepsilon_b)\varepsilon_P)C_T\left(\frac{1}{P}\frac{\partial P}{\partial t} - \frac{1}{T}\frac{\partial T}{\partial t}\right) + \varepsilon_b \frac{\partial v C_T}{\partial z} + \sum_{j=1}^{n} S_j = 0 \qquad (1)$$

$$(\varepsilon_b + (1-\varepsilon_b)\varepsilon_P)C_T \frac{\partial y_i}{\partial t} + \varepsilon_b C_T v \frac{\partial y_i}{\partial z} - y_i \sum_{j=1}^{n} S_j + S_i = 0 \qquad i = 1 \text{ to } N\text{-}1$$

(2a)

$$y_i + \sum_{j=1, j\neq i}^{n} y_j = 0 \qquad i = N \quad (2b)$$

with

$$C_T = \frac{P}{RT};\ S_i = (1-\varepsilon_b)\rho_P \frac{\partial q_i}{\partial t}$$

Where ε_p and ρ_p are the pellet porosity and density, respectively, ε_b is bulk porosity, v is the interstitial velocity, y_i is the molar fraction of species i in the gas phase, T is the temperature of both gas and solid phases, P is the pressure and q_i is loading of species i in the solid phase, R is the universal gas constant.

To determine the mass transfer rate for the particle for each gas one parameter non-isothermal macro pore model was used [Ref mass transfer paper]. The mass transfer of species i between the solid and gas phase is defined given by Eq. (3) (M.T.M.):

$$\frac{dq_i}{dt} = k_{M,eff}(q_i^*(P,T) - q_i) \tag{3}$$

where $k_{M,eff}$ is the overall effective macropore mass transfer coefficient, q_i^* is the adsorbed equilibrium concentration, i.e., $q_i^* = f(P,T)$ given by the isotherm and q_i is the average adsorbed concentration.

The overall effective macropore mass transfer coefficient is given by Ep. (5)

$$k_{M,eff} = \frac{1}{1 + \frac{RT\rho_p}{\varepsilon_p}\frac{\partial q^*}{\partial P}_{T,P_i}} k_M \tag{4}$$

Where ρ_P is the particle density, ε_P is the particle porosity, $\frac{\partial q^*}{\partial P}_{T,\bar{P}}$ is the slope of the isotherm, k_M macorpore mass transfer parameter. The fitting parameter for this model is k_M.

The equilibrium loading of component i, q_i^* is calculated from the Three Process Langmuir isotherm:

$$q_i^* = \sum_{k=1}^{3} \frac{b_{i,k} P_i q_{i,k,s}}{1 + \sum_{j=1}^{n} \left(b_{j,k} P_j\right)}$$

where $b_{i,k} = b_{i,k,o} \exp\left(\frac{B_{i,k}}{T}\right)$ and $q_{i,k,s} = q_{i,k,s}^* + q_{i,k,st} * T$ [k = 1 to 3]

where q_i^* is the total loading of component i in mol/kg, n is the number of components, $q_{i,k,s}$ is the saturation loadings of component i in mol/kg on sites k, P_i is the partial pressure of component I, T is the temperature in K.

The energy balance (E.B.) is expressed as

$$\left(\varepsilon_b + (1-\varepsilon_b)\varepsilon_P\right)\left(Cp_g C_T \frac{\partial T}{\partial t} - \frac{\partial P}{\partial t}\right) + \left((1-\varepsilon_b)\rho_P Cp_p\right)\frac{\partial T}{\partial t} + \varepsilon_b Cp_g C_T v \frac{\partial T}{\partial z} +$$

$$(1-\varepsilon_b)\rho_P \sum_{j=1}^{n}\left(Cp_{a,j} q_j \frac{\partial T}{\partial t} + \Delta H_i \frac{\partial q_i}{\partial t}\right) + \frac{2}{r_{b,i}} h_w (T - T_w) = 0 \qquad (5)$$

with

$$Cp_g = \sum_{i=1}^{n}\left(y_j Cp_{g,i}\right)$$

where $Cp_{g,i}$ and $Cp_{a,j}$ are the molar heat capacities of species i in the gas and adsorbed phase, respectively (typically assumed identical), Cp_p is the heat capacity of the pellet, ΔH_i is the heat of adsorption of species i, h_w is the heat transfer coefficient at the inner side of the wall of the bed and r_i is the internal radius of the bed and T_w is the wall temperature.

The pressure drop along the bed is evaluated via Ergun's equation, i.e. the momentum balance (E.B.):

$$\frac{\partial P}{\partial z} + 1.5\times10^{-1}\mu_g\left(\frac{1-\varepsilon_b}{2r_p\varepsilon_b}\right)^2 v + 1.75\times10^{-3} C_T M_g \frac{1-\varepsilon_b}{2r_p\varepsilon_b} v|v| = 0 \qquad (6)$$

where μ_g and M_g are the viscosity and the average molecular weight of the gas phase and r_p is the effective radius of the pellet.

At given boundaries the flow rate (F) whether it's goes in or out of the bed is defined according to the valve equation (V.E.), which is defined according to Eq (10):

$$F = C_v v_{sign} \frac{1}{\sqrt{S_g T_-}} min(49.08|P_-^2 - P_+^2|^{0.5}, 41.63P_-) \quad (7)$$

where c_v is the valve coefficient, S_g is the molecular weight of the gas relative to that of air, P_- and P_+ is the pressure upstream and downstream the valve, T_- is the temperature upstream the valve.

The equations described above constitute a complete mathematical model for multi-component pressure swing adsorption process once the initial and boundary conditions for particular steps are specified. For a system containing N components, there are a total of 2N+3 variables and equations that have to be solved at each node.

The initial and boundary conditions depends on the PSA process cycle configuration used. The initial and boundary conditions for different steps are given in **Table 3.2**:

3.3 Experimental Section

3.3.1 Adsorption Isotherm Measurement

Pure component adsorption equilibrium isotherms for CO_2 and N_2, on zeolite 13X were measured by using a volumetric system from micromeritics ASAP2010. Since ASAP-2010 is designed for surface area and porosimetry measurements and measures the nitrogen isotherm at 77 K it had to be modified to be able to measure different pure gas isotherms at various temperatures. Operation pressure range provided by this system is from 0 to 127 KPa. The molecular drag pump can create vacuums down to 1.3 $*10^{-6}$ KPa in the system.

Volumetric method involves measuring the pressure change in a known volume of sample gas exposed to an adsorbent sample. As the gas is adsorbed and allowed to come to equilibrium with the adsorbent, the measured decrease of pressure in the closed system indicates the amount of gas adsorbed under the given isothermal conditions.

Data were collected for the equilibrium pressure range of 0.001 to 110 KPa at 25, 50 and 75 degree Celsius. Obtaining each complete isotherm consists of 60 to 120 equilibrium point measurements and takes roughly about 12 hours. For each point when the rate of change for pressure is less than 0.01% criterion for equilibrium is satisfied and the system moves to the next point.

Prior to each isotherm measurement, the zeolite 13X was regenerated at 350 °C for 16 hours under a vacuum of less than 1 x 10^{-4} torr. In order to prevent structural damage caused by desorbing water steam a stepwise increase in temperature with simultaneous vacuum was applied to all samples.

The pure gas adsorption isotherm along with the model fit has been shown in **Figure 3.3**. The experimentally determined pure gas isotherms except for CO_2 have been fitted with the Dual Process Langmuir (DPL) model. The experimental isotherm of CO_2 was fitted with three-process Langmuir (TPL) isotherm. The isotherm model parameters have been summarized in **Table 3.4**.

3.3.2 Description of the 4-bed PSA apparatus

A complete and detailed schematic diagram of the 4-bed PSA apparatus is shown in **Figure 3.1**. This is a lab scale fully functional complete PSA experimental setup. There are identical four adsorbent beds, each was packed with 13X zeolite beads. There are

multiple valve manifold on top and bottom of each bed. By opening and closing each valves, a number of flow configuration in and out of each bed can be obtained. For example, for bed-1, at the top of the bed valve-1 was used to withdraw light product during the feed step, valve-2 was opened to equalize with another bed during the pressure equalization step, valve 38 was opened to withdraw the light product produced during the heavy reflux step, valve-3 was opened to feed the light product during the light reflux step, and valve 45 was used to pressurized the bed from the light end with light product. At bottom of the bed-1, valve 6 was opened to introduce the feed gas to the bed, valve-5 was opened during the counter current blowdown step to withdraw the heavy product, and valve-4 was used to feed the bed during the heavy reflux step. Four flow controllers F21, F22, F23 and F24 are used to blend individual pure gas to form the desired feed concentration. In this case, F22 was used for N_2 and F23 was used for CO_2, by setting appropriate flow rate of F22 and F23 the simulated flue gas containing 15% CO_2 in N_2 was produced. Each bed has dedicated line for feed, light product (LP), heavy product (HP), reflux gas isolated by several trains of solenoid valve. For example, Bed 1, 2, 3 and 4 were fed by opening valve 6, 12, 18 and 24 respectively. The light product was drawn from each bed by opening valve 1, 7, 13 and 19 and sent to the light product tank (LP Tank). The PSA cycle studied in this study is a 3-bed 7-step process, so only bed 1, 2 and 3 were used and bed-4 was kept isolated by closing all the valves connected to it. Seven exposed tip, K-type thermocouples were placed axially along the column to measure the temperature profiles. Bed 2,3 and 4 has only 3 thermocouple across the bed. The temperature profiles provided an estimate fo position of the concentration wave fronts within the column. A pressure transducer was placed few inches above each column to measure the column pressure. The

solenoid valves were operated using a spreadsheet based LabVIEW software and different process parameters were recorded in the computer using the same software.

3.3.3 PSA Experiments

The PSA cycle consist of seven different cycle steps namely feed (F), heavy reflux (HR), pressure equalization (E), counter-current blowdown, light reflux purge (LR), and light product pressurization (LPP). The cycle schedule studied is shown in **Table 3.1** and a simple schematic diagram is shown in **Figure 3.2:** Schematic diagram showing various cycle steps in a 3-bed 7-step dual-reflux stripping Pressure Swing Adsorption cycle with one equalization step. All the gas exiting from the light reflux (LR) step is taken out as heavy product (HP).. Simulated flue gas containing 15% CO_2 in N_2 was produced by blending pure CO_2 and N_2 using flow controller F23 and F22 respectively. Each flowmeter was calibrated using a gilibrator for every gas. Details of each of these cycle steps are given below:

The first step of the PSA cycle is the feed step (F) where simulated flue gas (16% CO_2 and 84% N_2) enters bed-1 at high pressure P_H through the heavy end or the feed end of the bed by opening valve 6. The heavy gas, CO_2 is preferentially adsorbed whereas N_2 rich gas leaves the column from the other end via valve 1 and enters the light product tank. The pressure of the bed remains constant during the F step and is equal to the highest operating pressure in the cycle denoted by P_H. A small portion of the light product was sent to bed-3 at low pressure P_L from the light product tank by setting the appropriate flow in flow controller F31 via valve 15 during the light reflux step. All of the light reflux gas coming out of bed-3 via valve 17 was sent to bed-2 via valve 10 to perform heavy reflux step. Flow meter F13 was used to record the flow of the heavy reflux gas. After the feed

step, bed-1 undergoes heavy reflux step, the gas as enters bed-1 at the high pressure P_H during this step via valve 4 and exit the bed via 1. When bed-1 undergoes heavy reflux step, bed-2 undergoes light reflux step. The light reflux gas enters bed-2 via valve 9. After undergoing the HR step bed-1 then equalizes with bed-2. Valve 2 of bed-1 and valve 8 of bed-2 were opened the pressures of these two bed were allowed to equalize and pressure of both bed becomes P_E. After the pressure equalization, step bed-1 was emptied counter currently by exposing it to the vacuum pump to low pressure P_L while keeping the other end closed. The pressure of the bed-2 While bed-1 and bed-2 undergoing pressure equalization step, the pressure of bed-3 was brought back to the feed temperature P_H by light product pressurization step by feeding the light product via valve 47. All three beds in the process undergoes the above mentioned seven steps in a cyclic manner.

3.3.4 PSA Cycle Process Performance Indicators

The PSA process was designed to produce enriched CO_2 as the heavy product and take out N_2 in the light product. The periodic state recovery and purity of CO_2 in the heavy product and the recovery and purity of the N_2 in the light product was used to judge the overall performance of the process, the average mole fraction of CO_2 in the heavy product during the CnD step was taken as the purity of CO_2 in the heavy product. The average mole fraction was calculated by averaging the mole fraction of the streams coming out of the CnD step. The recovery of this process was defined as the total amount of CO_2 produced divided by the total amount of CO_2 fed during the feed. The N_2 recovery in the light product is defined as the total moles of N_2 produced in the light product divided by the total amount of N_2 fed during feed, HR, LR and LPP steps.

Total twenty runs were carried out to study the effect of different process parameters on the overall process performance. The parameters studies was the light reflux ratio, CnD pressure, feed concentration, bed temperature. The bed properties and run conditions during each run (Runs 1 to 6) are shown in **Table 3.3**.

The performance indicators of the PSA process are evaluated in terms of purity, recovery and throughput, which are defined below for feed concentration y_F of CO_2:

$$Purity(\%) = \frac{CO_2(mol)obtained\ as\ product\ during\ A\ step.100}{total\ Product(mol)obtained\ during\ A\ step} \quad (11)$$

$$Recovery(\%) = \frac{CO_2(mol)obtained\ as\ product\ during\ CnD\ step.100}{COH_2(mol)\ fed\ during\ Feed\ step} \quad (12)$$

$$Throughput\left(\frac{L(STP)}{kg.h}\right) = \frac{Fresh\ total\ Feed(L(STP))\ used\ in\ Feed\ step.60}{Mass\ of\ adsorbent(kg)in\ all\ beds} \quad (13)$$

The compressor energy was calculated using the following formula:

$$E_i\left(\frac{kj}{mol}\right) = \frac{1}{n_{CO_2}}\int_0^{t_{step}}\left(\frac{\gamma}{\gamma-1}\right)RT\left[\left(\frac{P_{high}}{P(t)}\right)^{\frac{\gamma-1}{\gamma}}-1\right]\frac{1}{\eta}n(t)dt \quad (14)$$

where t_{step} is the duration of the step feeding the compressor, n_{CO2} is the total moles of CO_2 removed into the heavy product (HP) per cycle during the CnD step and P(t) and n(t) are the time varying pressure and molar flow, respectively, of the stream being fed into the compressor.

3.4 Results and Discussions

3.4.1 PSA Experimental Results

A number of PSA experiments were performed in the 4-bed PSA experimental setup to study the effect of different process parameters on the performance of the psa process. Total twenty runs were carried out to study the effect of various process parameters on the performance of the PSA process. The parameters studied include feed concentration, reflux or purge to feed ratio (γ) in the light reflux step, CnD pressure (P_L) or the pressure ratio (π) by keeping the high pressure constant (P_H) and bed temperature. **Table 3.3**. summarizes all the process conditions for the run E-1 through E-20. The base case is run 2 (E-2) which was conducted at 70 °C bed temperature, total cycle time was 720 sec, reflux ratio 3% and CnD pressure 5 kPa. The CnD pressure (P_L) was controlled by fine-tuning with a needle valve in the vacuum line. The mass balance of all the runs along with the percentage of error was summarized in **Error! Reference source not found.**. The experimental error in all the runs were no more than 4%, which is reasonably accurate.

Figure 3.4 shows the periodic state temperature profiles of three beds during experiment E-1. Only bed-1 is equipped with seven thermocouples (T-1 to T-7) along the bed. Bed 2 and 3 has only three thermocouple placed along the bed at a relative distance of 24.20% (bottom), 47.26% (middle) and 70.31% (top). **Figure 3.4** (a-c) shows the periodic state temperature profile of all three beds for the top, middle and bottom thermocouples. Since all the beds undergoes same cycle steps in a sequential manner, the temperature behavior of all the beds are similar at the periodic state. The periodic state temperature profiles of all seven thermocouples has been plotted in **Figure 3.4**(d). The temperature

profiles shows the progression of the concentration wave through the bed. The first temperature peak corresponds to the temperature rise due to the feed gas. However, the higher temperature peak corresponds to the temperature rise due to higher concentration heavy reflux stream. **Figure 3.5**(a) shows the periodic state pressure profiles of all three beds for a complete PSA cycle of the run E – 1. It is evident from **Figure 3.5**(a) how the beds interact with each other during the course of the PSA process and undergoes the same set of cycle steps in a sequential manner. **Figure 3.5**(b) shows the periodic state pressure profile for bed 1 for the run E-1.

The reflux ratio or the purge to feed ratio (γ) is the ratio of the flow of the purge gas entering the bed during the LR step to that of the feed gas entering the F step. γ is a very important design parameter that has a significant effect on the process performance in terms of recovery and purity of the heavy product [80-83]. A large γ means a lot of light gas enters the bed during the LR step enhancing desorption of the heavy product from the adsorbent and consequently better adsorbent regeneration. However, a large LR flow dilutes the effluent gas that exits the bed undergoing LR step. For a PSA process where the heavy product is produced from LR step, higher γ results in higher CO_2 recoveries but lower CO_2 purity in the heavy product [80-83]. A large γ is necessary to better regenerate the bed and reduce the breakthrough of CO_2 from the light end of the bed during the F and HR steps. The relative dilute LR effluent can be completely recycled back into the system as feed gas to the bed undergoing the HR step while the heavy product can only be produced only form the CnD step.

Experiments E-1, E-2 and E-3 were performed at three different γ by keeping other process parameters the same. **Table 3.6** shows that the CO_2 concentration in the HR stream

decreases as γ was increased (E-1 to E-3). The purity and recovery increases for increased γ. A high γ implies a higher flow of the purge gas which forces more CO_2 to desorb from the adsorbent and exit the bed during the LR step. The bed regenerates better by increasing γ resulting in less CO_2 breakthrough during the F step. As a result, the recovery of CO_2 in the heavy product increases with increasing γ. However, as the total effluent gas exiting the LR step was recycled back to the HR step, a higher γ pushes the high concentration wave front further down the bed. For a given value of γ chosen for operation, one of two scenarios can happen. The higher concentration wave front can be contained inside of the bed depending on how far it travelled through the bed during the HR step or it might breakthrough through the light of the bed for a higher value of γ resulting in loss of CO_2, which causes lower CO_2 recovery. The purity also increases as γ was increased. With increasing γ, the high concentration wave front propagates further down the bed during the HR step, which in turn increases the loading of CO_2 in the solid phase. All CO_2 adsorbed during the HR step subsequently desorb during the CnD step resulting in a high purity heavy product rich in CO_2. However, the higher γ also dilutes the effluent coming out of the LR step which enters the LR step. It is clear from the above discussion that the progression of the higher concentration wave front significantly affects the process performances such a CO_2 purity, CO_2 recovery in the heavy product.

The next important parameter in a PSA process design is the pressure ratio (π). The pressure ratio (π) is defined as the ratio of the highest pressure (P_H) to the lowest pressure (P_L) in the cycle. If the highest pressure P_H is kept constant then a higher π implies that the compressors are required to pull a deeper vacuum in the PSA beds during the regeneration steps. The desertion of CO_2 from the adsorbent strongly depends upon π and thus affects

the process performances in terms of CO_2 purity and recovery in the heavy product. A higher π for a constant P_H means a lower P_L, which results in better desorption of CO_2 during both CnD and LR steps resulting in higher CO_2 bed capacity. **Figure 3.7** shows the effect of π on CO_2 purity and CO_2 recovery in the heavy product for a constant throughput of 404 L_{STP}/hr/kg. The parameters held constant for each run are bed temperature (70 °C), high pressure (P_H = 120 kPa), purge to feed ration (γ = 3%), CO_2 feed concentration (16%), feed temperature (25 °C) and total feed flow rate. It is evident that both CO_2 purity and recovery decreases by increasing the low pressure PL. More CO_2 is desorbed for lower PL (increased π) and taken as heavy product during the CnD step. More CO_2 in the heavy product for lower PL increases the CO_2 purity and recovery. Lower PL also helps desorbs more CO_2 from the adsorbent thereby increasing the bed capacity resulting in less CO_2 breakthrough during F and HR steps. For a constant feed throughput, total moles entering the system is the same. As a result, if more moles of CO_2 is desorbed during the CnD step for a lower PL and removed as a heavy product during the CnD step, which in turn will hamper the progression of the higher concentration wave front through the bed. Despite a higher concentration wave font not penetrating deeper into the bed during the HR step for experiments with lower PL compared to an experiment with higher PL, a large CO_2 purity in the heavy product can be obtained provided a deeper vacuum is pulled in the beds. This proves that the purity of CO_2 in the heavy product does not only depend upon the propagation of the higher concentration wave front during the HR step but also on the low pressure during the CnD step.

The effect of temperature on the CO_2 recovery and purity is shown in **Figure 3.13**. Both CO_2 recovery and purity decreases initially for 70 C and then increases in the

experiment performed at 100 C. The temperature plays an important role in determining the working capacity of the adsorbent. A higher temperature also helps desorb the heavy component during CnD step and LR step.

3.4.2 Model Prediction of the PSA experimental results

In a previous study, the dynamic adsorption process simulator (DAPS) was validated against the experiments performed in the 1-bed PSA apparatus. The DAPS model was validated against the experimental data obtained in the five runs in single bed psa apparatus described in previous study. This validated DAPS was used to predict the experimental results of the 4-bed psa apparatus. The simulations was performed using the equilibrium and kinetic information of the 13X zeolite for the given gases independently in separate measurement methods. As explained before the equilibrium isotherm of both CO_2 and N_2 on 13X zeolite was obtained using the micromeritics ASAP 2010 for three different operating temperatures. The mass transfer coefficients of CO_2 and N_2 was obtained using the rapid pressure swing apparatus (RPSA). In these simulations one parameter mass transfer coefficient with energy balance was used. The main heat transfer resistance is between the solid and gas phase inside of the column wall. In order to remove the heat transfer of the wall and outside the wall thickness was considered negligible. The heat transfer coefficient was obtained by fitting the temperature profile of the bed of a pure N_2 purge run. Heat transfer and mass transfer coefficients were not changed in any simulation. Only the valve coefficient of different steps was changed in order to match the pressure history of the bed during a complete cycle.

In **Figure 3.9**, the model predicted pressure profile of the bed was plotted against the experimental pressure profile of the bed-1 at the periodic state for the entire PSA cycle

of run E-1. The PSA cycle consists of 7 steps namely feed step (F), heavy reflux step (HR), pressure equalization down step (E), counter-current blowdown step (CnD), light reflux step (LR), equalization step up (E*) and light product pressurization step (LPP). The experimental data was represented as the open circle whereas the solid line shows the model prediction. As it can be seen from the figure the DAPS can predict exactly the experimental pressure profile of the bed. It is very important to have a correct estimation of the individual component isotherms, mass transfer coefficients and heat transfer coefficients. The pressure profile was matched only adjusting the respective valve coefficients of each step no other parameter was adjusted.

In **Figure 3.10**, the experimental temperature profiles at periodic state for seven different thermocouples in the bed-1 was plotted against the DAPS predicted temperature profiles for the run E-1. The open circles represent the experimental data whereas the solid lines represent the model predictions. The experimental and model prediction of seven thermocouples (T-1 to T-7) were plotted separately in **Figure 3.10**(a) – (g) in order for better comparison. In **Figure 3.10**(h) the model prediction of all the thermocouples (T-1 to T-7) are plotted together. The relative locations of the thermocouples along the bed-1 are T-1: 12.68%, T-2: 24.02%, T-3: 35.73%, T-4: 47.26%, T-5: 58.78%, T-6: 70.31%, and T-7: 81.83%. Because of a higher heat of adsorption of CO_2 there is a temperature rise during adsorption and the temperature rise indicates the location of the concentration front in the bed. The first peak in the **Figure 3.10**(a) – (g) is due to the feed gas. The second peak in **Figure 3.10**(a) - (d) is due to the heavy reflux gas. The temperature rise during the heavy reflux is more than that happens during feed because CO_2 concentration is higher in the heavy reflux stream. The feed concentration is 15% CO_2 whereas the concentration in the

heavy reflux stream is in the range 75 - 85% CO_2. The progression of the concentration front can be tracked by observing the temperature rise peak in the temperature profile of all the thermocouple. It can be seen that the second peak only reaches until thermocouple T-4 which is 47.26% in the bed that means the front location is between 47.26% and 58.78% of the bed. However, the feed wave front reached until T-7 and a very small amount of CO_2 broke through during this experiment. Using the equilibrium isotherms of individual component determined using micromeritics ASAP 2010 and mass transfer coefficients determined from the single gas cyclic experiment in RPSA setup, the model was able to predict accurately the temperature profiles and position of the higher concentration front during the heavy reflux step for the entire PSA cycle for E – 1. The comparison of the experiment with simulation prediction of CO_2 purity and CO_2 recovery in the heavy product for all five runs are shown in **Table 3.7**. The results show a close agreement between experiments and model.

The energy consumed for each run was calculated using equation (14) and summarized in **Table 3.8**. The effect on the energy consumed by the PSA process for change in the reflux ratio, CnD pressure and bed temperature were studied. **Figure 3.11** shows the energy consumed (kJ/mol of CO_2 removed) by the PSA unit cumulatively during the CnD step and the LR step for changing the light reflux ratio (γ). For each case the energy consumption was calculated for the compressor efficiency 80%. **Figure 3.11** shows that the energy consumption increases by increasing γ. Operating at higher γ means more gas exit the LR step, which recycled back completely to the HR step. The more energy consumption is due to the higher flow rate. The base case met the DOE criteria of 90%

CO_2 recovery, 95% CO_2 purity and energy consumption of less than 20 kJ/mol CO_2 captured.

Figure 3.12 shows the energy consumption for three different CnD pressures (PL), 5, 7 and 10 kPa. The highest pressure of the process (PH) was kept constant for all three runs. As it be seen from **Figure 3.12** that the energy consumption is lower for 7 kPa as compared to 5 kPa as expected. However, the energy consumption increases for 10 kPa compared to that of 7 kPa. For each case, the energy consumption was calculated for compressor efficiency 80%. The higher PL (i.e. lower π) is not sufficient enough to effectively regenerate the bed during the CnD and LR steps which lowers the CO_2 recovery in the HP. Therefore, a higher PL means less work done by the compressor (kJ), the energy consumed (kJ/mol of CO_2 produced) is high due to low CO_2 recovery in the heavy product.

Figure 3.13 shows the effect of energy consumption (kJ/mol of CO_2 captured) for three different temperatures 25, 70 and 100 °C. The energy consumption increases by increasing temperature. From equation (14), it can be seen that the energy consumption is directly proportional to the operating temperature, which explains the increase in energy for increasing temperature.

3.5 Conclusion

A pressure swing adsorption (PSA) process described that is cable of separating CO_2 from flue gas using 13X zeolite as adsorbent by a dual-reflux PSA cycle. The feed gas considered as a simulated dry flue gas consisting of 15.9% CO_2 and balance N_2 that was fed at 121 kPa and at 25 °C. A unique combination of cycle steps consisting of three beds

was able to produce high purities (>90%) and high recoveries (>90%) of CO_2 in the heavy product. The throughput achieved experimentally was 404 L_{STP}/hr/kg. A comprehensive experimental study was performed to determine the effect of different process conditions such as feed concentration, purge to reflux ratio, pressure ratio, bed temperature on the CO_2 purity, CO_2 recovery in the heavy product and the energy consumption (kJ/mol CO_2 captured) by the PSA process.

The study showed that purge to feed ratio has significant effect on the process performance. The CO_2 recovery increased as the purge to feed ratio was increased. For all the experiment, the total effluent coming out of the LR step was recycled back as the feed to the HR step. By increasing, the purge to feed ratio more CO_2 desorbs during the LR step and the bed regenerated better, but it also pushes the high concentration wave front further up the bed during the HR step. A smaller value of the purge to feed ratio causes less regeneration of the bed and the high concentration wave front does not travel though the bed more. Increasing value of the purge to feed ratio also increases the purity and recovery of the CO_2. A higher value of the purge to feed ratio physically means large flow rates exiting from the LR step, which increases the energy consumption of the PSA process.

Pressure ratio also had a significant effect on the CO_2 recovery and CO_2 purity in the heavy product. Operating at a deeper vacuum resulted in greater CO_2 desorption and better bed regeneration. As the CnD pressure (P_L) was increased, i.e. pressure ratio decreased the CO_2 purity and CO_2 recovery both were decreased. The CO_2 recovery was decreased when operated at lower pressure ratio causing the energy consumption increase.

The effect of temperature and feed concentration was also studies. The CO_2 recovery and CO_2 purity in the heavy product increased by increasing the temperature. The energy consumption also increased upon increasing temperature. Three different feed concentration was used 15.9%, 14.59% and 10%. The CO_2 recovery and CO_2 purity in the heavy product was increased with increasing CO_2 concentration in the feed.

A validated dynamic adsorption process simulator (DAPS) was used to predict a number of experimental results. The dynamic adsorption process simulator (DAPS) was used to predict the experimental results for different process conditions using equilibrium isotherms of the individual components measured at three different temperatures independently using micromeritics ASAP 2010 and the mass transfer coefficients determined using the single gas cycling using a rapid pressure swing adsorption apparatus. The model successfully predicts the pressure and temperature profiles and performance of each experiment. DAPS successfully capture the location of the concentration front in the bed without any adjustable parameters. The agreement between the experiment and simulation results also validate the single component adsorption isotherm and mass transfer coefficient measure independently. The reason simulation predicted temperature profiles did not match perfectly with the experiment was that there is only one lumped heat balance was used. However, the model does excellent job in predicting the location of the temperature peaks.

3.6 Tables

Table 3.1: The cycle schedule of the experiment performed.

FEED			HR	E	CnD	LR	E*	LPP
HR	E	CnD	LR	E*	LPP	FEED		
LR	E*	LPP	FEED			HR	E	CnD
120	20	100	120	20	100	120	20	100

Table 3.2: Initial and boundary conditions for different steps of the PSA process.

Step	Time and Bed Location	Initial, Boundary conditions and balances
		PSA cycles
Feed (F)	t = 0	$y_i=y_{i,LPP}$, $T = T_{LPP}$, $q_i = q_{i,LPP}$ (at all z)
	z/L = 0	$y = y_{i,F}$, $F = F_F$, LDFE, $T = T_F$, M.B. (at all t)
	z/L = 1	C.M.B., O.M.B., LDFE, E.B. ($T_o = T_F$), V.E. ($P_o=P_H$) (at all t)
Heavy Reflux (HR)	t = 0	$y_i=y_{i,F}$, $T = T_F$, $q_i = q_{i,F}$ (at all z)
	z/L = 0	$y = y_{i,HR}$, $F = F_{HR}$, LDFE, $T = T_{HR}$, M.B. (at all t)
	z/L = 1	C.M.B., O.M.B., LDFE, E.B. ($T_o = T_F$), V.E. ($P_o=P_H$) (at all t)
Equalization (E)	t = 0	$y_i=y_{i,HR}$, $T = T_{HR}$, $q_i = q_{i,HR}$ (at all z)
	z/L = 0	C.M.B., v = 0, LDFE, E.B. ($T_o = T_F$) (at all t)
	z/L = 1	C.M.B., O.M.B., LDFE, E.B. ($T_o = T_F$), V.E. ($P_o=P_H$) (at all t)
Counter-current depressurization (CnD)	t = 0	$y_i=y_{i,HR}$, $T = T_{HR}$, $q_i = q_{i,HR}$ (at all z)
	z/L = 0	C.M.B., O.M.B., LDFE, E.B. ($T_o = T_F$), V.E. (at all t)
	z/L = 1	C.M.B., v = 0, LDFE, E.B. ($T_o = T_F$) (at all t)
Light reflux (LR)	t = 0	$y_i=y_{i,CnD}$, $T = T_{CnD}$, $q_i = q_{i,CnD}$ (at all z)
	z/L = 0	C.M.B., O.M.B., LDFE, E.B. ($T_o = T_F$), V.E. (at all t)
	z/L = 1	$y = y_{i,LR}$, $F = -F_{LR}$, LDFE, $T = T_F$, M.B. (at all t)
Equalization (E*)	t = 0	$y_i=y_{i,LR}$, $T = T_{LR}$, $q_i = q_{i,LR}$ (at all z)
	z/L = 0	C.M.B., O.M.B., LDFE, E.B. ($T_o = T_F$), v = 0 (at all t)
	z/L = 1	$y = y_{i,E1D,z/L=1}$, $F = -F_{E1D,z/L=1}$, LDFE, $T = T_F$, M.B. (at all t)
Light Product pressurization (LPP)	t = 0	$y_i=y_{i,E1R}$, $T = T_{E1R}$, $q_i = q_{i,E1R}$ (at all z)
	z/L = 0	C.M.B., v = 0, LDFE, E.B. ($T_o = T_F$) (at all t)
	z/L = 1	$y = y_{i,LPP}$, $F = -F_{LPP}$, LDFE, $T = T_F$, M.B. (at all t)

Table 3.3: Properties and Operating conditions

Properties	Values
Bed Characteristics	
Length (m)	0.50165
Internal Radius (m)	0.0254
Bed porosity	0.425
Bulk density (kg/m^3)	632.8
External Heat transfer Coefficient ($kW/m^2/K$	0.0024
Wall	
Material	SS 316
Thickness (mm)	4.0
Heat capacity (kJ/kg/K)	0.468
Density (kg/m^3)	8.24
Adsorbent	
Material	Zeolite 13X
Pellet density (kg/m^3)	1100.0
Pellet porosity	0.54
Pellet heat capacity (kJ/kg/K)	1.1
Operation	See table 3
Feed flow (SLPM)	13.0
CO_2 concentration (Balance N_2, %)	15.9
Feed and external temperature (^oC)	25.0
Light reflux ratio*	0.02-0.05
High pressure, P_H (kPa)	121.0
Low pressure, P_L (kPa)	5.0, 7.0, 10.0
Cycle time (s)	720
Feed step (s)	240
Counter current depressurization (CND) step (s)	100
Light reflux step (LR) (s)	120
Light product pressurization (LPP) step (s)	100
Heavy Reflux (HR) step (s)	120
Equalization (Eq) step (s)	20
Gasses	
CO_2	
Isotherm	See Table 4
LDF Mass transfer Coefficient (1/s)	
Nitrogen	
Isotherm	See Table 4
LDF Mass transfer Coefficient (1/s)	

*** Volume fraction of the product flow leaving the feed step used in LR step**

Table 3.4: Three process Langmuir isotherm parameters for CO_2 and N_2.

Parameter	CO_2	N_2
ns1 [mole/kg]	1.338	0.438
ns2 [mole/kg]	2.238	0.733
ns3 [mole/kg]	1.853	0.607
b01 [1/kPa]	2.4419E-08	7.595E-07
b02 [1/kPa]	4.5204E-08	7.595E-07
b03 [1/kPa]	1.3737E-08	7.595E-07
B21 [K]	5757.03	2370.32
B22 [K]	4606.08	2370.32
B23 [K]	4224.86	2370.32

Table 3.5: Experimental Conditions of the PSA Experiments.

Bed Temp [°C]	Exp. No	Feed Throughput [L_{STP}/hr/kg]	Feed CO_2 Conc. [%]	Reflux Ratio [%]	P_H [kPa]	P_L [kPa]	P_H/P_L
70	E-1	404	16.00	2.0	122.61	5.02	24.41
	E-2	404.31	16.05	3.0	121.6	5.0	24.29
	E-3	404.29	16.05	4.0	121.2	5.1	23.66
	E-4	404	16.00	3.0	122.70	7.01	17.51
	E-5	404	16.00	4.0	122.56	6.94	17.65
	E-6	404	16.00	4.0	122.41	10.28	11.91
	E-7	397.39	14.59	2.0	121.3	5.0	24.14
	E-8	397.39	14.59	3.0	120.8	7.2	16.83
	E-9	397.40	14.59	4.0	120.7	7.0	17.33
	E-10	397.35	14.59	4.0	122.1	10.0	12.26
	E-11	405.72	10.04	3.0	121.65	5.06	24.06
	E-12	405.64	10.04	5.0	121.34	5.06	23.98
100	E-13	404	16.00	3.0	121.16	5.02	24.13
	E-14	404	16.00	2.0	121.33	5.04	24.06
	E-15	397.32	14.59	3.0	121.8	5.0	24.21
	E-16	397.31	14.59	2.0	121.1	5.1	23.56
25	E-17	404	15.99	3.0	121.09	5.50	22.01
	E-18	404	15.99	2.0	122.62	4.97	24.69
	E-19	404	15.99	3.0	121.1	5.5	22.01
	E-20	404	15.99	2.0	122.6	4.97	24.69

Table 3.6: Summary of PSA Cycle experimental results.

Temp	Exp	Feed CO_2 Conc.	P_L	R.R.	CO_2 Conc HR	CO_2 HP		N_2 LP	
[°C]		[%]	[kPa]	[%]	[%]	% Pur	% Rec	% Pur	% Rec
70	E-1	16.00	5.02	2.0	85.09	96.83	91.68	98.70	98.35
	E-2	16.05	5.01	3.0	78.67	95.43	90.81	98.48	96.52
	E-3	16.05	5.12	4.0	75.07	96.54	94.06	98.48	96.28
	E-4	16.00	7.01	3.0	80.17	94.44	82.32	96.40	96.82
	E-5	16.00	6.94	4.0	80.23	95.93	[illegible]	.25	98.18
	E-6	16.00	10.28	4.0	77.12	93.68	70.39	94.50	97.80
	E-7	14.59	5.02	2.0	85.39	95.57	88.34	98.04	96.34
	E-8	14.59	7.18	3.0	82.79	93.43	81.74	97.17	96.67
	E-9	14.59	6.97	4.0	78.23	94.01	84.22	97.59	96.20
	E-10	14.59	9.96	4.0	79.24	91.04	71.26	95.43	96.34
	E-11	10.04	5.06	3.0	73.19	86.79	90.62	99.16	96.54
	E-12	10.04	5.06	5.0	66.76	86.46	97.01	99.53	96.52
100	E-13	16.00	5.02	3.0	81.29	97.61	93.17	98.64	97.62
	E-14	16.00	5.04	2.0	85.67	97.47	89.58	98.16	98.23
	E-15	14.59	5.03	3.0	80.51	91.23	89.76	91.23	89.76
	E-16	14.59	5.14	2.0	90.43	94.27	89.01	97.89	97.17
25	E-17	15.99	5.50	3.0	83.58	96.05	91.66	98.27	97.83
	E-18	15.99	4.97	2.0	87.73	96.81	91.68	98.44	97.98
	E-19	14.59	4.99	3.0	90.43	94.23	92.70	97.89	95.43
	E-20	14.59	5.04	2.0	80.85	93.93	87.62	98.58	95.30

Table 3.7: Summary of PSA cycle experimental results compared with Simulation results.

Temp	Exp	P_L	R.R.	HP CO_2 Rec [%]		HP CO_2 Pur [%]	
[°C]		[kPa]	[%]	Experiment	Modeling	Experiment	Modeling
70	E-1	5.02	2.0	91.68	88.64	96.83	95.87
	E-2	5.01	3.0	90.81	90.11	95.43	95.58
	E-3	5.12	4.0	94.06	92.10	96.54	95.60
	E-5	6.94	4.0	87.16	86.15	95.93	95.72
	E-6	10.28	4.0	70.39	70.00	93.68	94.28
	E-11	5.06	3.0	90.62	87.32	86.79	86.24
100	E-13	5.02	3.0	93.17	91.00	97.61	96.86
25	E-17	5.50	3.0	91.66	81.13	96.05	93.60

Table 3.8: Energy consumption of some of the experiment evaluated from simulation.

Experiment	Energy [kJ]	Energy [kJ/mol of CO_2]
E-1	5.92	17.93
E-2	6.26	18.63
E-3	6.58	19.17
E-5	5.39	16.73
E-6	4.42	17.10
E-11	4.48	22.02
E-13	6.80	20.12
E-17	5.03	16.70

3.7 Figures

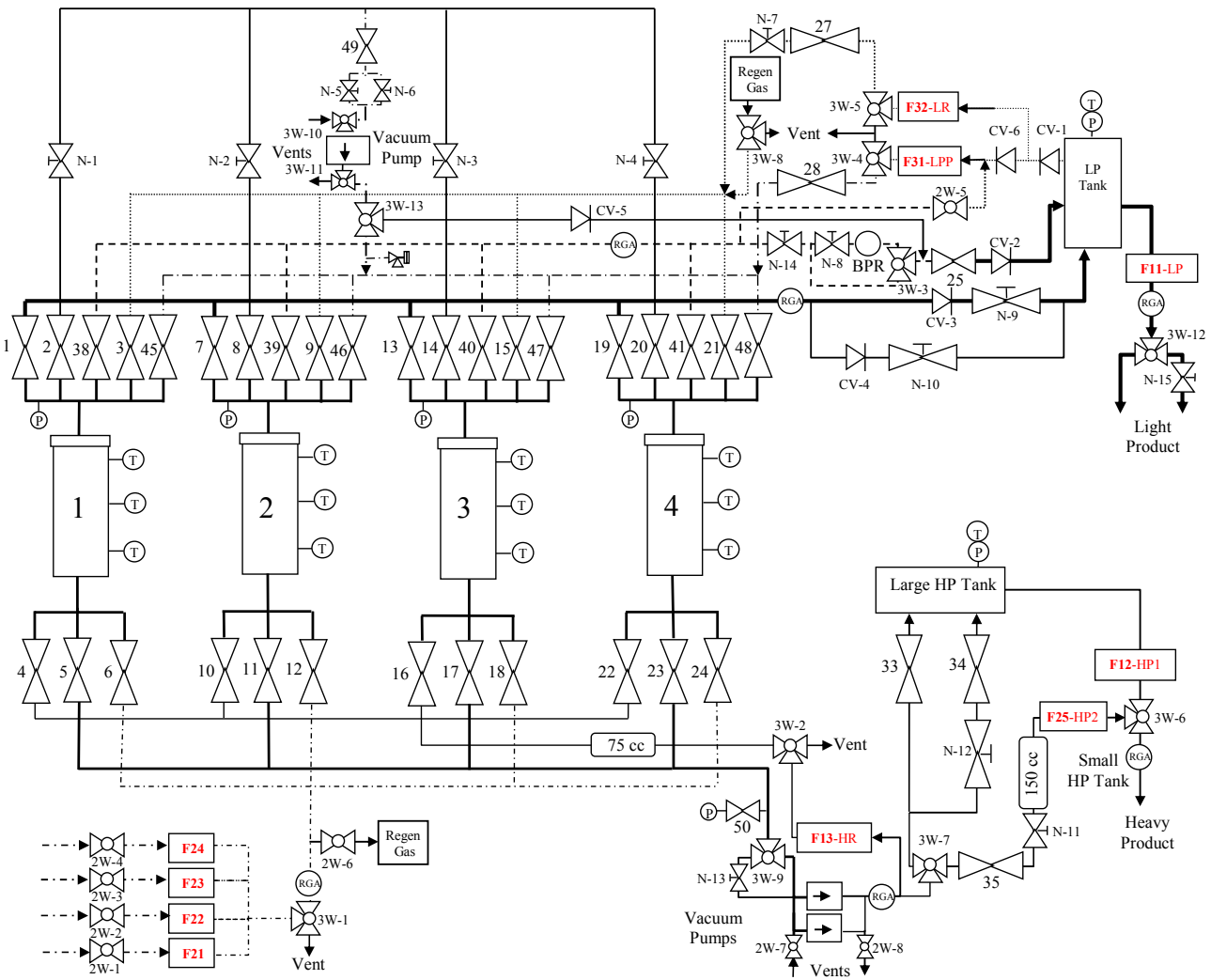

Figure 3.1: A detailed schematic diagram of the 4-bed PSA apparatus.

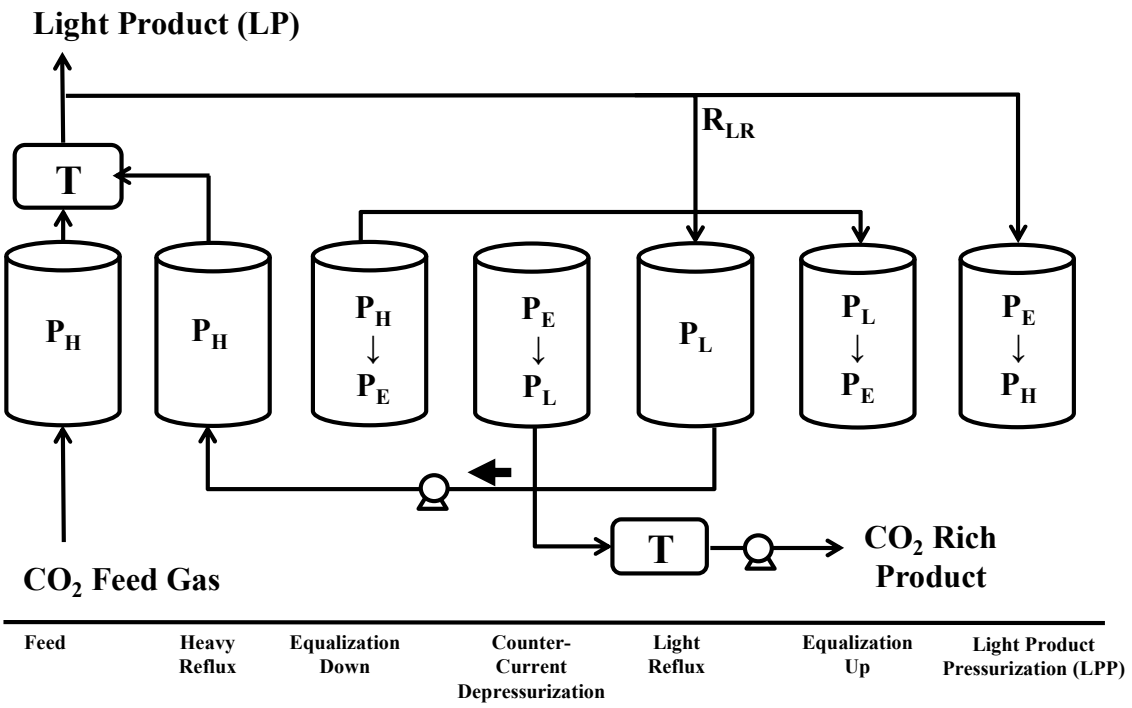

Figure 3.2: Schematic diagram showing various cycle steps in a 3-bed 7-step dual-reflux stripping Pressure Swing Adsorption cycle with one equalization step. All the gas exiting from the light reflux (LR) step is taken out as heavy product (HP).

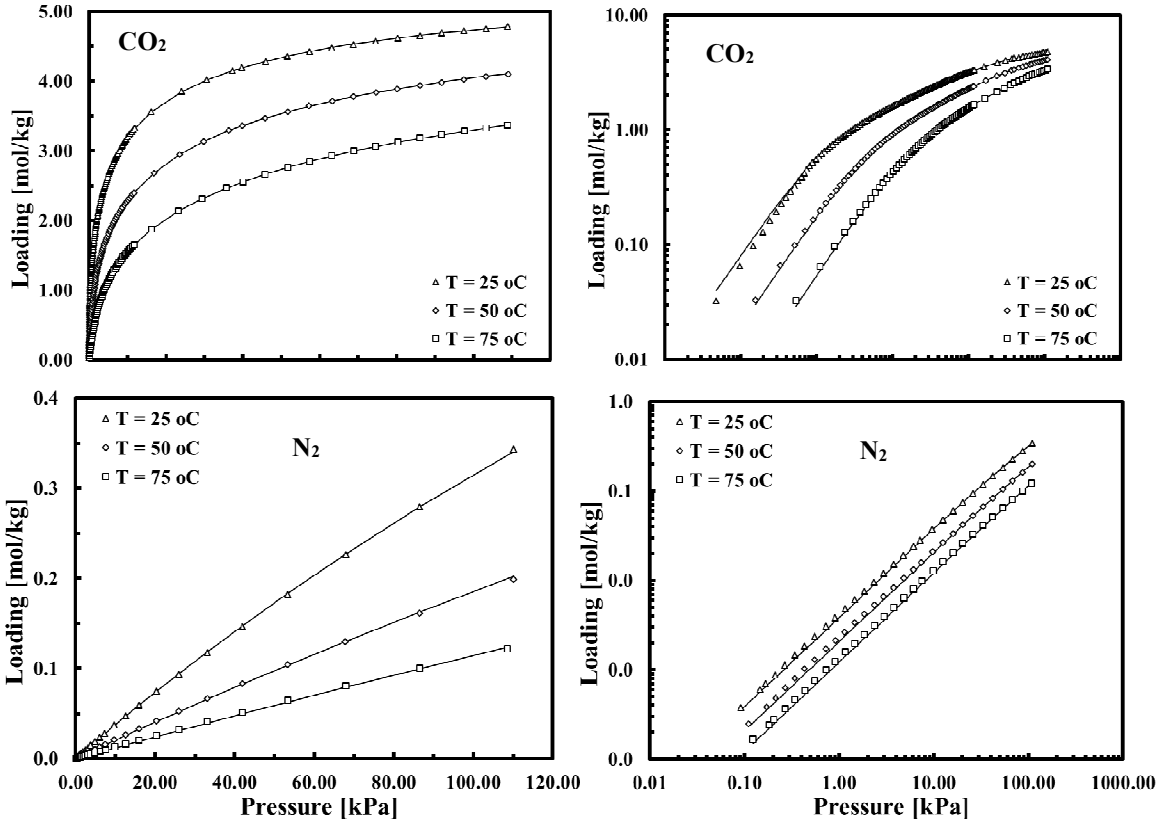

Figure 3.3: Isotherms of Carbon dioxide and Nitrogen at three different temperatures in linear (left) and log-log scale (right). The solid lines represent the model fits and the markers represent the experimental data.

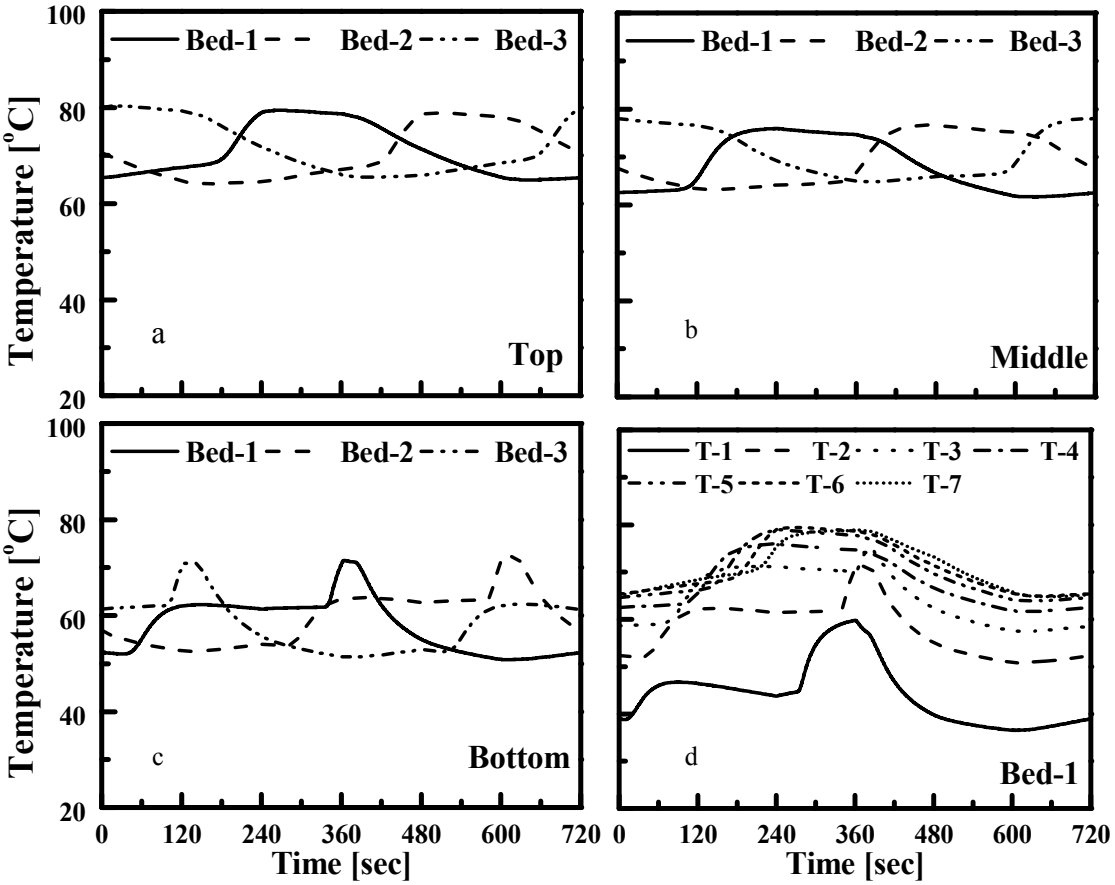

Figure 3.4: Periodic state temperature profiles of bed-1,2 and 3 for the experiment E-1; a) top thermocouple placed at 70.31% of length of each bed, b) middle thermocouple placed at the 47.26% of length of each bed, c) bottom thermocouple placed at the 24.20% of the length of each bed, d) temperature history of bed-1 at 7 different equidistant locations along the bed (1:12.68%, 2:24.20%, 3:35.73%, 4:47.26%, 5:58.78%, 6:70.31%, 7:81.83%).

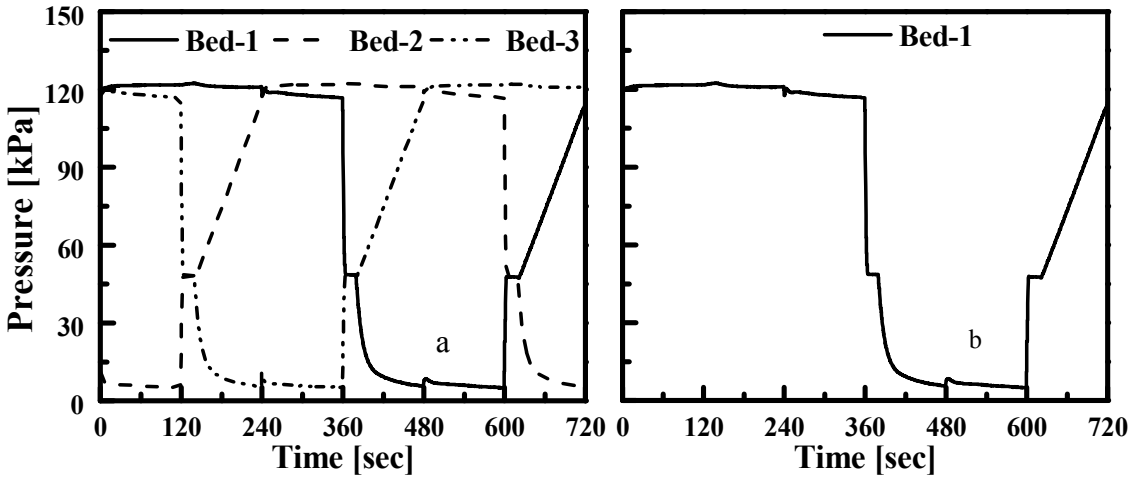

Figure 3.5: Pressure history for all 3 beds during one entire cycle (left) and pressure history for only bed-1 during one entire cycle (right) of experiment E-1.

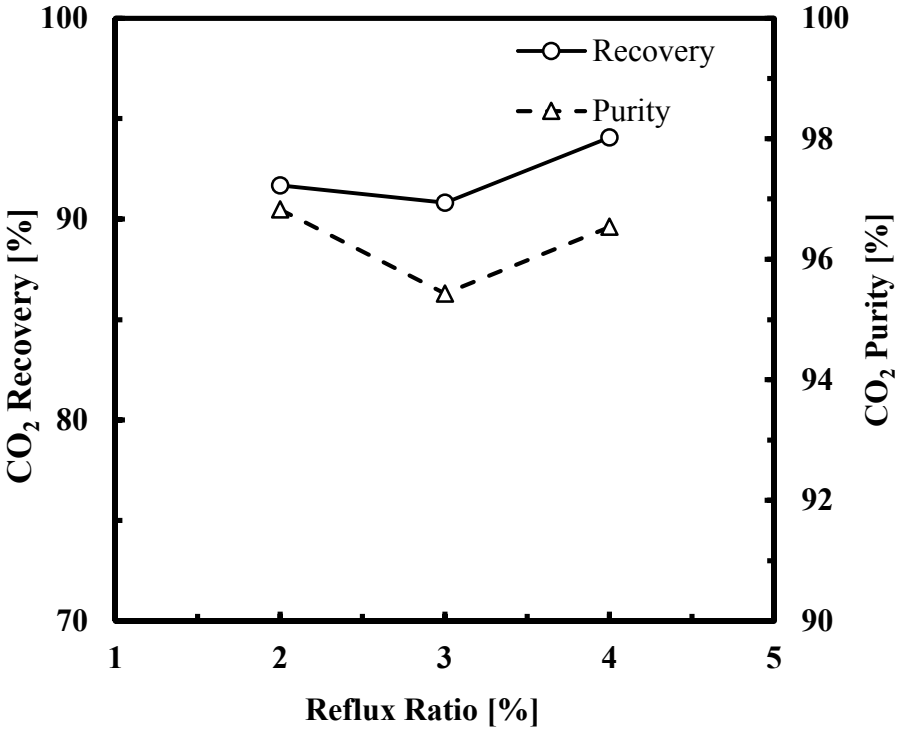

Figure 3.6: Effect of reflux ration on the CO_2 purity and CO_2 recovery in the heavy product.

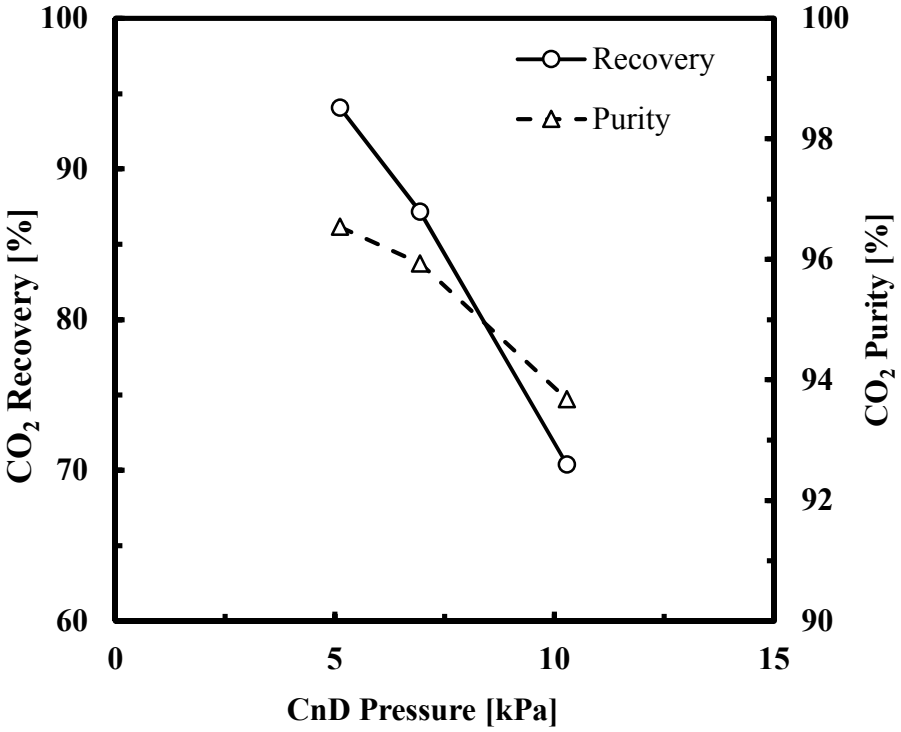

Figure 3.7: Effect of CnD pressure (i.e. pressure ratio, π) on CO_2 purity and CO_2 recovery in the heavy product.

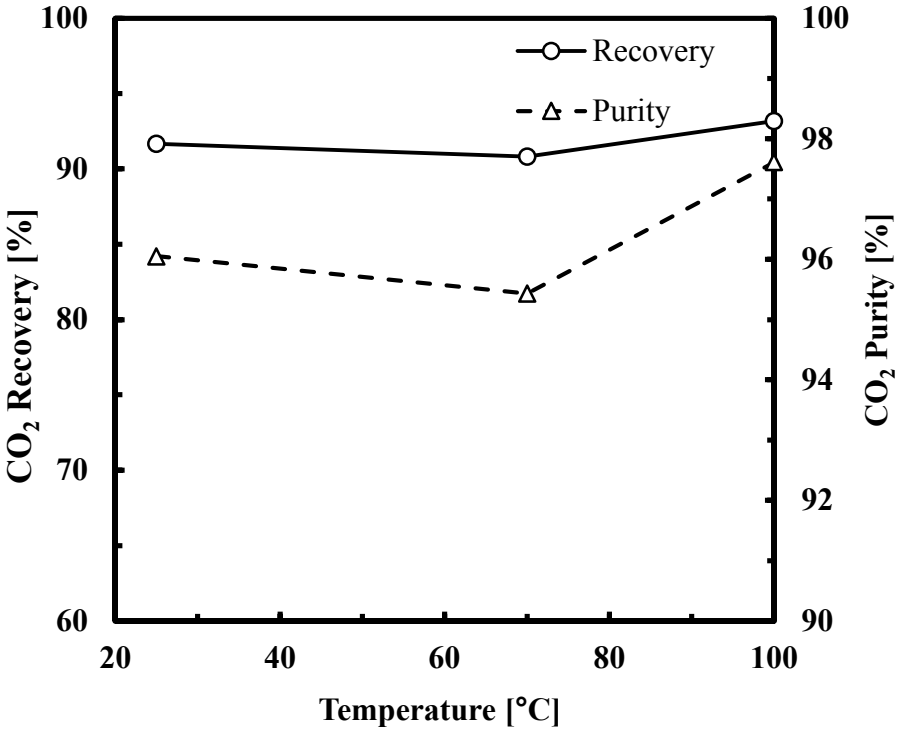

Figure 3.8: Effect of temperature on the CO_2 purity and CO_2 recovery in the heavy product.

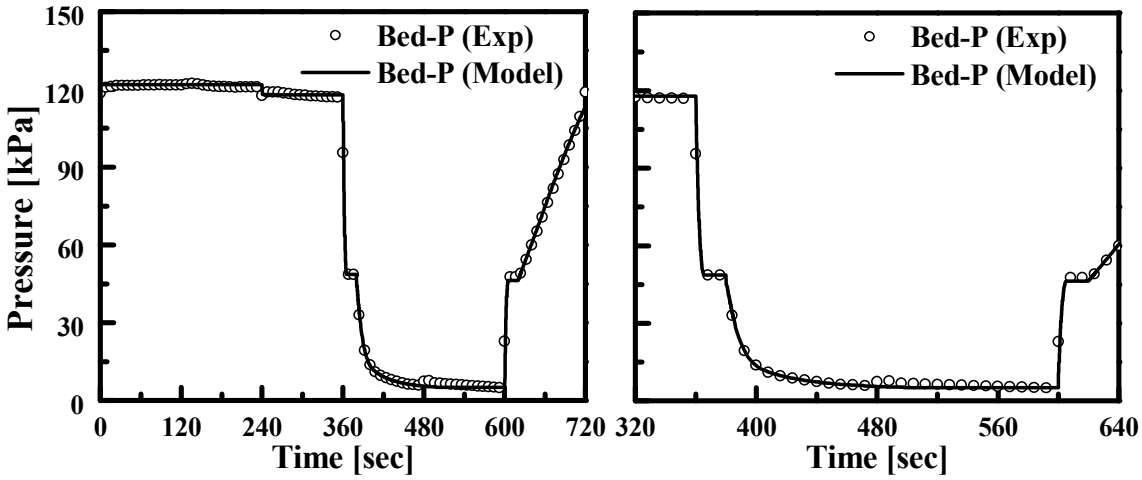

Figure 3.9: Pressure history of Bed-1 during one entire cycle for E1, plotted against the pressure history as predicted by simulation (M-1).

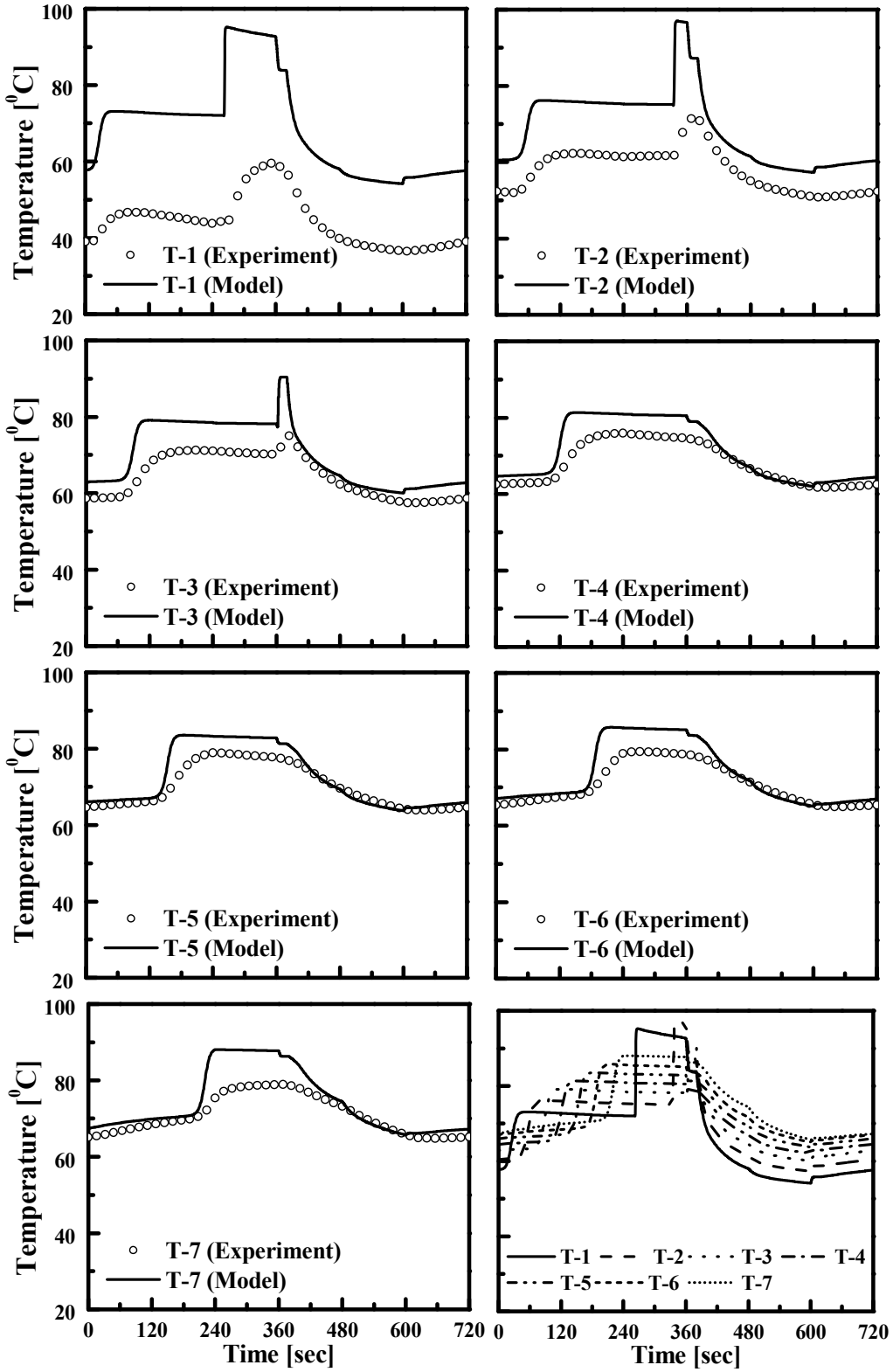

Figure 3.10: Comparison of experiment and model temperature histories for E-1 & M-1. (1:12.68%, 2:24.20%, 3:35.73%, 4:47.26%, 5:58.78%, 6:70.31%, 7:81.83%).

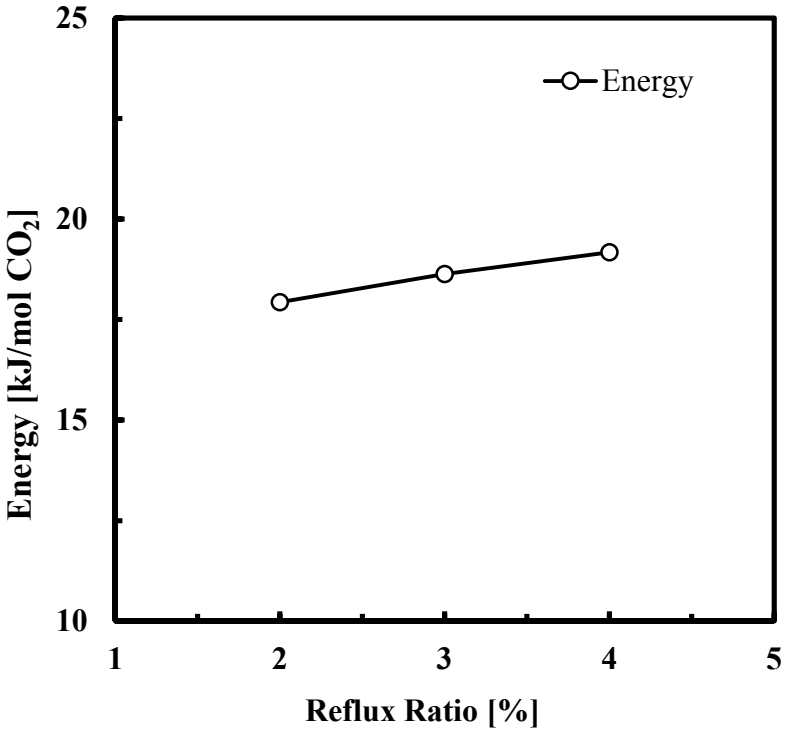

Figure 3.11: Effect of reflux ratio on the energy consumption of the psa process.

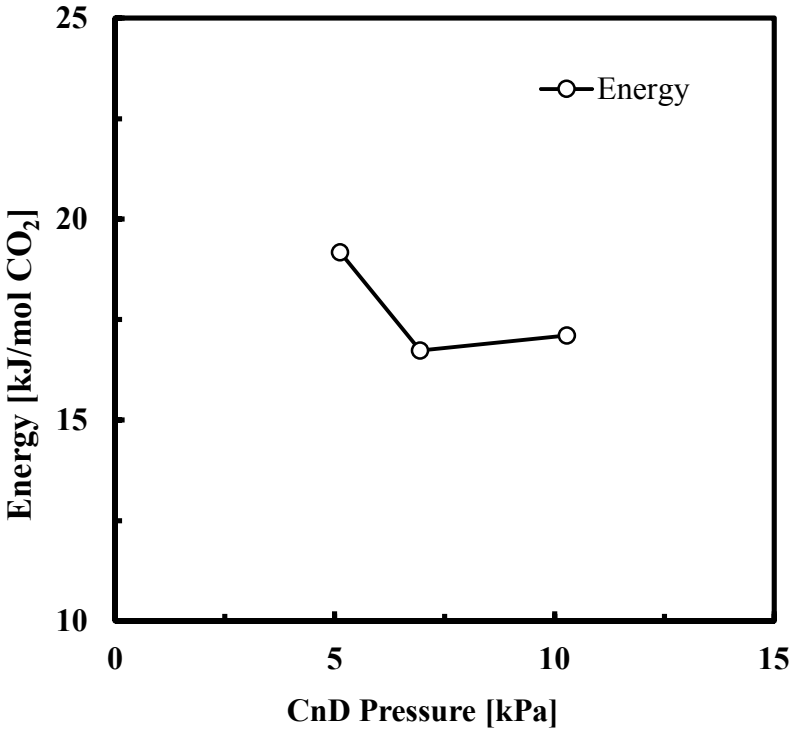

Figure 3.12: Effect of CnD pressure on the energy consumption of the psa process.

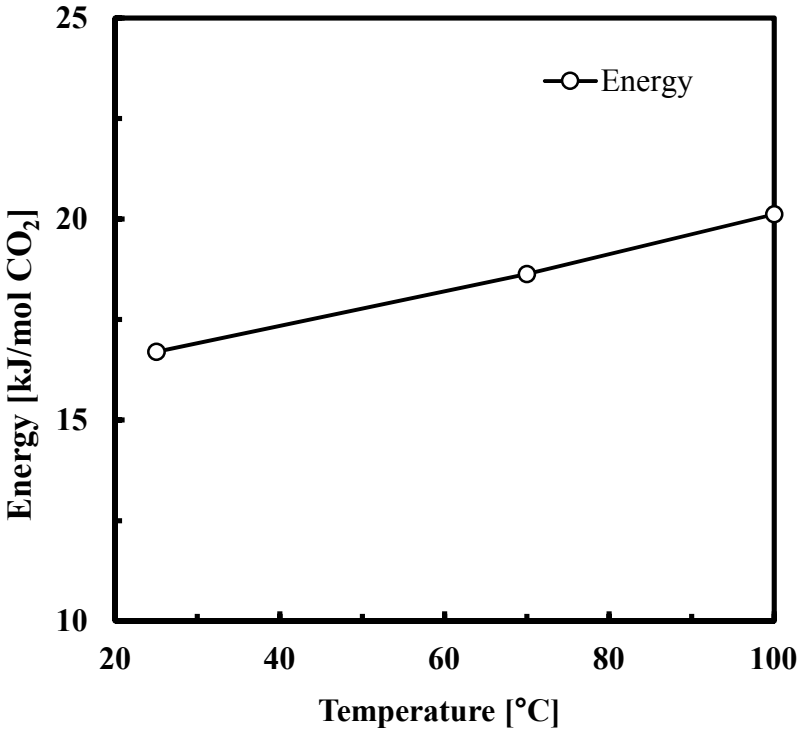

Figure 3.13: Effect of temperature on the energy consumption of the psa process.

REFERENCES

[1] D. Aaron and C. Tsouris, "Separation of CO_2 from Flue Gas: A Review," *Separation Science and Technology,* vol. 40, pp. 321-348, 2005.

[2] A.-T. Vu, Y. Park, P. R. Jeon, and C.-H. Lee, "Mesoporous MgO sorbent promoted with KNO3 for CO2 capture at intermediate temperatures," *Chemical Engineering Journal,* vol. 258, pp. 254-264, 12/15/ 2014.

[3] N. Díez, P. Álvarez, M. Granda, C. Blanco, R. Santamaría, and R. Menéndez, "CO2 adsorption capacity and kinetics in nitrogen-enriched activated carbon fibers prepared by different methods," *Chemical Engineering Journal,* vol. 281, pp. 704-712, 12/1/ 2015.

[4] D. Bahamon and L. F. Vega, "Systematic evaluation of materials for post-combustion CO2 capture in a Temperature Swing Adsorption process," *Chemical Engineering Journal,* vol. 284, pp. 438-447, 1/15/ 2016.

[5] R. T. Yang, *Gas separation by adsorption processes*: Butterworth-Heinemann, 2013.

[6] J. Yang and C.-H. Lee, "Adsorption dynamics of a layered bed PSA for H2 recovery from coke oven gas," *AIChE Journal,* vol. 44, pp. 1325-1334, 1998.

[7] K. T. Chue, J. N. Kim, Y. J. Yoo, S. H. Cho, and R. T. Yang, "Comparison of Activated Carbon and Zeolite 13X for CO_2 Recovery from Flue Gas by Pressure Swing Adsorption," *Industrial & Engineering Chemistry Research,* vol. 34, pp. 591-598, 1995.

[8] H. Yang, Z. Xu, M. Fan, R. Gupta, R. B. Slimane, A. E. Bland*, et al.*, "Progress in carbon dioxide separation and capture: A review," *Journal of Environmental Sciences,* vol. 20, pp. 14-27, // 2008.

[9] M. Hefti, D. Marx, L. Joss, and M. Mazzotti, "Adsorption equilibrium of binary mixtures of carbon dioxide and nitrogen on zeolites ZSM-5 and 13X," *Microporous and Mesoporous Materials,* vol. 215, pp. 215-228, 10/1/ 2015.

[10] T.-H. Bae, M. R. Hudson, J. A. Mason, W. L. Queen, J. J. Dutton, K. Sumida*, et al.*, "Evaluation of cation-exchanged zeolite adsorbents for post-combustion carbon dioxide capture," *Energy & Environmental Science,* vol. 6, pp. 128-138, 2013.

[11] M.-B. Kim, Y.-S. Bae, D.-K. Choi, and C.-H. Lee, "Kinetic Separation of Landfill Gas by a Two-Bed Pressure Swing Adsorption Process Packed with Carbon Molecular Sieve: Nonisothermal Operation," *Industrial & Engineering Chemistry Research,* vol. 45, pp. 5050-5058, 2006/07/01 2006.

[12] H.-H. Lee, H.-J. Kim, Y. Shi, D. Keffer, and C.-H. Lee, "Competitive adsorption of CO2/CH4 mixture on dry and wet coal from subcritical to supercritical conditions," *Chemical Engineering Journal,* vol. 230, pp. 93-101, 8/15/ 2013.

[13] T. Montanari, E. Finocchio, I. Bozzano, G. Garuti, A. Giordano, C. Pistarino*, et al.*, "Purification of landfill biogases from siloxanes by adsorption: A study of silica and 13X zeolite adsorbents on hexamethylcyclotrisiloxane separation," *Chemical Engineering Journal,* vol. 165, pp. 859-863, 12/15/ 2010.

[14] T. Montanari, E. Finocchio, E. Salvatore, G. Garuti, A. Giordano, C. Pistarino*, et al.*, "CO2 separation and landfill biogas upgrading: A comparison of 4A and 13X zeolite adsorbents," *Energy,* vol. 36, pp. 314-319, 1// 2011.

[15] S. Cavenati, C. A. Grande, and A. E. Rodrigues, "Removal of Carbon Dioxide from Natural Gas by Vacuum Pressure Swing Adsorption," *Energy & Fuels,* vol. 20, pp. 2648-2659, 2006/11/01 2006.

[16] A. Kapoor and R. T. Yang, "Kinetic separation of methane—carbon dioxide mixture by adsorption on molecular sieve carbon," *Chemical Engineering Science,* vol. 44, pp. 1723-1733, 1989/01/01 1989.

[17] S. Cavenati, C. A. Grande, and A. E. Rodrigues, "Layered Pressure Swing Adsorption for Methane Recovery from CH4/CO2/N2 Streams," *Adsorption,* vol. 11, pp. 549-554.

[18] J. Schell, N. Casas, D. Marx, and M. Mazzotti, "Precombustion CO2 Capture by Pressure Swing Adsorption (PSA): Comparison of Laboratory PSA Experiments and Simulations," *Industrial & Engineering Chemistry Research,* vol. 52, pp. 8311-8322, 2013/06/19 2013.

[19] P. A. Webley, "Adsorption technology for CO2 separation and capture: a perspective," *Adsorption,* vol. 20, pp. 225-231, 2014.

[20] G. Li, P. Xiao, J. Zhang, P. A. Webley, and D. Xu, "The role of water on postcombustion CO2 capture by vacuum swing adsorption: Bed layering and purge to feed ratio," *AIChE Journal,* vol. 60, pp. 673-689, 2014.

[21] C.-T. Chou and C.-Y. Chen, "Carbon dioxide recovery by vacuum swing adsorption," *Separation and Purification Technology,* vol. 39, pp. 51-65, 2004.

[22] A. D. Ebner and J. A. Ritter, "State-of-the-art Adsorption and Membrane Separation Processes for Carbon Dioxide Production from Carbon Dioxide Emitting Industries," *Separation Science and Technology,* vol. 44, pp. 1273-1421, 2009/04/03 2009.

[23] V. G. Gomes and K. W. K. Yee, "Pressure swing adsorption for carbon dioxide sequestration from exhaust gases," *Separation and Purification Technology,* vol. 28, pp. 161-171, 2002.

[24] M. Ishibashi, H. Ota, N. Akutsu, S. Umeda, M. Tajika, J. Izumi*, et al.*, "Technology for removing carbon dioxide from power plant flue gas by the physical adsorption method," *Energy Conversion and Management,* vol. 37, pp. 929-933, 1996.

[25] E. S. Kikkinides, R. T. Yang, and S. H. Cho, "Concentration and recovery of carbon dioxide from flue gas by pressure swing adsorption," *Industrial & Engineering Chemistry Research,* vol. 32, pp. 2714-2720, 1993.

[26] G. N. Nikolaidis, E. S. Kikkinides, and M. C. Georgiadis, "Model-Based Approach for the Evaluation of Materials and Processes for Post-Combustion Carbon Dioxide Capture from

Flue Gas by PSA/VSA Processes," *Industrial & Engineering Chemistry Research,* vol. 55, pp. 635-646, 2016/01/27 2016.

[27] G. Li, P. Xiao, P. Webley, J. Zhang, R. Singh, and M. Marshall, "Capture of CO2 from high humidity flue gas by vacuum swing adsorption with zeolite 13X," *Adsorption,* vol. 14, pp. 415-422, 2008/06/01 2008.

[28] P. J. E. Harlick and F. H. Tezel, "An experimental adsorbent screening study for CO2 removal from N2," *Microporous and Mesoporous Materials,* vol. 76, pp. 71-79, 12/1/ 2004.

[29] R. V. Siriwardane, M.-S. Shen, and E. P. Fisher, "Adsorption of CO2, N2, and O2 on Natural Zeolites," *Energy & Fuels,* vol. 17, pp. 571-576, 2003/05/01 2003.

[30] S. Cavenati, C. A. Grande, and A. E. Rodrigues, "Adsorption Equilibrium of Methane, Carbon Dioxide, and Nitrogen on Zeolite 13X at High Pressures," *Journal of Chemical & Engineering Data,* vol. 49, pp. 1095-1101, 2004/07/01 2004.

[31] S. Dasgupta, N. Biswas, Aarti, N. G. Gode, S. Divekar, A. Nanoti*, et al.*, "CO2 recovery from mixtures with nitrogen in a vacuum swing adsorber using metal organic framework adsorbent: A comparative study," *International Journal of Greenhouse Gas Control,* vol. 7, pp. 225-229, 3// 2012.

[32] G. Onyestyak, D. Shen, and L. V. C. Rees, "Frequency-response study of micro- and macro-pore diffusion in manufactured zeolite pellets," *Journal of the Chemical Society, Faraday Transactions,* vol. 91, pp. 1399-1405, 1995.

[33] G. Onyestyák and L. V. C. Rees, "Frequency Response Study of Adsorbate Mobilities of Different Character in Various Commercial Adsorbents," *The Journal of Physical Chemistry B,* vol. 103, pp. 7469-7479, 1999/09/01 1999.

[34] G. Onyestyák, "Comparison of Dinitrogen, Methane, Carbon Monoxide, and Carbon Dioxide Mass-Transport Dynamics in Carbon and Zeolite Molecular Sieves," *Helvetica Chimica Acta,* vol. 94, pp. 206-217, 2011.

[35] T. J. Giesy, Y. Wang, and M. D. LeVan, "Measurement of Mass Transfer Rates in Adsorbents: New Combined-Technique Frequency Response Apparatus and Application to CO2 in 13X Zeolite," *Industrial & Engineering Chemistry Research,* vol. 51, pp. 11509-11517, Sep 5 2012.

[36] T. J. Giesy, Y. Wang, and M. D. LeVan, "Measurement of Mass Transfer Rates in Adsorbents: New Combined-Technique Frequency Response Apparatus and Application to CO2in 13X Zeolite," *Industrial & Engineering Chemistry Research,* vol. 51, pp. 11509-11517, 2012.

[37] J. Valyon, F. Lónyi, G. Onyestyák, and J. Papp, "DRIFT and FR spectroscopic investigation of N2 and O2 adsorption on zeolites," *Microporous and Mesoporous Materials,* vol. 61, pp. 147-158, 7/18/ 2003.

[38] H. Ahn, J.-H. Moon, S.-H. Hyun, and C.-H. Lee, "Diffusion Mechanism of Carbon Dioxide in Zeolite 4A and CaX Pellets," *Adsorption,* vol. 10, pp. 111-128, 2004/06/01 2004.

[39] J. A. C. Silva, K. Schumann, and A. E. Rodrigues, "Sorption and kinetics of CO2 and CH4 in binderless beads of 13X zeolite," *Microporous and Mesoporous Materials,* vol. 158, pp. 219-228, 8/1/ 2012.

[40] X. Hu, E. Mangano, D. Friedrich, H. Ahn, and S. Brandani, "Diffusion mechanism of CO2 in 13X zeolite beads," *Adsorption,* vol. 20, pp. 121-135, 2013.

[41] F. Rezaei and P. Webley, "Structured adsorbents in gas separation processes," *Separation and Purification Technology,* vol. 70, pp. 243-256, 2010.

[42] T. J. Giesy and M. D. LeVan, "Mass transfer rates of oxygen, nitrogen, and argon in carbon molecular sieves determined by pressure-swing frequency response," *Chemical Engineering Science,* vol. 90, pp. 250-257, 3/7/ 2013.

[43] T. J. Giesy, L. A. Mitchell, and M. D. LeVan, "Mass Transfer of Binary Mixtures of Oxygen and Argon in a Carbon Molecular Sieve," *Industrial & Engineering Chemistry Research,* p. 140106083817003, 2014.

[44] DOE/NETL. (2010, DOE/NETL carbon dioxide capture and storage RD&D roadmap.

[45] A. S. Bhown and B. C. Freeman, "Analysis and Status of Post-Combustion Carbon Dioxide Capture Technologies," *Environmental Science & Technology,* vol. 45, pp. 8624-8632, 2011/10/15 2011.

[46] R. Steeneveldt, B. Berger, and T. A. Torp, "CO2 Capture and Storage: Closing the Knowing–Doing Gap," *Chemical Engineering Research and Design,* vol. 84, pp. 739-763, 9// 2006.

[47] J. Davison and K. Thambimuthu, "An overview of technologies and costs of carbon dioxide capture in power generation," *Proceedings of the Institution of Mechanical Engineers, Part A: Journal of Power and Energy,* vol. 223, pp. 201-212, May 1, 2009 2009.

[48] J. Zhang, P. Webley, and P. Xiao, "Effect of process parameters on power requirements of vacuum swing adsorption technology for CO2 capture from flue gas," *Energy Conversion and Management,* vol. 49, pp. 346-356, 2008.

[49] R. Haghpanah, A. Majumder, R. Nilam, A. Rajendran, S. Farooq, I. A. Karimi*, et al.*, "Multiobjective Optimization of a Four-Step Adsorption Process for Postcombustion CO2 Capture Via Finite Volume Simulation," *Industrial & Engineering Chemistry Research,* vol. 52, pp. 4249-4265, 2013/03/20 2013.

[50] (2002, International Energy Agency Working Party on Fossil Fuels, Solutions for the 21st century: zero emissions technologies for fossil fuels. 1-50.

[51] (2003, International Energy Agency Working Party on Fossil Fuels, CO2 capture at power stations and other major point sources. 1-12.

[52] A. L. Chaffee, G. P. Knowles, Z. Liang, J. Zhang, P. Xiao, and P. A. Webley, "CO_2 capture by adsorption: Materials and process development," *International Journal of Greenhouse Gas Control,* vol. 1, pp. 11-18, 2007.

[53] S. Farooq and D. M. Ruthven, "Numerical simulation of a kinetically controlled pressure swing adsorption bulk separation process based on a diffusion model," *Chemical Engineering Science,* vol. 46, pp. 2213-2224, // 1991.

[54] S. J. Wilson, C. C. K. Beh, P. A. Webley, and R. S. Todd, "The Effects of a Readily Adsorbed Trace Component (Water) in a Bulk Separation PSA Process: The Case of Oxygen VSA," *Industrial & Engineering Chemistry Research,* vol. 40, pp. 2702-2713, 2001/06/01 2001.

[55] A. Malek and S. Farooq, "Hydrogen purification from refinery fuel gas by pressure swing adsorption," *AIChE Journal,* vol. 44, pp. 1985-1992, 1998.

[56] S. Sircar and T. C. Golden, "Purification of Hydrogen by Pressure Swing Adsorption," *Separation Science and Technology,* vol. 35, pp. 667-687, 2000/01/05 2000.

[57] C. A. Grande and A. E. Rodrigues, "Propane/Propylene Separation by Pressure Swing Adsorption Using Zeolite 4A," *Industrial & Engineering Chemistry Research,* vol. 44, pp. 8815-8829, 2005/11/01 2005.

[58] J. A. Ritter and R. T. Yang, "Pressure swing adsorption: experimental and theoretical study on air purification and vapor recovery," *Industrial & Engineering Chemistry Research,* vol. 30, pp. 1023-1032, 1991/05/01 1991.

[59] A. Agarwal, L. T. Biegler, and S. E. Zitney, "Superstructure-Based Optimal Synthesis of Pressure Swing Adsorption Cycles for Precombustion CO2 Capture," *Industrial & Engineering Chemistry Research,* vol. 49, pp. 5066-5079, 2010/06/02 2010.

[60] F. V. S. Lopes, C. A. Grande, and A. E. Rodrigues, "Activated carbon for hydrogen purification by pressure swing adsorption: Multicomponent breakthrough curves and PSA performance," *Chemical Engineering Science,* vol. 66, pp. 303-317, 2/1/ 2011.

[61] C. A. Grande, F. V. S. Lopes, A. M. Ribeiro, J. M. Loureiro, and A. E. Rodrigues, "Adsorption of Off-Gases from Steam Methane Reforming (H2, CO2, CH4, CO and N2)

on Activated Carbon," *Separation Science and Technology,* vol. 43, pp. 1338-1364, 2008/04/01 2008.

[62] A. M. Ribeiro, C. A. Grande, F. V. S. Lopes, J. M. Loureiro, and A. E. Rodrigues, "Four beds pressure swing adsorption for hydrogen purification: Case of humid feed and activated carbon beds," *AIChE Journal,* vol. 55, pp. 2292-2302, 2009.

[63] Y. Swesi, P. Kerleau, I. Pitault, F. Heurtaux, and D. Ronze, "Purification of hydrogen from hydrocarbons by adsorption for vehicles application," *Separation and Purification Technology,* vol. 56, pp. 25-37, 8/1/ 2007.

[64] J.-G. Jee, M.-B. Kim, and C.-H. Lee, "Adsorption Characteristics of Hydrogen Mixtures in a Layered Bed: Binary, Ternary, and Five-Component Mixtures," *Industrial & Engineering Chemistry Research,* vol. 40, pp. 868-878, 2001/02/01 2001.

[65] A. Malek and S. Farooq, "Kinetics of hydrocarbon adsorption on activated carbon and silica gel," *AIChE Journal,* vol. 43, pp. 761-776, 1997.

[66] N. Casas, J. Schell, R. Pini, and M. Mazzotti, "Fixed bed adsorption of CO2/H2 mixtures on activated carbon: experiments and modeling," *Adsorption,* vol. 18, pp. 143-161, 2012.

[67] M. M. Islam, H. A. Mohammadpour, A. Ghaderi, C. Brice, and S. Yong-June, "Time-frequency based instantaneous power components for transient disturbances according to IEEE Standard 1459," in *Power & Energy Society General Meeting, 2015 IEEE*, 2015, pp. 1-1.

[68] Md. Moinul Islam, Roger A. Dougal, and Charles W. Brice,, "Analysis of Real-World Power Quality Disturbances Employing Time-Frequency Distribution," presented at the Power Systems Conference, IEEE, Clemson, SC, 2016.

[69] H. A. Mohammadpour, M. M. Islam, D. Coats, E. Santi, and S. Yong-June, "Sub-synchronous resonance mitigation in wind farms using gate-controlled series capacitor," in *Power Electronics for Distributed Generation Systems (PEDG), 2013 4th IEEE International Symposium on*, 2013, pp. 1-6.

[70] H. A. Mohammadpour, M. M. Islam, E. Santi, and Y. J. Shin, "SSR Damping in Fixed-Speed Wind Farms Using Series FACTS Controllers," *Power Delivery, IEEE Transactions on,* vol. 31, pp. 76-86, 2016.

[71] P. Stone, M. Islam, and Y. J. Shin, "Power quality impact of wind turbine generators on the electrical grid," in *Energytech, 2012 IEEE*, 2012, pp. 1-6.

[72] M. Islam, H. A. Mohammadpour, A. Ghaderi, C. W. Brice, and S. Yong-June, "Time-Frequency-Based Instantaneous Power Components for Transient Disturbances According to IEEE Standard 1459," *Power Delivery, IEEE Transactions on,* vol. 30, pp. 1288-1297, 2015.

[73] M. Islam, H. A. Mohammadpour, P. Stone, and S. Yong-June, "Time-frequency based power quality analysis of variable speed wind turbine generators," in *Industrial Electronics Society, IECON 2013 - 39th Annual Conference of the IEEE*, 2013, pp. 6426-6431.

[74] M. M. Islam, "Advanced Digital Signal Processing Based Redefined Power Quality Indices, and Their Applications to Wind Power.," PhD, Electrical Engineering, University of South Carolina, Columbia, SC, 2014.

[75] M. M. Islam, M. N. Kabir, and C. W. Brice, "Time-frequency-based assessment of grid frequency deviation caused by wind power fluctuations," in *Industrial Electronics Society, IECON 2015 - 41st Annual Conference of the IEEE*, 2015, pp. 001061-001066.

[76] M. Hirose, I. Omori, M. Oba, and T. Kawai, "Carbon Dioxide Separtion and Recovery System," Japan Patent 2005262001, 2005.

[77] K. Ito, K. Otake, and M.Itoi, "Carbon Dioxide Desorption Method," Japan Patent 2004202393, 2004.

[78] A. Sasaki, S. Matsumoto, M. Fujitsuka, T. Shinoki, T. Tanaka, and J. Ohtsuki, "CO_2 recovery in molten carbonate fuel cell system by pressure swing adsorption," *Energy Conversion, IEEE Transactions on,* vol. 8, pp. 26-32, 1993.

[79] T. Yokoyama. (2004, Japanese R&D on Large-Scale CO_2 Capture. *ECI Symposium Series on Separations Technology VI: New Perspectives on very Large-Scale Opeations RP3*.

[80] S. P. Reynolds, A. D. Ebner, and J. A. Ritter, "New Pressure Swing Adsorption Cycles for Carbon Dioxide Sequestration," *Adsorption,* vol. 11, pp. 531-536, 2005.

[81] S. P. Reynolds, A. D. Ebner, and J. A. Ritter, "Carbon dioxide capture from flue gas by pressure swing adsorption at high temperature using a K-promoted HTlc: Effects of mass transfer on the process performance," *Environmental Progress,* vol. 25, pp. 334-342, 2006.

[82] S. P. Reynolds, A. D. Ebner, and J. A. Ritter, "Stripping PSA Cycles for CO2 Recovery from Flue Gas at High Temperature Using a Hydrotalcite-Like Adsorbent," *Industrial & Engineering Chemistry Research,* vol. 45, pp. 4278-4294, 2006.

[83] S. Reynolds, A. Mehrotra, A. Ebner, and J. Ritter, "Heavy reflux PSA cycles for CO_2 recovery from flue gas: Part I. Performance evaluation," *Adsorption,* vol. 14, pp. 399-413, 2008.

[84] Y. Takamura, S. Narita, J. Aoki, S. Hironaka, and S. Uchida, "Evaluation of dual-bed pressure swing adsorption for CO_2 recovery from boiler exhaust gas," *Separation and Purification Technology,* vol. 24, pp. 519-528, 2001.

[85] J.-H. Park, H.-T. Beum, J.-N. Kim, and S.-H. Cho, "Numerical Analysis on the Power Consumption of the PSA Process for Recovering CO_2 from Flue Gas," *Industrial & Engineering Chemistry Research,* vol. 41, pp. 4122-4131, 2002.

[86] D. Ko, R. Siriwardane, and L. T. Biegler, "Optimization of Pressure Swing Adsorption and Fractionated Vacuum Pressure Swing Adsorption Processes for CO2 Capture," *Industrial & Engineering Chemistry Research,* vol. 44, pp. 8084-8094, 2005.

[87] C. A. Grande, S. Cavenati, and A. E. Rodrigues, "Pressure Swing Adsorption for Carbon Dioxide Sequestration," 2005.

[88] P. Xiao, J. Zhang, P. Webley, G. Li, R. Singh, and R. Todd, "Capture of CO_2 from flue gas streams with zeolite 13X by vacuum-pressure swing adsorption," *Adsorption,* vol. 14, pp. 575-582, 2008.

[89] J. Zhang and P. A. Webley, "Cycle Development and Design for CO2 Capture from Flue Gas by Vacuum Swing Adsorption," *Environmental Science & Technology,* vol. 42, pp. 563-569, 2007.